FINAL REPORT

Continued Discrimination Demonstration Using Advanced EMI Models at Live UXO Sites: Data Quality Assessment and Residual Risk Mitigation in Real Time

ESTCP Project MR-201227

APRIL 2018

Dr. Fridon Shubitidze
White River Technologies, Inc.

Page Intentionally Left Blank

Page Intentionally Left Blank

REPORT DOCUMENTATION PAGE

Form Approved
OMB No. 0704-0188

1. REPORT DATE *(DD-MM-YYYY)*	**2. REPORT TYPE**	**3. DATES COVERED** *(From - To)*
31-03-2017	ESTCP Final Report	30 April 2012 – 31 March 2017

4. TITLE AND SUBTITLE

Continued Discrimination Demonstration Using Advanced EMI Models at Live UXO Sites: Data Quality Assessment and Residual Risk Mitigation in Real Time

5a. CONTRACT NUMBER
W912HQ-12-C-0056

5b. GRANT NUMBER

5c. PROGRAM ELEMENT NUMBER

6. AUTHOR(S)

Dr. Fridon Shubitidze

5d. PROJECT NUMBER
MR-201227

5e. TASK NUMBER

5f. WORK UNIT NUMBER

7. PERFORMING ORGANIZATION NAME(S) AND ADDRESS(ES)

White River Technologies, Inc.
1242 Chestnut Street
Newton, MA 02464

8. PERFORMING ORGANIZATION REPORT NUMBER

MR-201227

9. SPONSORING / MONITORING AGENCY NAME(S) AND ADDRESS(ES)

Environmental Security Technology Certification Program
4800 Mark Center Drive, Suite 17D03, Alexandria, VA 22350-3605

10. SPONSOR/MONITOR'S ACRONYM(S)
ESTCP

11. SPONSOR/MONITOR'S REPORT NUMBER(S)
MR-201227

12. DISTRIBUTION / AVAILABILITY STATEMENT

DISTRIBUTION A. Approved for public release: distribution unlimited.

13. SUPPLEMENTARY NOTES

14. ABSTRACT

This project demonstrated the capability of advanced electromagnetic induction (EMI) models to perform discrimination of unexploded ordnance (UXO) at live sites; to achieve a high probability of UXO discrimination in situations involving widespread clutter; to minimize the number of false positives in such cases; to identify all UXO with high confidence; to assess the quality of the data; and to provide a robust dig threshold that will minimize the risk to regulators. Specific technical objectives were to:

1. Use advanced physics-based EMI models to extract robust features that will allow reliable classification when starting from dynamic or cued EMI sensor data. Establish the validity and limitations of these advanced models, taking into account the number of objects in a given cell, their size and material heterogeneity, the geology, and the level of background noise.

2. Combine the advanced models with a statistical model-based approach to select robust classification feature vectors for a specific live UXO site that can reliably and effectively discriminate hazardous targets of interest (TOI) from nonhazardous items.

3. Deploy advanced EMI and statistical signal processing tools to assess EMI data quality onsite and provide a robust dig-threshold point; as a last step, use the different targets' extracted extrinsic parameters to mitigate the residual risk due to UXO and to increase the confidence of regulators at the site.

15. SUBJECT TERMS

Electromagnetic Induction, EMI, UXO, Classification, Dynamic Classification,

16. SECURITY CLASSIFICATION OF:			**17. LIMITATION OF ABSTRACT**	**18. NUMBER OF PAGES**	**19a. NAME OF RESPONSIBLE PERSON**
a. REPORT	**b. ABSTRACT**	**c. THIS PAGE**			Fridon Shubitidze
U	U	U	SAR	133	**19b. TELEPHONE NUMBER** *(include area code)* (603) 727-9673

Standard Form 298 (Rev. 8-98)
Prescribed by ANSI Std. Z39.18

Page Intentionally Left Blank

COST & PERFORMANCE REPORT

Project: MR-201227

TABLE OF CONTENTS

Page

EXECUTIVE SUMMARY ES-1

1.0 INTRODUCTION 1

1.1 BACKGROUND 1

1.2 OBJECTIVE OF THE DEMONSTRATIONS 2

1.3 REGULATORY DRIVERS 3

2.0 TECHNOLOGY 5

2.1 SENSING TECHNOLOGIES 6

2.2 EMI DATA PRE-PROCESSING AND BACKGROUND CORRECTION 6

2.3 TARGETS DETECTION 7

2.4 FORWARD MODELS: ONVMS 8

2.5 JOINT DIAGONALIZATION FOR DATA PREPROCESSING 10

2.6 EMI DATA INVERSION 13

2.7 EXTRACTING CLASSIFICATION PARAMETERS 15

2.8 CLASSIFICATION USING CLUSTERING 15

2.9 CLASSIFICATION USING TEMPLATE MATCHING 17

2.10 ADVANTAGES AND LIMITATIONS OF THE TECHNOLOGY 18

2.11 FORT ORD, CA, DATA INVERSION AND CLASSIFICATION SCHEME 19

3.0 PERFORMANCE OBJECTIVES 31

3.1 OBJECTIVE: MAXIMIZE CORRECT CLASSIFICATION ON MUNITIONS 31

3.1.1 Metric 31

3.1.2 Data Requirements 32

3.1.3 Success Criteria Evaluation and Results 32

3.2 OBJECTIVE: MAXIMIZE CORRECT CLASSIFICATION OF NON-MUNITIONS 32

3.2.1 Metric 32

3.2.2 Data Requirements 32

3.2.3 Success Criteria Evaluation and Results 32

3.3 OBJECTIVE: SPECIFICATION OF NON-DIG THRESHOLD 32

3.3.1 Metric 32

3.3.2 Data Requirements 32

3.3.3 Success Criteria Evaluation and Results 33

3.4 OBJECTIVE: MINIMIZE NUMBER OF ANOMALIES THAT CANNOT BE ANALYZED 33

3.4.1 Metric 33

TABLE OF CONTENTS (Continued)

Page

3.4.2 Data Requirements 33
3.4.3 Success Criteria Evaluation and Results 33
3.5 OBJECTIVE: CORRECT ESTIMATION OF TARGET PARAMETERS 33
3.5.1 Metric 33
3.5.2 Data Requirements 33
3.5.3 Success Criteria Evaluation and Results 34
4.0 SITE DESCRIPTION 35
4.1 SITE DESCRIPTION 36
4.1.1 Former Spencer Artillery Range, TN 36
4.1.2 Massachusetts Military Reservations, MA 38
4.1.3 Former CampEllis, IL 39
4.1.4 Fort Rucker, AL 40
4.1.5 New Boston Air Force Station, NH 41
4.1.6 Former Southwestern Proving Ground, AR 42
4.1.7 Waikoloa Maneuver Area, HI 43
4.1.8 Andersen Air Force Base, Guam 44
4.1.9 Fort Bliss, TX 45
4.1.10 West Mesa, NM 46
4.1.11 Former Fort Ord, CA 47
4.2 BRIEF SITE HISTORY 48
4.2.1 Spencer Artillery Range, TN 48
4.2.2 Massachusetts Military Reservations, MA 48
4.2.3 Camp Ellis, IL 48
4.2.4 Ft. Rucker, AL 49
4.2.5 New Boston Air Force Station, NH 49
4.2.6 SWPG, AR 49
4.2.7 Waikoloa, HI 50
4.2.8 Andersen AF Base, Guam 50
4.2.9 Castner Range Fort Bliss, TX 50
4.2.10 West Mesa, NM 50
4.2.11 Fort Ord, CA 51
4.3 SITE GEOLOGY 51
4.3.1 Spencer Range, TN 51
4.3.2 Massachusetts Military Reservation, MA 51
4.3.3 Camp Ellis, IL 52
4.3.4 Fort Rucker, AL 52
4.3.5 New Boston AF Station, NH 52
4.3.6 SWPG, AR 53
4.3.7 Waikoloa, HI 53
4.3.8 Andersen AF Base, Guam 53
4.3.9 Castner Fort Bliss, TX 53

TABLE OF CONTENTS (Continued)

Page

4.3.10 West Mesa, NM 54
4.3.11 Fort Ord, CA 54
4.4 MUNITIONS CONTAMINATION 54
4.4.1 Spencer Range, TN 54
4.4.2 MMR, MA 54
4.4.3 Former Camp Ellis, IL 54
4.4.4 Fort Rucker, AL 55
4.4.5 New Boston Air Force Station, NH 55
4.4.6 Southwestern, AR 55
4.4.7 Waikoloa, HI 55
4.4.8 Andersen Air Force Base, Guam 56
4.4.9 Fort Bliss, TX 56
4.4.10 West Mesa, NM 56
4.4.11 Fort Ord, CA 56
5.0 TEST DESIGN 57
5.1 SITE PREPARATION 57
6.0 DATA ANALYSIS AND PRODUCTS 59
6.1 EMI DATA INVERSION AND CLASSIFICATION STEPS 59
6.2 DATA PRODUCTS 60
7.0 PERFORMANCE ASSESSMENT 61
7.1 CORRECT CLASSIFICATION OF MUNITIONS 61
7.1.1 Results for Spencer Range, TN 61
7.1.2 Massachusetts Military Reservation, MA 68
7.1.3 Camp Ellis, IL 71
7.1.4 Fort Rucker, AL 76
7.1.5 New Boston AF Station, NH 77
7.1.6 SWPG, AR 78
7.1.7 Waikoloa Maneuver Area, HI 80
7.1.8 Andersen AF Base, Guam 89
7.1.9 Castner Range Fort Bliss, TX 90
7.1.10 West Mesa, NM 91
7.1.11 Fort Ord, CA 92
7.2 OBJECTIVE: MAXIMIZE CORRECT CLASSIFICATION OF NON-MUNITIONS 93
7.3 RESULTS 93
7.4 OBJECTIVE: SPECIFY A NO-DIG THRESHOLD 95
7.5 RESULTS 95
7.6 OBJECTIVE: MINIMIZE THE NUMBER OF ANOMALIES THAT CANNOT BE ANALYZED 97
7.7 RESULTS 97

TABLE OF CONTENTS (Continued)

Page

7.8 OBJECTIVE: CORRECT ESTIMATION OF TARGET PARAMETERS 97
7.9 RESULTS 97
8.0 COST ASSESSMENT 99
8.1 COST FOR CUED DATA SET PROCESSING AND CLASSIFICATIONS 99
8.2 COST FOR DYNAMIC DATA SET PRE-PROCESSING, DATA INVERSION AND CLASSIFICATIONS 99
9.0 IMPLEMENTATION ISSUES 101
10.0 REFERENCES 103
APPENDIX A HEALTH AND SAFETY PLAN (HASP) A-1
APPENDIX B POINTS OF CONTACT B-1

LIST OF FIGURES

Page

Figure 1. A Screen Shot of the Graphical User Interface of EMClass v-2.1.6 5
Figure 2. Color Map: Mapped Response Amplitude [mV/A] 7
Figure 3. Difference Between the Predicted and Actual Locations for TOIs 8
Figure 4. Time-decay Curves of Dipole Moment for a Target at a UXO Live Site 10
Figure 5. Estimated Log(K), β and γ *parameters* for Eigenvalues from all the Data Points in a Lane 13
Figure 6. Blue Dots: Extracted Locations from a Dynamic Data Set using the Combined ONVMS-DE Algorithm; Red Dots: Centers of Clusters 17
Figure 7. Inverted Total ONVMS Time-decay Profiles for Fort Sill, OK (Left) and Camp Beale, CA (Right) Seeded ISO Targets 18
Figure 8. Fort Bliss, TX, 2x2 TT Targets Classification Results in the Form of ROC Curves Obtained by Our Team and Two Other Teams 19
Figure 9. Multi-static Response Matrix Eigenvalues Versus Time for a Seeded 155-mm Projectile 22
Figure 10. MM Multi-static Response Matrix Eigenvalues Versus Time for a Seeded 75-mm Projectile (Top Figure) and Small ISO (Bottom Figure), Respectively 23
Figure 11. Multi-static Response Matrix Eigenvalues Versus Time for a Seeded Medium ISO (Top Figure) and 37-mm Projectile (Bottom Figure), Respectively 24
Figure 12. MM Multi-static Response Matrix Eigenvalues Versus Time for a Native 40 mm (Top Figure) and 60 mm (Bottom Figure) Projectiles, Respectively 25
Figure 13. Multi-static Response Matrix Eigenvalues Versus Time for Multi Targets 26
Figure 14. Multi-static Response Matrix Eigenvalues Versus Time for (Top Figure) a Native Deeply Buried 155-mm Projectile and a Set of Shallow Clutters and (Bottom Figure) a Native 37-mm Projectile and Clutter Buried at 30 cm and 10 cm, Respectively 27
Figure 15. One Source Inversion Result Shows: a) Extracted Total ONVMS (Effective Polarizability) for a Library TOI (Red Lines); and b) Fort Ord Anomaly #40070 .. 28
Figure 16. Total ONVMS for Fort Ord Anomaly #40070 Using Two Source Inversion for: a) Source 1/2; b) Source 2/2; c) Source 1+ Source 2 28
Figure 17. Three Source Inversion for Fort Ord Anomaly #40070 29
Figure 18. Fort Ord TOIS, From Left to Right: 20-mm, Small ISO, 37-mm, 35-mm, 40-mm, 60-mm, Medium ISO, 75-mm, 81-mm, 4.2" Mortar, 155-mm Projectiles 30
Figure 19. Wooded, Open and Dynamic Areas in a Portion of the Former Spencer Artillery Range MRS 37
Figure 20. Boundaries of MM and 2x2 TT Demonstration Study Areas at the MMR Site 38
Figure 21. Former Camp Ellis ETCP UXO Live Site Classification Study Area with Geophysical Anomaly Density 39
Figure 22. An Aerial Photo of the ESTCP UXO Live Site Classification Site Located at Fort Rucker, AL 40
Figure 23. ESTCP Demonstration Area MU705, Located within the New Boston Air Force Station, NH 41

LIST OF FIGURES (CONTINUED)

Page

Figure 24. Boundary of the ESTCP UXO Live Site Classification Area Located at the Former Southwestern Proving Ground, AK 42
Figure 25. ESTCP Data Collection Boundaries at WMA, HI 43
Figure 26. Boundary of Demonstration Area at NRP, Andersen AFB, Guam 44
Figure 27. ESTCP Classification Demonstration Area at Castner Range, Ft. Bliss, TX 45
Figure 28. Boundary of ESTCP Live Site Area at the Former Kirtland AFB Precision Bombing Range, West Mesa, NM 46
Figure 29. Locations of Cued MM Anomalies During ESTCP UXO Live Site at Units 11 and 12 in the Impact MRA, Former Fort Ord, CA 47
Figure 30. Comparisons Between Effective Polarizabilities Extracted from MM, MPV and 2x2 TEMTADS Data for a 60 mm Mortar (SR-1661), Small (SR-1502) and Medium (SR-1555) Size ISOs, 105 mm (SR-1569), 75 mm (SR-1725) and 37 mm (SR-1576) Projectiles 62
Figure 31. ROC Curve for the Spencer Artillery Range 5x5 TEMTADS Data 63
Figure 32. ROC Curve for the MM Data in the Spencer Artillery Range Open Area 64
Figure 33. ROC Curves for MM, MPV and 2x2 TEMTADS Anomalies from the Spencer Range Dynamic Area 65
Figure 34. ROC Curves for MPV and 2x2 TEMTADS Anomalies in Spencer Range Wooded Area 66
Figure 35. Time-dependent Total ONVMS Inverted from MPV-II Data for the Spencer Range Anomaly #2355 using Three-target Inversion 67
Figure 36. Six-target Inversion Results: Time-dependent Total ONVMS, Inverted from MPV-II Data, for Spencer Range Anomaly #2355 68
Figure 37. ROC Curve for the MMR 2x2 TEMTADS Data 69
Figure 38. ROC Curve for the MMR MM Data 70
Figure 39. ROC Curves of MM and 2x2 TEMTADS Systems Develop for the Same Set of Anomalies 71
Figure 40. ROC Curve for the Camp Ellis MM Data 72
Figure 41. ROC Curve for the Camp Ellis 2x2 TEMTADS Data 73
Figure 42. Ground Truth Photos for Camp Ellis MM Anomalies (Left to Right) #EL-33, EL-132 and EL-941 73
Figure 43. Inverted Total ONVMS Time-decay Profiles for Camp Ellis Seeded Rifle Grenades 74
Figure 44. Ground Truth Photos for Camp Ellis TEMTADS Anomalies #EL-319 and #EL-941 75
Figure 45. Inverted Total ONVMS Time-decay Profiles for the Camp Ellis Seeded Rifle Grenades, 2x2 TEMTADS Data Set 75
Figure 46. S2-V2 ROC Curve for the Camp Ellis 2x2 TEMTADS Data 76
Figure 47. ROC Curve for the Camp Rucker MM Data 77
Figure 48. ROC Curve for the NBAFS MPV Data 78
Figure 49. ROC Curve for the SWPG 2x2 TEMTADS Data 79
Figure 50. ROC Curve for the SWPG 2x2 MM Data 80
Figure 51. ROC Curve for the WMA, HI, MM Data 81
Figure 52. Eigenvalues Versus Time for Three WMATest Areas: T017, T020 A and T020 B 82

LIST OF FIGURES (CONTINUED)

Page

Figure 53. Total ONVMS and Eigenvalues for Missed Small ISO (anomaly #1027) and 60 mm Mortar (anomaly #1047) Targets 83
Figure 54. Photos of Intrusive Investigated Anomalies #29, #36, #199, #441, #442 85
Figure 55. Top Row: Comparisons Between Total ONVMS for a Library 37-mm Projectile (Red Lines), with a Copper Band, and for Anomalies #36 and #442. Bottom Row: Eigenvalues Versus Time for Anomalies #36 and #442 86
Figure 56. Top Row: Comparison Between Total ONVMS for a Library 37-mm Projectile (Red Lines), Without a Copper Band, and for Anomalies #29 and #441. Bottom Row: Eigenvalues Versus Time for Anomalies #29 and #441 87
Figure 57. Top: Comparisons Between Total ONVMS for a Library 60-mm Projectile (Red Lines) and for Anomaly #199. Bottom: Eigenvalues Versus Time for Anomaly #199 88
Figure 58. ROC Curve for the Andersen Air Force Base, Guam, 2x2 TEMTADS Data 89
Figure 59. ROC Curve for the Fort Bliss, TX , 2x2 TEMTADS Data 90
Figure 60. ROC Curve for the West Mesa, NM, MM Data 91
Figure 61. ROC for Fort Ord Primary Objective (Finding all Large TOIs to a Depth of 2 Feet) 92
Figure 62. Final Scoring Result for Fort Ord Secondary Objective (Classify all TOI) 93
Figure 63. Cost Savings for Achieved by Our and Two Other Teams at Fort Bliss, TX, and Fort Ord, CA, UXO Live Sites 96
Figure 64. Extracted Total ONVMS Time-decay Profiles for MM Anomaly #2504 101

LIST OF TABLES

Page

Table 1. Inverted Locations for Fort Ord, CA, Anomaly #40070 Using One, Two and Three Source Inversions 29
Table 2. Performance Objectives 31
Table 3. ESTCP UXO Live Site Classification Studies 36
Table 4. Sites, Targets, Sensors and Survey Modes 37
Table 5. Efficiency and False Positive Rejections Rates for 2x2 TEMTADS and MPV System in Spencer Range Wooded Area 67
Table 6. Classification Performance Results for all Eleven UXO Live Sites 94
Table 7: Average Time and Cost Model for Processing Cued Data Set Using Advanced EMI Models 99
Table 8: Average Time Spent by an Analyst on Camp Hale, CO, Dynamic Data Processing and Classification 100
Table 9. Points of Contact for the Advanced EMI Models Demonstration B-1

ACRONYMS AND ABBREVIATIONS

2D	two-dimensional
3D	three-dimensional
AFSCF	Air Force Satellite Control Facility
AFSPC	Air Force Space Command
AL	Alabama
APG	Aberdeen Proving Ground
AR	Arkansas
BRAC	Base Realignment and Closure
BSS	Blind Source Separation
BUD	Berkley UXO Discriminator
CA	California
CIA	Central Impact Area
cm	Centimeter
CO	Colorado
DE	Differential evolution
DoD	Department of Defense
EMI	Electromagnetic Induction
ESTCP	Environmental Security Technology Certification Program
GPS	global positioning system
HE	high explosive
HI	Hawaii
IDA	Institute for Defense Analyses.
IL	Illinois
Inc	Incorporated
JD	Joint Diagonalization
lb	pound
MA	Massachusetts
MEC	Munitions and Explosives of concern
MILCON	military construction
µs	Microsecond
mm	Millimeter
MM	MetalMapper
MMR	Massachusetts Military Reservation

MPV	Man-Portable Vector
MRA	Munitions Response Area
MRS	Munition Response Site
ms	Millisecond
MSR	Multi-static response
NBAFS	New Boston Air Force Station
NC	North Carolina
NH	New Hampshire
NM	New Mexico
NRL	Naval Research Laboratory
NRP	North Ramp Parking
NSMS	Normalized surface magnetic source
NV/SMS	Normalized volume or surface magnetic source models
ONVMS	Orthogonal normalized volume magnetic source
ONV/SMS	Orthonormalized volume or surface magnetic source models
OPTEMA	One pass transient electromagnetic array
PNN	Probabilistic Neural Network
RF	Recovery Field
ROC	receiver operating characteristic
SERDP	Strategic Environmental Research and Development Program
SLO	San Luis Obispo
SNR	Signal to noise ratio
SVM	Support vector machine
SWPG	Southwestern Proving Ground
TD	Time Domain
TEMTADS	Time Domain Electromagnetic Towed Array Detection System
TOI	Target of Interest
TONVMS	Total Orthonormalized volume magnetic source
TX	Texas
Tx/Rx	Transmitter / Receiver
USACE	U.S. Army Corps of Engineers
UXO	Unexploded Ordnance
WMA	Waikoloa Maneuver Area
WRT	White River Technologies

ACKNOWLEDGEMENTS

Funding for this project was provided by the Environmental Security Technology Certification Program (ESTCP). We wish to express our sincere appreciation to Dr. Anne Andrews, Dr. Herb Nelson, and the staff of the ESTCP and SERDP Offices for their support.

The Principal Investigator, Dr. Fridon Shubitidze of White River Technologies, Inc. and Thayer School of Engineering, at Dartmouth University, conceived the implementation of advanced electromagnetic induction (EMI) data pre-processing, data inversion and classification approaches. He successfully applied them to all unexploded ordnance (UXO) data sets collected on all ESTCP Live Sites presented here.

Dr. Irma Shamatava of White River Technologies, Inc. an expert in forward and inverse EMI problems, conducted advanced EMI sensor data inversion and UXO discrimination studies on ESTCP Live Sites presented here.

Mr. Joe Keranen and Mr. Jon Miller of White River Technologies, Inc., performed inversion and classification analysis on ESTCP Live Site data collected at Spencer Range, TN, New Boston, NH, and Fort Rucker, AL.

Page Intentionally Left Blank

EXECUTIVE SUMMARY

Unexploded ordnance (UXO) Live Site classification demonstrations described in this report were conducted in fulfilment of the ESTCP Project MR-201227, "Continued Discrimination Demonstration Using Advanced EMI Models at Live UXO Sites: Data Quality Assessment and Residual Risk Mitigation in Real Time." This project was executed as part of the 2012 ESTCP solicitation, "Military Munitions Detection, Classification, and Remediation: *Classification Technologies.*"

The primary objectives of Project MR-201227 were to:

1. Implement and demonstrate robust procedures and approaches for advanced electromagnetic induction (EMI) sensor data pre-processing, inversion and sub-surface target classification;
2. Assess quantitatively the quality and utility of advanced EMI sensor data in terms geologic and background noise effects, and the use of multi-object inversion algorithms to de-couple the EMI response of targets in the presence of high-density metal contamination;
3. Validate processing technology based on extracted intrinsic (effective dipole polarizability) and extrinsic (location) target parameters from measured data, and identify robust classification features in order to distinguish UXO targets from non-hazardous objects; and,
4. Fully characterize the discrimination ability and limitations of the advanced models with regard to the number of objects, target size and material heterogeneity, geology, and background noise.

UXO classification procedures consist of the following sequential steps: background corrections, target detection/picking, data inversion and target feature parameter estimation, ranking, training, and finally classification, i.e., separating UXO from non-hazardous anomalies. Under this project we have developed and tested a user-friendly software package for advanced EMI sensor data pre-processing, inversion and classification. The software package, which supports both cued and dynamic survey datasets, allows the efficient execution of the following procedures:

a. **Background correction:** during this process each EMI dataset is first normalized by a corresponding transmit (Tx) current. Next, in the case of cued datasets, background data files are selected for a process of subtracting background levels from the original EMI anomaly dataset, and in the case of dynamic survey datasets, a median filter approach is employed for removing background noise from target signals.
b. **Data inversion:** after background EMI levels have been applied and corrupted channels removed, the combined Orthogonal Normalized Volume Magnetic Source – Differential Evolution (ONVMS-DE) algorithms are applied to the anomaly datasets using a multiple source inversion approach. The intrinsic and extrinsic parameters of the targets are then extracted and used for ranking.

c. **Targets picking using survey data set**: once background levels are removed from the survey data, two approaches are used to pick targets for cued interrogations: (1) The traditional method that utilizes signal amplitudes on a 2D map and identifies peaks of signals above a prescribed threshold level; and (2) A semi-supervised Gaussian clustering process which clusters the inverted extrinsic (source locations) parameters into a 3D space and identifies targets using cluster centers.

d. **Ranking:** this process uses extracted intrinsic classification features of the targets, such as total ONVMS-effective polarizabilities, (via one, two and three sources), to rank anomalies.

e. **Training:** typically, target classification feature parameters are clustered and site-specific training target lists are used to support final classification. Specifically, these training data are used to assess background noise levels, validate inversion results, confirm preliminary target ranking results, and (more importantly) determine an optimal "stop-dig" point which optimizes classification performance. The stop-dig point is established through evaluation of training data derived from "uncertain anomalies," which are located between targets which are definitely targets of interest (TOI) and those targets which are definitely clutter in the preliminary ranked list.

f. **Classification:** once the ground truth is obtained from the training targets, all anomalies are classified as TOI or clutter, and the optimal stop-dig point is defined.

During the course of Project MR-201227 our team processed multiple datasets collected at eleven ESTCP UXO Live Site demonstrations, including:

1. Spencer Range, TN;
2. Camp Edwards Massachusetts Military Reservation (MMR), MA;
3. Camp Elis, IL;
4. Fort Rucker, AL;
5. New Boston Airforce Station, NH;
6. Southwestern Proving Ground, AR;
7. Waikoloa Maneuver Area (WMA), HI;
8. Andersen AF base, Guam;
9. Fort Bliss, TX;
10. West Mesa, NM; and
11. Fort Ord, CA.

The advanced EMI data inversion and classification technology was demonstrated at these eleven UXO live sites for identifying all TOI and eliminating more than 75% of the clutter. The technology has applied to cued and dynamic data sets collected by the next generation EMI sensors: such as MM, 5x5 and 2x2 TEMTADS, MPV, BUD and OPTEMA. The demonstrations have showed that for most sites the advanced classification technology identified all TOI while correctly classifying 75% to 92% of the clutter at specified Stop-Dig points.

However, there were few sites where the algorithm did not correctly classify one or more TOI due to insufficient data quality, magnetic soil and inaccurately documenting the intrusive results. These illustrated the importance of a well-defined data collection procedure and accounting magnetic soil responses during intrusive investigations. A comparison of the classification results for different sensors showed that they perform equally well when data are analyzed using the advanced EMI models. We come to similar conclusion when compared between classification results for cued and survey data sets. The choice of which sensor in with mode to deploy on site can therefore be driven by cost and which system can most efficiently survey the terrain.

Page Intentionally Left Blank

1.0 INTRODUCTION

1.1 BACKGROUND

Clean-up of unexploded ordnance (UXO) contaminated lands at Department of Defense (DoD) and Department of Energy (DoE) has been identified as one of the military's most pressing environmental problems. As a result of past military training and weapon-testing activities, UXO are found at both active and formerly used defense sites, including closed, transferred and transferring ranges, munitions burning and open detonation areas. In the United States alone, more than 900 sites (about 11 million acres of land) are potentially contaminated with UXO. The costs of excavating all geophysical anomalies are well-known and are one of the greatest impediments to the efficient clean-up of UXO, particularly at highly contaminated UXO sites, when the multiple objects are present simultaneously in the sensor's field of view. It is estimated that UXO cleanup costs may be in the range of tens of billions of dollars [1]. To reduce the cost and accelerate the pace of cleanup, advanced EMI sensors and associated data processing and analysis methods were developed to distinguish buried UXO from the vast quantity of harmless scrap metal found on all munitions response site. These advanced classification technologies allow resources to be directed to removing only the UXO.

To reduce UXO cleanup costs, a new and recently advanced geophysical classification approach has been developed using electromagnetic induction technology. The technology has three main stages: detection, inversion, and classification [2]. Detection of UXO can be considered a binary-hypothesis problem in which one must determine whether there are objects present or not. Great developments have been made on this first stage by the introduction of a series of sophisticated ultra-wideband sensors designed to increase detection and classification probabilities. Current state-of-the-art EMI sensors are capable of recording target responses, whether in scalar [3]-[9] or vector form [7], [10]-[12], with unprecedented spatial resolution and spectral range that allows for a comprehensive characterization of buried objects.

During the second step of the process, background-corrected data are inverted to extract target parameter information. Both intrinsic target information (classification features) and extrinsic target information (location and orientation) are determined simultaneously. Our team has developed a physically complete, fast, accurate, robust, and clutter-tolerant forward model, called the ONVMS method for representing targets EMI responses. The method starts from the assumption that the measurable secondary magnetic field from the target is radiated by a set of elementary dipole sources infused throughout a volume at a set of singular points [13]. The Green's Functions that connects these sources with the measured field are transferred into orthonormal basis functions to streamline the calculations. The spatial distribution of the responding dipoles (their amplitudes scaled by the primary magnetic field) traces a map of "response activity" that reveals the targets below. This ONVMS model [13] is a generalization of the dipole model that simultaneously allows for the presence of several targets in the field of view of the sensor. Additionally, ONVMS supports the possibility that one or more of the targets is of such complexity—by being large or heterogeneous, for example—that it requires more than one dipole to account for the spatial or temporal nuances of its response. The need to determine the source locations and their intrinsic features results in a computationally costly nonlinear inversion. The inversion defines an objective function that provides a measure of the misfit between predictions and measurements and performs a least-squares minimization.

These objective functions tend to have many local minima, resulting in incorrect predictions. There is a procedure that uses elementary sources to locate a singularity directly but its generalization to multi-target scenarios is not straightforward. To avoid this difficulty, our group has employed a two-step inversion approach that combines the ONVMS technique with DE, a continuous genetic algorithm [15], [16]. The procedure alternates between linear ONVMS time-dependent-amplitude determinations and DE location searches, iterating until it reaches convergence.

At the final stage of the process it is necessary to classify the detected objects as UXO or clutter and, if the former, to determine the type of UXO. This classification step uses data derived from training and pre-existing library anomalies, associated intrusive ground truth data, and statistical classification tools.

This report describes and quantifies the performance and cost of UXO discrimination process that is based on advanced EMI models, such as orthonormalized volume magnetic source joint diagonalization and the differential evolution approach, which were applied to both cued and dynamic ESTCP UXO Live Site datasets.

1.2 OBJECTIVE OF THE DEMONSTRATIONS

The principal objective of this project was to apply advanced EMI models to ESTCP UXO Live Site data sets collected using next-generation EMI systems in cued and dynamic models, to demonstrate the capability and reliability of new classification models under real world scenarios. Specific technical objectives were:

- Process EMI datasets collected via next-generation geophysical instrumentation using advanced physics-based EMI models, particularly the ONVMS model and the JD technique. Establish the limitation and valid range of application of advanced models for subsurface targets classification using Live Site EMI data. Specifically, take into account the number of objects in a close proximity to the sensor, the size and material heterogeneity of those targets, the local geologic conditions influencing successful application of the methods, and the performance of the methods based on background noise levels.
- Identify robust classification features which successfully and robustly distinguish UXO targets from non-hazardous objects. Specifically, the technology should:
  - Identify all seeded and native UXO; and
  - Eliminate at least 75% of targets that do not correspond to targets of interest (TOI).
- Combine advanced EMI modeling and statistical signal processing tools to assess and quantify the quality of the survey data and provide a robust Stop-Dig threshold point.
- Document the applicability and limitations of the advanced EMI technologies for processing dynamic data.

- Demonstrate a robust target-picking and background-noise-subtraction approach for advanced EMI dynamic data using Joint Diagonalization and inverted extrinsic parameters. This entails the extraction of discrimination features like the total ONVMS (i.e., the effective polarizability) and use of a statistical model-based approach to select robust classification feature vectors for a specific UXO Live Site that can reliably and effectively discriminate hazardous TOI from non-hazardous items.

1.3 REGULATORY DRIVERS

Advanced EMI models (non-dipole models) have been developed under the SERDP MM-1572 project and successfully applied to next-generation EMI sensor datasets collected at ESTCP UXO Live Sites located at Camp Sibert, AL, Aberdeen Proving Ground (APG), MD, San Luis Obispo, CA and Camp Butner, NC [19]. As advanced UXO classification methods have been thoroughly documented via ESTP to perform reliably, the challenge of implementing the classification approach into the actual UXO cleanup process is to convince the regulatory community of the reliability of the classification information that these models and advanced EMI sensors can provide. To address this issue, the ESTCP Program Office conducted a series of blind UXO Live Site classification studies. The demonstrations included work at eleven former of active military facilities, including; Spencer Range, TN, Camp Edwards Massachusetts Military Reservation (MMR), MA, Camp Elis, IL, Fort Rucker, AL, New Boston Airforce Station, NH, Southwestern Proving Ground, AR, Waikoloa Maneuver Area (WMA), HI, Andersen AF base, Guam, Fort Bliss, TX, West Mesa, NM and the Former Fort Ord, CA. To gain regulator acceptance, the ESTCP Program Office involved regulators in the sites selection and other aspects of test design.

Page Intentionally Left Blank

2.0 TECHNOLOGY

New advanced EMI models and statistical signal processing approaches were developed and tested under SERDP Project MM-1572, which was completed in 2012. These methods were shown to be able to detect and identify buried UXO ranging in caliber from 25 mm up to 155 mm. The techniques were demonstrated to be physically complete, fast, accurate, and clutter-tolerant. They provided accurate and repeatable classification capabilities in both single- and multiple-target scenarios when combined with multi-axis/transmitter/receiver sensors like TEMTADS [5] and the MM [11]. The methodology, augmented to include a suite of classifiers, was also adapted to handheld sensors like the MPV and the 2×2-3D TEMTADS [19], [20]. Under this project, we have created a user-friendly program package called "*EMClass*" for advanced EMI data pre-processing, targets selection for cued interrogation, data inversion, extraction of target extrinsic and intrinsic parameters, and classification. In this section, we briefly describe the main functionalities of *EMClass*, along with related underline mathematical techniques one by one. More detailed descriptions of mathematical techniques can be found in [21].

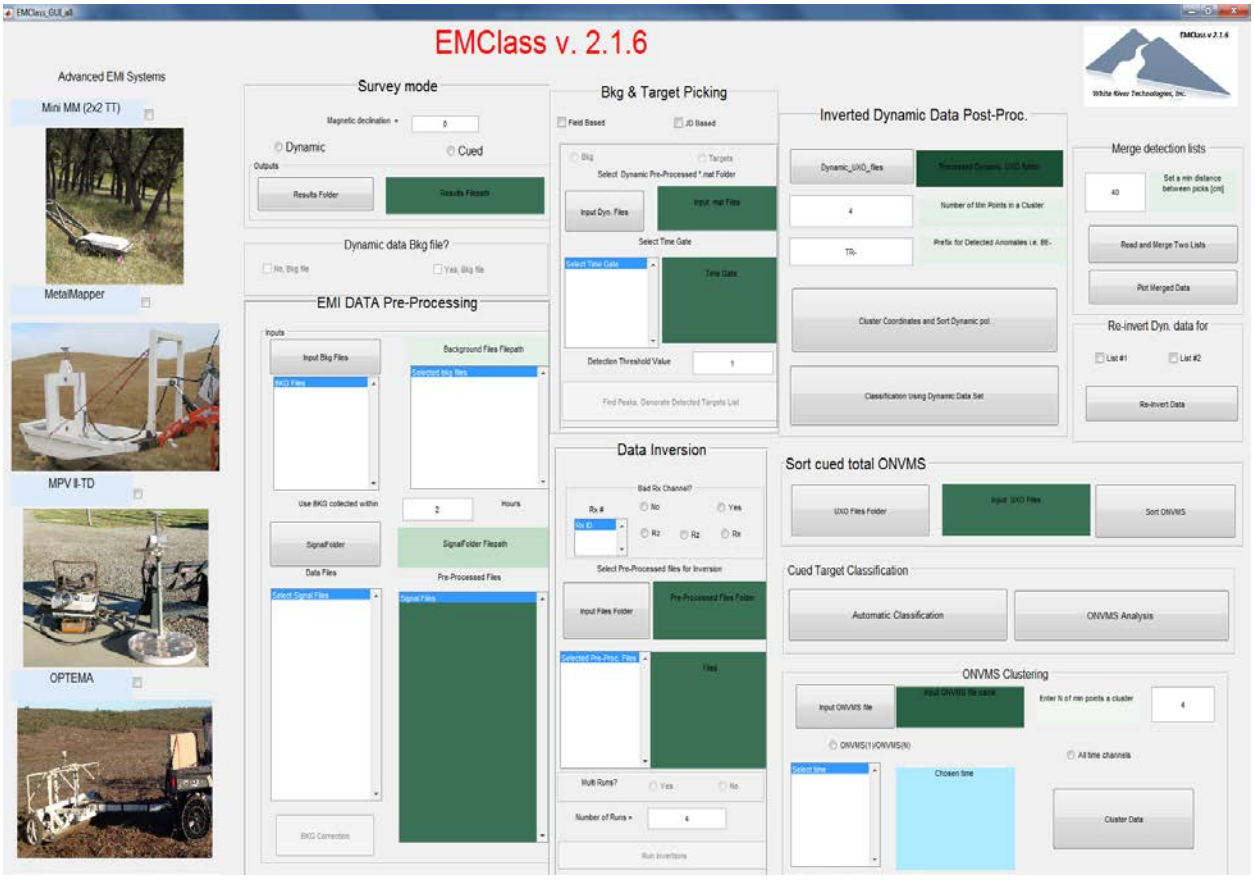

Figure 1. A Screen Shot of the Graphical User Interface of EMClass v-2.1.6

2.1 SENSING TECHNOLOGIES

A wide range of different electromagnetic induction sensing technologies, with novel waveforms, multi-axis transmitters, and scalar/vector receivers have been recently developed under SERDP-ESTCP programs. These advanced EMI sensors—including the MM, the 5x5 and 2x2-3D TEMTADS arrays, the OPTEMA, and the man-portable vector (MPV) sensor—provide measurements that feature a combination of high spatial diversity, different viewpoints, and a very wide dynamic range and which do full justice to the vector character of the electromagnetic field. Current state-of-the-art EMI systems thus offer data of unprecedented richness for use by discrimination processing algorithms. The *EMClass* software package supports 2x2 TEMTADS (Mini MM), MM, MPV and OPTEMA systems in both dynamic and cued survey modes (see Figure 1). To support modeling of multiple systems, the transmitter loops are divided into subsections and the primary field produced at any observation point is calculated as a sum of fields produced by the Tx current in each sub-section using the Biot-Savart law. Similarly, the receiver's area is divided into sub-areas, and the measured signal is modeled as sum of magnetic field fluxes into sub-areas using Faraday's induction law. For more details see [19].

2.2 EMI DATA PRE-PROCESSING AND BACKGROUND CORRECTION

Once a user chooses a sensor type and survey mode, the next steps include data pre-processing and background corrections. All sensors are equipped with a Global Positioning System (GPS) that geo-registers all collected EMI data (see Figure 1). In addition, sensors have an inertial measurement unit (IMU) that provides sensor orientations with respect to magnetic north. The software adjusts the angle between magnetic north and true north by entering the site-specific magnetic declination.

As part of the initial processing step, the measured transient signals $S_{k,m}(t_q)$ for kth -Tx, m^{th}-*Rx*, q^{th}-time channels are normalized to the corresponding transmitter currents maximum $max(I_k)$ as

$$D_k^m(t_q) = \frac{S_{k,m}(t_q)}{max(I_k)} \tag{1}$$

The background files, which are typically collected once every two hours during a survey, are pre-processed in the same manner as anomaly target files in Equation 1. All background data are compared to each other over the period of the project to estimate background fluctuation statistics.

Cued Data Sets: Following analysis of the background data collected each day, all cued data files for that day are background corrected as follows:

$$Data_{k,m}(t_q) = S_{k,m}(t_q) - 0.5 \cdot (B_{1\ k,m}(t_q) + B_{2\ k,m}(t_q)) \tag{2}$$

Where $B_{\alpha\ k,m}(t_q), \alpha = 1,2$ are normalized background data collected before and after $S_{k,m}(t_q)$; i.e., each target dataset is corrected using the respective background data collected closest in time. In order to achieve proper background leveling, the user must specify a time window of collected background data files (see Figure 1).

Dynamic Data Set: After dynamic data are pre-processed using equation (1), background levels are removed from signals using the median filter line-by-line.

2.3 TARGETS DETECTION

EMCLass software has two ways to pick targets from a dynamic data set for cued interrogations: (1) using the traditional amplitude response matric approach – using measured peak values above a prescribed threshold; and (2) using an advanced anomaly selection procedure exploiting the advanced orthogonal methods approach, i.e., ONVMS and joint diagonalization.

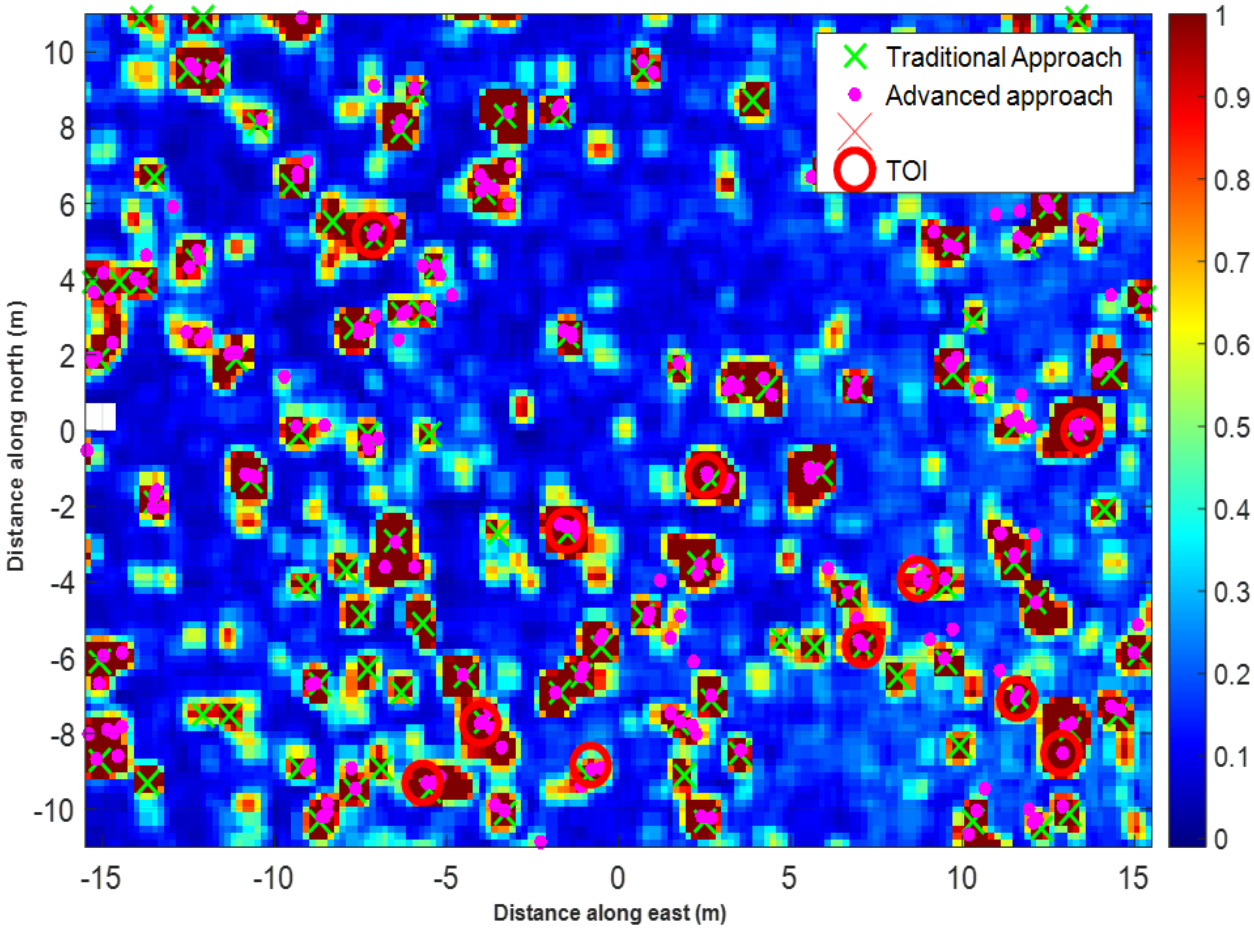

Figure 2. Color Map: Mapped Response Amplitude [mV/A]

Locations of detected targets using the traditional response metric (green crosses) and advanced anomaly section approach (magenta dots), respectively. Red circles: ground truth of TOIs locations.

Comparisons between predicted target locations, estimated using traditional and advanced target picking/classification algorithms, and actual target locations measured intrusively at a UXO Live Site are showed in Figure 2 and Figure 3. The comparisons show that the advanced anomaly selection approach maps the subsurface targets accurately and provide significantly improved anomaly locations compared to the traditional amplitude thresholding approach, particularly at dense metallic areas, see Figure 3.

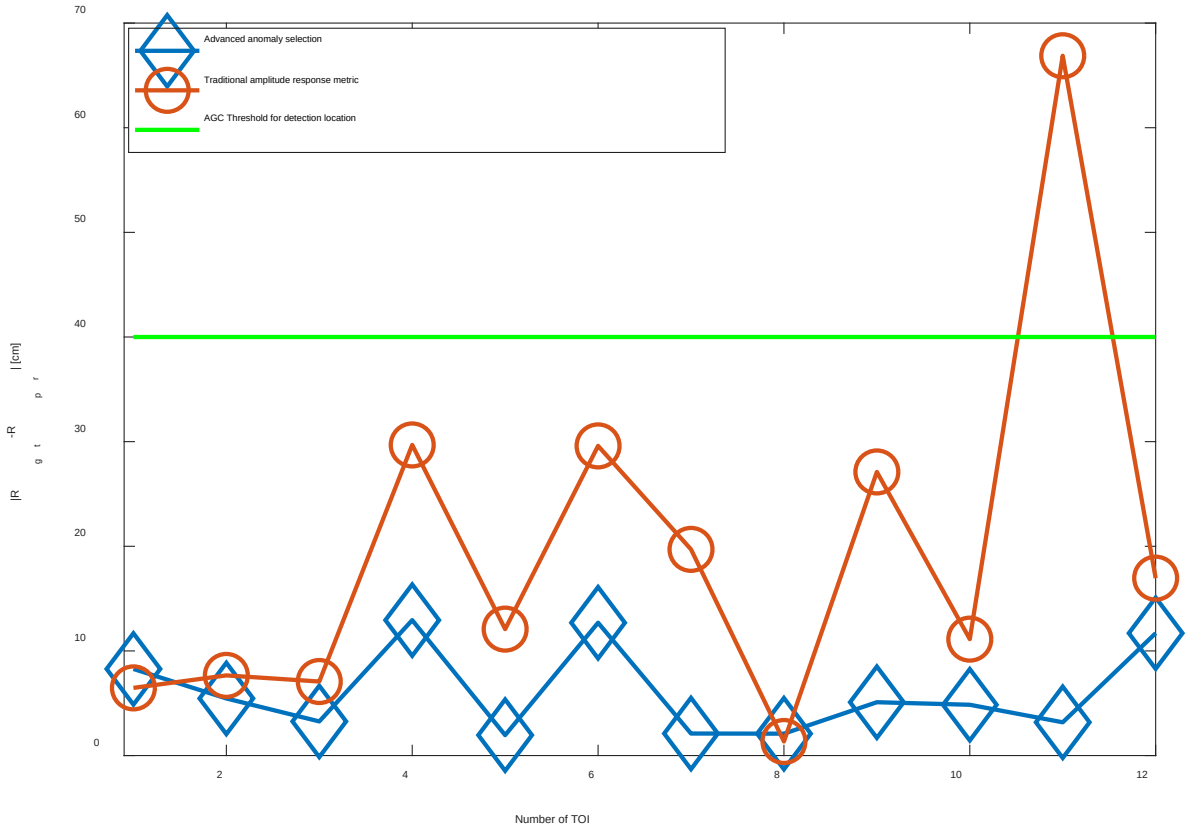

Figure 3. Difference Between the Predicted and Actual Locations for TOIs

In addition, the advanced anomaly selection algorithms, such as the ONVMS and JD methods, output the intrinsic parameters of subsurface targets for each dynamic data point. These extracted features, such as the effective magnetic dipole polarizabilities, allow us to classify targets as TOI and no-TOI with high confidence. Namely, comparison of the data collected via dynamic survey mode and stationary cued mode revealed that dynamic data is not significantly inferior to cued data in terms of the information that can be extracted and exploited for target classification. Our analysis has shown that when advanced models are applied to dynamic datasets, we are able to completely characterize and classify anomalies and eliminate or reduce significantly the number of cued measurements required for complete target classification across a site.

2.4 FORWARD MODELS: ONVMS

Advanced EMI forward models, which are distinctly different than traditional dipole models, were developed under the SERDP via Project MM-1572 and successfully applied to former Camp Sibert, AL ESTCP UXO Live Site datasets [33]. One such model routinely utilized is the ONVMS. This computational paradigm provides a physically complete, fast, accurate, and clutter-tolerant forward model used for effective UXO classification. ONVMS can be considered as a generalized volume dipole model, and in fact contains the point dipole model as a limiting case. The model assumes that a collection of scatterers can be replaced with a set of magnetic dipole sources, distributed over a volume, that mimic the eddy currents and magnetic responses induced on the targets by the sensor, that in turn establish observable secondary magnetic fields.

These induced dipoles and currents are distributed inside the objects in question, and thus the spatial distribution of the responding dipoles (their amplitudes scaled by the primary field) traces a map of "response activity" with a clustering pattern that reveals the locations and orientations of the targets present within. The scattered magnetic field at any point outside the volume of targets is represented as a superposition of magnetic fields due to a volumetric distribution of magnetic dipole density:

$$\boldsymbol{H}^{\mathrm{SC}}(\boldsymbol{r},p)=\int_V \frac{1}{4\pi R^3}(3\hat{\boldsymbol{R}}\hat{\boldsymbol{R}}-\bar{\bar{\boldsymbol{I}}})\cdot\boldsymbol{m}(\boldsymbol{r}'_v,p)dv'=\int_V \bar{\bar{\boldsymbol{G}}}(\boldsymbol{r},\boldsymbol{r}')\cdot\boldsymbol{m}(\boldsymbol{r}'_v,p)\,dv', \tag{3}$$

where $p=\{t,f\}$ is time or frequency, $\hat{\boldsymbol{R}}$ is the unit vector along $\mathbf{R}=\mathbf{r}-\mathbf{r}'_v$, $\mathbf{r}'_v$ is the position of the v'-th infinitesimal dipole in the volume V, $\mathbf{r}$ is the observation point, and $\bar{\bar{\mathbf{I}}}$ and $\bar{\bar{G}}(\mathbf{r},\mathbf{r}')$ are respectively the identity and Green dyads. The induced magnetic dipole moment $\mathbf{m}(\mathbf{r}_{v'},p)$ at point $\mathbf{r}_{v'}$ on the surface is related to the primary field through $\mathbf{m}(\mathbf{r}_{v'},p)=\bar{\bar{\mathbf{M}}}(\mathbf{r}_{v'},p)\cdot\mathbf{H}^{\mathrm{pr}}(\mathbf{r}_{v'})$, where $\bar{\bar{\mathbf{M}}}(\mathbf{r}_{v'},p)$ is the symmetric polarizability tensor. The secondary magnetic field at any point can be expanded in a set of orthonormal functions $\bar{\bar{\psi}}_i(\mathbf{r})$ as

$$\mathbf{H}(\mathbf{r})=\sum_{i=1}^{N_v}\bar{\bar{\psi}}_i(\mathbf{R}_i)\cdot\mathbf{b}_i\,, \tag{4}$$

where we have also introduced the expansion coefficients $\mathbf{b}_i$. The $\bar{\bar{\psi}}_i$ functions are linear combinations of dipole Green dyads guaranteed to be orthonormal by the Gram–Schmidt process. Based on this property, the amplitudes of the tensor elements of $\bar{\bar{\mathbf{M}}}_i(p)$ can be determined without having to solve a linear system of equations. The significant advantages of ONVMS are: (1) it takes into account the mutual couplings between different sections of the targets; (2) it avoids matrix singularity problems in multi-object cases, and (3) it is noise-tolerant and can thus be applied to UXO Live Site applications.

ONVMS is readily applicable for single- and multi-target scenarios based on the same conceptual and numerical formulation. Once the tensor elements and locations of the responding dipoles are determined, one can group them within the volume and for each group calculate the total polarizability, which at the end is joint-diagonalized. The ONVMS is applicable for cued as well as dynamic mode data sets. In order to illustrate the applicability of the ONVMS for target classification in dynamic mode, we show comparisons between effective polarizabilities for a library 37-mm projectile and a UXO Live Site anomaly.

Figure 4 shows a comparison between extracted effective magnetic polarizabilities for a 37-mm projectile contained in a DoD TOI target library (red line, which is same in six graphs) and six nearby dynamic data points in a dynamic lane (green, blue and black lines) for a subsurface anomaly. The results show that even though dynamic data is generally noisier and only recorded over a shorter time-period, the total ONVMS extracted from dynamic data points are comparable to the DoD TOI library target effective polarizabilities extracted from the cued test-stand data.

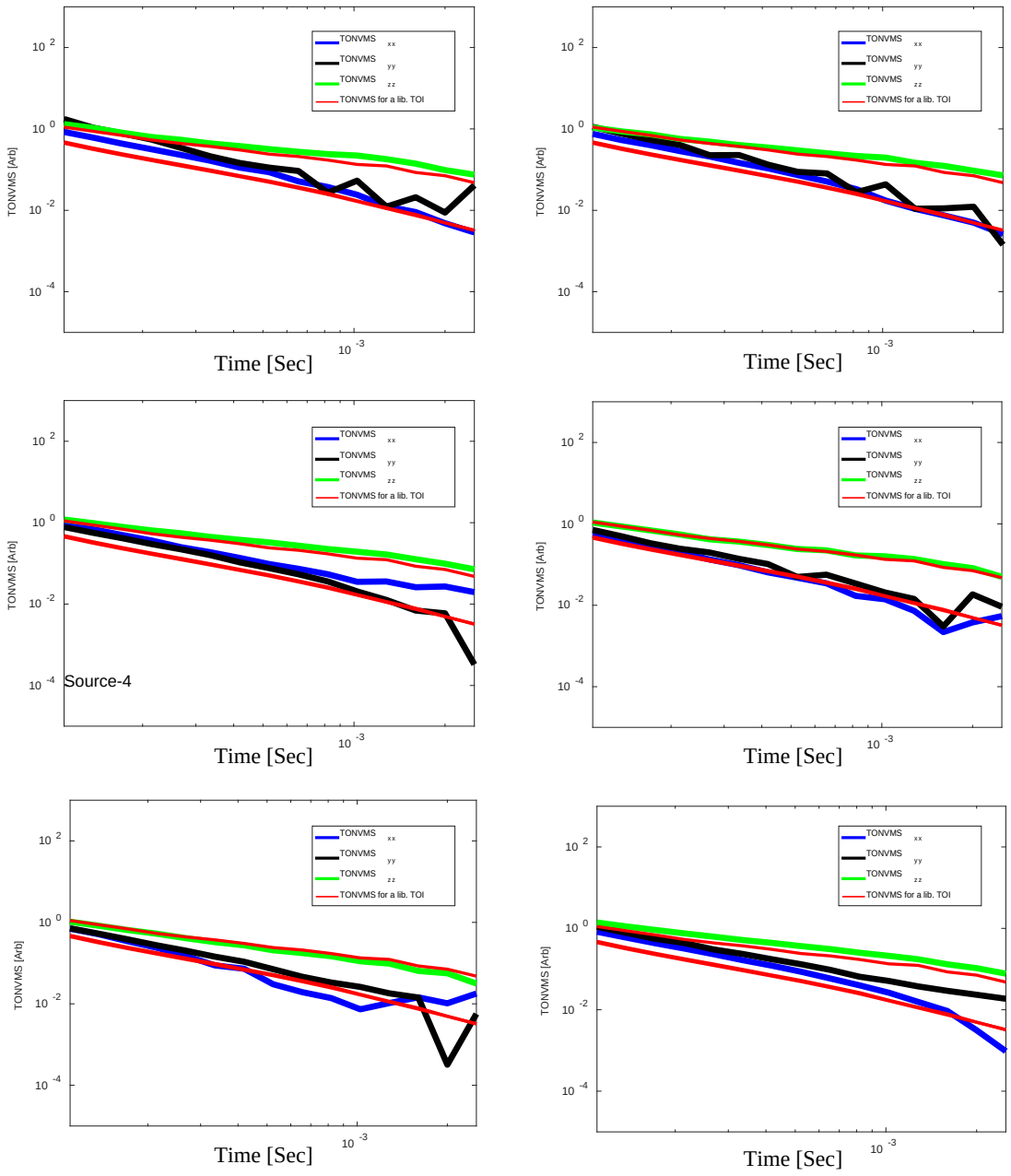

Figure 4. Time-decay Curves of Dipole Moment for a Target at a UXO Live Site

The red lines are for a 37-mm projectile from the DoD TOI library while green, black and blue lines are from dynamic data collected at six nearby points.

2.5 JOINT DIAGONALIZATION FOR DATA PREPROCESSING

Joint Diagonalization, also referred to as simultaneous matrix diagonalization, is a numerical approach for estimating the common eigenvalues and eigenvectors of a set of related square matrices. The approach has become an essential tool for independent component analysis and blind source separation (BSS) [22]–[25], common principal component analysis [26], various signal processing applications [27], and, more recently, kernel-based nonlinear BSS [27], [28].

We apply JD to the problem of detecting and discriminating subsurface targets by adapting the method to next-generation EMI sensor data. The main task of the JD technique is the following: given the measured MSR matrices $[\mathbf{H}_i^d]$ of size $M_T \times M_R$, where M_T and M_R (= M_T by assumption) respectively represent the numbers of Tx and Rx coils, JD finds an orthogonal matrix [**V**] such that the products $[\mathbf{V}]^T[\mathbf{H}_i^d][\mathbf{V}]$ are as diagonal as possible for all $i = 1,2,\ldots,N_t$, where N_t is the number of time gates and $[\mathbf{V}]^T$ denotes the transpose of [**V**]. (The fact that the resulting products are "as diagonal as possible" suggests that [**V**] results from a convergence process and that the matrix products are diagonal only within a given tolerance. In rigor we should call the method "Approximate JD," but we use the shorter name here to be consistent with the published literature.)

As an example, let us briefly describe how one can set up JD for the TEMTADS system. TEMTADS illuminates targets using $N = 25$ rectangular transmitter antennas positioned at $R_1, R_2, \ldots, R_N$. The primary magnetic field at point $\mathbf{r}_i$ due to the j-th transmitter is

$$\boldsymbol{B}_{ij}^{\mathrm{pr}}(\boldsymbol{r}_i,\boldsymbol{r}_j) = \frac{\mu_0}{4\pi}\oint_{\mathrm{Tx}_j}\frac{I_j d\ell\times(\boldsymbol{r}_i-\boldsymbol{r}_j)}{|\boldsymbol{r}_i-\boldsymbol{r}_j|^3} \equiv \frac{\mu_0 I_j}{4\pi}\oint_{\mathrm{Tx}_j}\frac{d\ell\times\boldsymbol{R}_{ij}}{|\boldsymbol{R}_{ij}|^3} \equiv \boldsymbol{G}_{ij}^{\mathrm{pr}} I_j, \tag{5}$$

where $\mathbf{G}_{ij}^{\mathrm{pr}}$ is the primary magnetic field at $\mathbf{r}_i$ due to a unit current flowing through the j-th transmitter; the closed line integral is over the transmitter coil. The primary magnetic field $\mathbf{B}_{ij}^{\mathrm{pr}}$ penetrates the object and induces a magnetic dipole moment $\mathbf{m}_{ij}$ that in turn establishes a secondary magnetic that induces electromotive forces (or voltages) in the receivers. From Faraday's Law, the voltage induced in a receiver is given by the negative rate of increase of magnetic flux through its surface,

$$V_{mi}^{j}(\boldsymbol{r}_m,\boldsymbol{r}_i) = -\frac{\partial}{\partial t}\int_{\mathrm{Rx}_m}\nabla\times\boldsymbol{A}(\boldsymbol{r}_m,\boldsymbol{r}_i)\cdot d\boldsymbol{s} = \frac{\partial \boldsymbol{m}_{ij}}{\partial t}\cdot\left[-\frac{\mu_o}{4\pi}\oint_{\mathrm{Rx}_m}\frac{d\ell\times\boldsymbol{R}_{mi}}{|\boldsymbol{R}_{mi}|^3}\right] = \boldsymbol{G}_{mi}^{\mathrm{sc}}\cdot\frac{\partial \boldsymbol{m}_{ij}}{\partial t}, \tag{6}$$

where $\mathbf{G}_{ij}^{\mathrm{sc}}$ is the secondary magnetic flux through Rx_m, the m-th receiver, due to a unit magnetic dipole, and the closed line integral is now over the receiver coil. The induced magnetic dipole moment $\boldsymbol{m}_{ij}$ at point $\boldsymbol{r}_i$ in space is related to the primary field via $\mathbf{m}_{ij} = [\mathbf{M}]_{ij}\cdot\mathbf{B}_{ij}^{pr}$, where $[\mathbf{M}]_{ij}$ is the symmetric polarizability tensor. Combining (5) and (6), we see that the total induced voltage for all transmitter/receiver orientations can be summarized as

$$[V] = [\mathbf{G}^{\mathrm{sc}}]\,[M]\,[\mathbf{G}^{\mathrm{pr}}]^T I = [\mathbf{A}][I]. \tag{7}$$

The matrix $[\mathbf{A}]$ is called the "multi static response" (MSR) or information matrix. Let us analyze the MSR matrix and determine the physical meaning of its diagonal elements.

First, let us define two new matrices, $G_r = [\mathbf{G}^{\mathrm{sc}}][\mathbf{G}^{\mathrm{sc}}]^T$ and $G_t = [\mathbf{G}^{\mathrm{pr}}]^T[\mathbf{G}^{\mathrm{pr}}]$. If the matrix $[G^{\mathrm{sc}}]$ has rank $k_r \le N$ and $[\mathbf{G}^{\mathrm{pr}}]$ has rank $k_t \le N$, then G_r and G_t have rank k_r and k_t respectively. When $k_r = k_t = N$, G_r and G_t are positive definite and invertible. Using the polar decomposition, we can further write $[\mathbf{G}^{\mathrm{sc}}] = U_r(G_r)^{1/2}$ and $[\mathbf{G}^{\mathrm{pr}}] = U_t(G_t)^{1/2}$, where the matrices $U_r \in \Sigma^{N_r\times N}$ and $U_t \in \Sigma^{N_t\times N}$ have orthonormal columns (*i.e.*, $U_r^T U_r = U_t^T U_t = I_N$, where I_N is the $N \times N$ identity matrix).

The MSR matrix can thus be expressed as

$$[\boldsymbol{A}] = U_r(G_r)^{1/2}\,[M]\,(G_r{}^{1/2})^T U_t^T = U_r \Xi U_t^T, \tag{8}$$

and $\Xi = (G_r)^{1/2}[M](G_r{}^{1/2})^T$ can be further decomposed via the SVD to give

$$[\boldsymbol{A}] = U_r U_\Xi\; D_\Xi\,(U_t V_\Xi)^T, \tag{9}$$

where D_Ξ is a diagonal matrix whose elements are the eigenvalues of [**A**], and $U_r U_\Xi$and $U_t V_\Xi$ are respectively its left and right eigenvectors. Thus, the eigenvalues of the MSR matrix correspond to the diagonal elements of the normalized induced magnetic polarization tensor $(\mathrm{G}_r)^{1/2}\,[M]\,(\mathrm{G}_r^{1/2})^T$. In the EMI regime the matrices $(\mathrm{G}_r)^{1/2}$ and $(\mathrm{G}_r^{1/2})^T$ are independent of time, and therefore the time dependence is carried directly by the polarizability tensors of the targets, which can then be used for classification. The joint diagonalization (JD) technique finds an orthogonal (*i.e.*, real and unitary) matrix $\bar{\bar{V}} = U_r U_\Xi$ that minimizes the $\{D_\Xi(t_q)\}_{q=1}^{N_q}$ matrices' off-diagonal elements [29]. The diagonal matrices $\{D_\Xi(t_q)\}_{q=1}^{N_q}$ contain information about the targets that contribute to the signal. Our studies have shown that each set of three above-threshold diagonal elements of the measured multi-static response (MSR) data matrix describe one target. We have also demonstrated that the JD technique is a robust method for extracting target information in cases with a low signal-to-noise-ratio [21]. In addition, to take advantage of the rich datasets from these sensors, we recently developed and successfully demonstrated a discrimination procedure based on the JD [30].

EMClass uses the JD technique to assess data quality, estimate number of potential sources/targets, classify targets as TOI and non-TOI, as well as for detecting targets from the dynamic data set. Namely, for the latter approach, the JD technique is applied to each dynamic data point and eigenvalues-versus-time functions are extracted. The extracted eigenvalues are fitted to the power decay model ($d_m(t) = kt^{-\beta}e^{-\gamma t}$) and the associated model parameters represented by k, β and γ are extracted. In addition to these parameters, the average fitting error σ^2, a biased sample variance, is introduced as the measurement of fluctuation in one eigenvalue curve, defined as follows,

$$\sigma^2 = \frac{1}{N_t}\sum_{q=1}^{N_t}\left(log\left(d(t_q)\right) - log\left(d_m(t_q)\right)\right)^2 \tag{10}$$

where N_t is number of time channels. The log(k), β and γ parameters are extracted using a standard least square fit. The results depicted in Figure 5 show that there is a good separation between the eigenvalues associated with a target signal (blue dots with small σ^2) and eigenvalues associated with noise in the log(k), β and γ feature space. The log(k), β and γ parameters of the signal eigenvalues, which have low σ^2 and high log(K), are separated for the noise eigenvalues. Based on these distribution, a user separate signal and noise eigenvalues for the entire dynamic data set, by using the extracted high log(K), and low σ^2 as signal eigenvalues and high σ^2 as the noise eigenvalues.

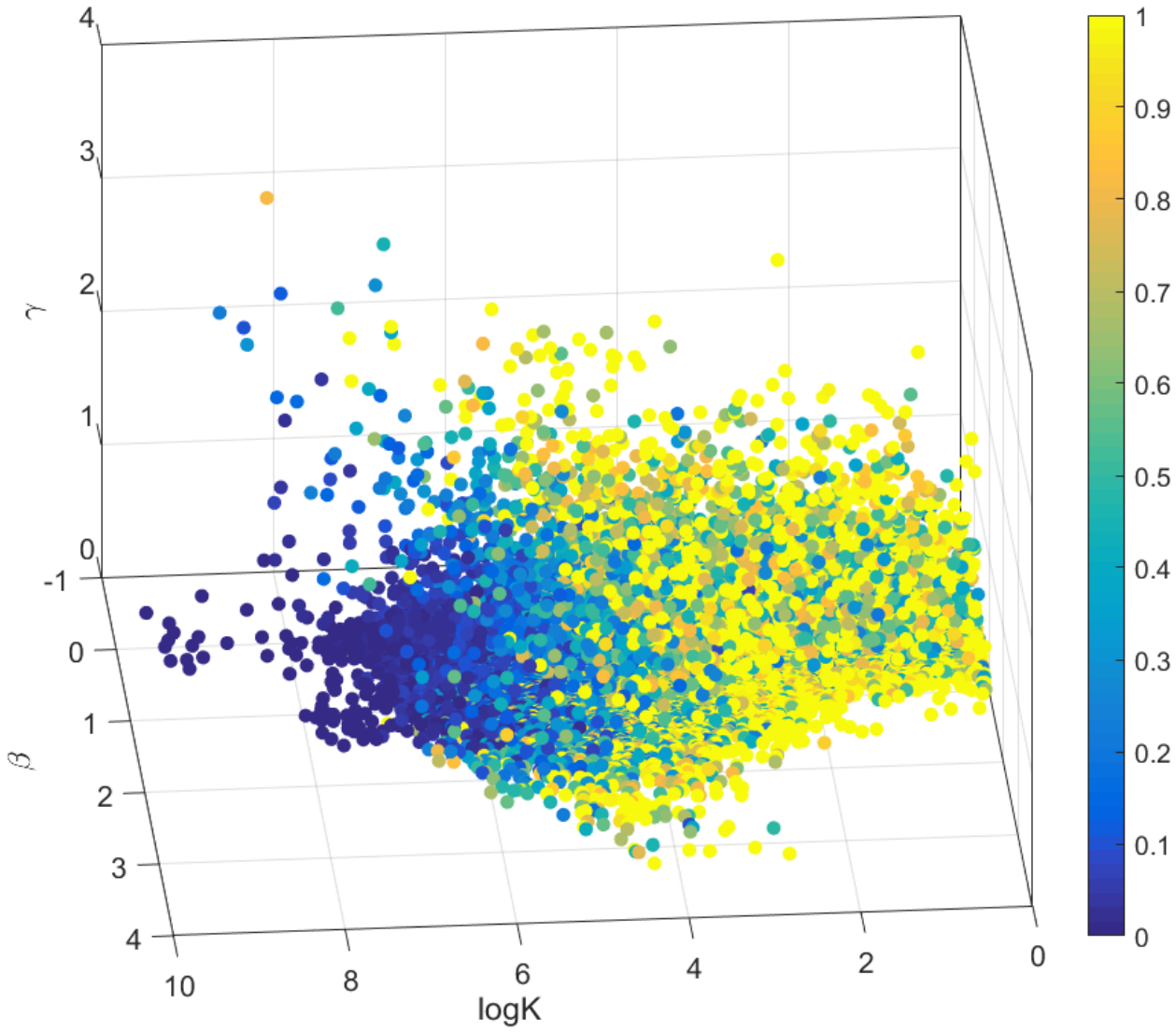

Figure 5. Estimated Log(K), β and γ *parameters* for Eigenvalues from all the Data Points in a Lane

σ^2 is used as the color scale.

2.6 EMI DATA INVERSION

Determining the orientation and location of a buried object is a non-linear problem. The data inversion is carried out by: (1) choosing a forward model (*e.g.*, dipole, NSMS, ONVMS, spheroidal) that mixes free parameters with *a priori* information (such as the global location of the sensor and the spatial behavior of its primary field) to make quantitative predictions for measurable quantities, and (2) defining an objective function that measures the misfit between those predictions and measured data.

The method of least squares is routinely used to recover the parameter vector **v**, which in our case contains intrinsic information about the object and also its location and orientation. Specifically, if $\mathbf{d}^{\text{obs}}$ is the vector of the measured secondary field, and $\mathbf{F}(\mathbf{v})$ the forward problem solution, then the least squares approach uses as criterion

$$\underset{\mathbf{v}}{\text{minimize}} \quad \phi(\mathbf{v}) = \frac{1}{2}\left\|\mathbf{d}^{\text{obs}} - \mathbf{F}(\mathbf{v})\right\|^2 + \frac{\alpha}{2}\left\|\mathbf{v} - \mathbf{v}_{\text{ref}}\right\|^2, \tag{11}$$

where the regularization parameter α is used to take into account uncertainties originating from the sensor, measurement error, or background noise. The second term on the right-hand side of (11) determines how close we want the final solution to be to a reference model $\mathbf{v}_{\text{ref}}$. Through the choice of $\mathbf{v}_{\text{ref}}$ it is possible to introduce prior information into the inversion. Constraints to the model can also be included in the inversion procedure, which is usually carried out by iteration. Solving for the perturbation at each iteration is equivalent to solving the least-squares problem, which can be done by using a Gauss-Newton or Marquardt-Levenberg algorithm. The value of α, which dictates the relative importance of the data misfit and penalty terms within the minimization problem, must be determined at every-iteration. Two approaches are primarily used in the literature to derive regularization parameters in the framework of ill-posed problems: generalized cross-validation and L-curve analysis. Usually both approaches often suffer from a surfeit of local minima that sometimes result in incorrect estimates for location and orientation. To avoid this problem, we recently developed a different class of global optimization search algorithms. One such technique is the DE method [31], [32], [13]-[16], a global-search algorithm developed to bypass the local-minima problem that often leads standard gradient-search approaches to make incorrect predictions for location and orientation. The DE methodology is a heuristic, parallel, direct-search method for minimizing nonlinear functions of continuous variables. Similar in concept to the genetic algorithms that have been used with much success on problems with discrete variables, DE is straightforward to implement and has good convergence properties.

We have combined the DE algorithm with the above-discussed ONVMS technique to routinely invert advanced geophysical EMI sensors data. The scattered field from any object whose location and orientation are known depends linearly on the magnitudes of its responding sources, and the procedure starts by assigning initial values of the attitude parameters and using these estimates, along with the measured data, to determine the source amplitudes by using orthogonality of $\bar{\bar{\psi}}_i(\mathbf{r})$ basis function and integrating a linear system of equations. The amplitudes thus found are fed into a nonlinear objective function that quantifies the mismatch between measured data and model predictions and whose minimum, determined via DE, serves to refine the estimates for location and orientation. The procedure continues to alternate between these linear and nonlinear stages until it reaches convergence (or a preset maximum number of iterations). The responding amplitudes are then stored and used in a later classification step, while the location and orientation parameters are used; a) to assess data inversion performance, and b) to assist with the target excavation process [21].

2.7 EXTRACTING CLASSIFICATION PARAMETERS

To classify targets in this demonstration we used ONVMS combined with DE optimization and joint diagonalization to invert for the locations of the targets of TOI. The model provides at least three independent total ONVMS parameters along the principal axes for each potential target that can be used for classification. During the inversion stage the total time-dependent ONVMS, which depends on the size, geometry, and material composition of the object in question, is determined for each potential target. Early time gates measure the high-frequency response of the TOI until the shutdown of the exciting field; the induced eddy currents in this range are superficial, and a large total ONVMS amplitude at early times correlates with large objects and large surface areas. At later times, when the eddy currents have diffused completely into the object and low-frequency harmonics dominate, the EMI response relates to the metal content (i.e., the volume) of the target. Thus, a smaller but compact object has a relatively weak early response that dies down slowly, while a large but thin (or hollow) object has a strong initial response that decays quickly. These parameters are used to form feature vectors for classification. The success of classification depends on the selection of features, the separation of different classes in feature space, and the ability of the sensor data to constrain the estimated features. In some cases, due to poor signal-to-noise ratio, the feature vectors from UXO targets can be corrupted or could be similar with clutter anomalies. In such cases, we must recognize that discrimination may be limited, or a classification decision will require an override using an expert's judgment. When discrimination is possible we use both template-matching and statistical procedures—such as Gaussian Mixture models [35], support vector machines (SVM) [36].

2.8 CLASSIFICATION USING CLUSTERING

Success in classification depends on the selection of input features, the separation of the different classes in feature space, and the ability of the sensor data to constrain the estimated features. In some extreme cases, a poor signal-to-noise ratio can result in feature vectors from different-sized targets being similar, forcing us to recognize that discrimination via statistical methods may be limited. For that reason and given moreover that class labels and features are likely to be dependent on the type of data and may be quite variable, we always use and compare several different clustering/classification approaches to each other and library matching techniques.

The distribution of power-law / exponential-decay parameters extracted from the total ONVMS profiles is key to performing classification. This is because TOIs with similar total ONVMS have similar patterns under various conditions. By comparing the total ONVMS time-decay parameters of unknown targets to those of known objects, one can predict the class/cluster to which the unknown targets belong. Routinely, we use Gaussian Mixture modelling [35] and Support Vector Machines [36] for targets classification.

The time decay curve of the inverted total ONVMS is fitted to an exponential decay function ($S(t) = kt^{-\beta}e^{-\gamma t}$), known as Pasion-Oldenburg model, and classification feature parameters such as k (or $\log_{10}(k)$), β, γ and $S(t_1)/S$ (t_q) , q=1,2, 3,…$N_{time,}$ are extracted.

The extracted classification feature parameters are clustered into classes. The algorithm assumes that: a) there are K clusters, and each cluster is mathematically given by a parametric continuous or discrete distribution function, for example a Gaussian distribution; and b) the total ONVMS time decay parameters data are arranged in an $N_p \times M$ matrix denoted by $\mathbf{Y} = [\mathbf{Y}_1, \mathbf{Y}_2, \ldots, \mathbf{Y}_M]$, where $\mathbf{Y}_i$, $i = 1, 2, \ldots, M$, is a vector, M is the number of anomalies, and N_p is the length of $\mathbf{Y}_i$, vector i.e., the number of parameters, (*e.g.*, k (or $\log_{10}(k)$), β, γ and $S(t_1)/S(t_q)$ etc.). Each $\mathbf{Y}_i$ is considered to follow an N_p-dimensional mixture of normal distributions and estimated using the Gaussian mixture model. Mathematically, the mixture Gaussian distribution for K clusters is expressed as:

$$F(\mathbf{Y}_i) = \sum_{k=1}^{K} w_k \, f_i(\mathbf{Y}_i \mid \boldsymbol{\mu}_k, \boldsymbol{\sigma}_k), \tag{12}$$

where w_k, is the mixing weight of cluster k, $\sum_{k=1}^{K} w_k = 1$, and:

$$f_i(\mathbf{Y}_i \mid \boldsymbol{\mu}_k, \boldsymbol{\sigma}_k) = \frac{1}{\sqrt{\boldsymbol{\sigma}_k (2\pi)^m}} \exp\left(-\frac{1}{2}\left(\mathbf{Y}_i - \boldsymbol{\mu}_k\right)^T \boldsymbol{\sigma}_k^{-1} \left(\mathbf{Y}_i - \boldsymbol{\mu}_k\right)\right) \tag{13}$$

$f_i(\boldsymbol{Y}_i|\mu_k, \sigma_k)$ is the probability density of the k-th normal distribution with a mean vector $\boldsymbol{\mu}_k$ (an $N_p \times 1$ vector) and a variance-covariance matrix $\boldsymbol{\sigma}_k$ (an $M \times M$ matrix). The mixing weight w_k is defined as the proportion of anomalies that belong to the k-th cluster. The parameters $\boldsymbol{\mu}_k$, $\boldsymbol{\sigma}_k$ and w_k are estimated from blind test data using the maximum likelihood (ML) criterion using the Expectation Maximization algorithm [37]. Once all $\boldsymbol{\mu}_k$, $\boldsymbol{\sigma}_k$ and w_k parameters are determined then the $f_i(\boldsymbol{Y}_i|\mu_k, \sigma_k)$ probability density function is used to rank anomalies [35].

Using the combined algorithms of ONVMS-DE, *EMClass* inverts EMI data from subsurface targets to produce intrinsic and extrinsic parameters. Once these parameters are extracted, they are clustered using the described classification algorithm. To illustrate applicability of the combined technique for actual UXO Live Site dynamic data processing and targets selection, Figure 6 shows inverted locations for a dynamic data set (blue dots) using the combined ONVMS-DE approach. These estimated locations are clustered using the clustering algorithm, and the center of each cluster is calculated (shown as red dots in Figure 6). Each cluster contains more than four inverted estimated locations. This approach separates anomalies and provides sub-surface target locations more accurately than the standard amplitude response metric approach, see Figure 3.

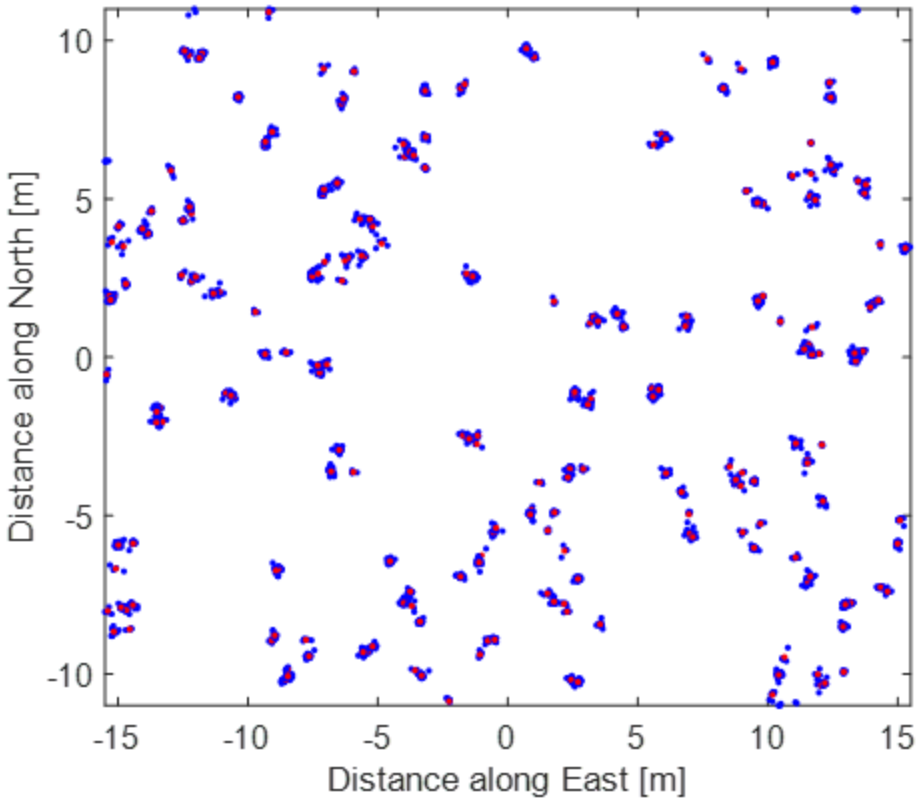

Figure 6. Blue Dots: Extracted Locations from a Dynamic Data Set using the Combined ONVMS-DE Algorithm; Red Dots: Centers of Clusters

2.9 CLASSIFICATION USING TEMPLATE MATCHING

The template matching technique is a classification approach that classifies unknown targets within a TOI by comparing the extracted target features—in our case the total ONVMS—to a set of features stored in a target library. There are two ways to execute the template-matching technique; (1) using an algorithm that estimates a least-square error between the unknown and library targets ONVMS, and (2) by visual inspection. We used both template matching and feature clustering approaches when classifying the targets. Namely, we used the error function (also called the Gaussian error function) to estimate the probably of the extracted effective polarizabilities falling in a defined range. The error function is defined as

$$erf(x) = \frac{1}{\sqrt{\pi}} \int_0^x e^{-\varepsilon^2} dt, \tag{14}$$

where error ε is the weighted misfit between the extracted $\boldsymbol{P(t_k)} = \boldsymbol{log_{10}(M(t_k))}$, $\mathbf{k=1,2,\ldots,N_t}$ and a given library target's mean $\widehat{\boldsymbol{P}} = \boldsymbol{log_{10}}(\widehat{\boldsymbol{M}}\ \ (\boldsymbol{t_k}))$ effective magnetic polarizabilities. The misfit is estimated as

$$\varepsilon = -\frac{1}{2}\big(\boldsymbol{P}(t_k) - \widehat{\boldsymbol{P}}(t_k)\big)^T \sigma_{t_k}^{-1}\big(\boldsymbol{P}(t_k) - \widehat{\boldsymbol{P}}(t_k)\big).; \tag{15}$$

Here $\boldsymbol{\sigma}_{t_k}^{-1}$ (an $N_t \times N_t$ matrix) is the variance-covariance matrix and N_t is number of time gates. At each time gate the both $\widehat{\boldsymbol{P}}(t_k)$ mean and $\boldsymbol{\sigma}_{t_k}^{-1}$ the covariance matrix are estimated using the exiting library and/or site-specific training data sets. For an example, Figure 7 shows extracted polarizabilities for the small ISO TOI for Camp Beale, CA and Fort Sill, OK sites. The comparisons show that the ISOs effective polarizabilities at Fort Sill, OK are more clustered then at Camp Beale, CA. under this circumstance. As a result, a user should update and define a site-specific $\widehat{\boldsymbol{P}}(t_k)$ mean and $\boldsymbol{\sigma}_{t_k}^{-1}$ covariance matrix values.

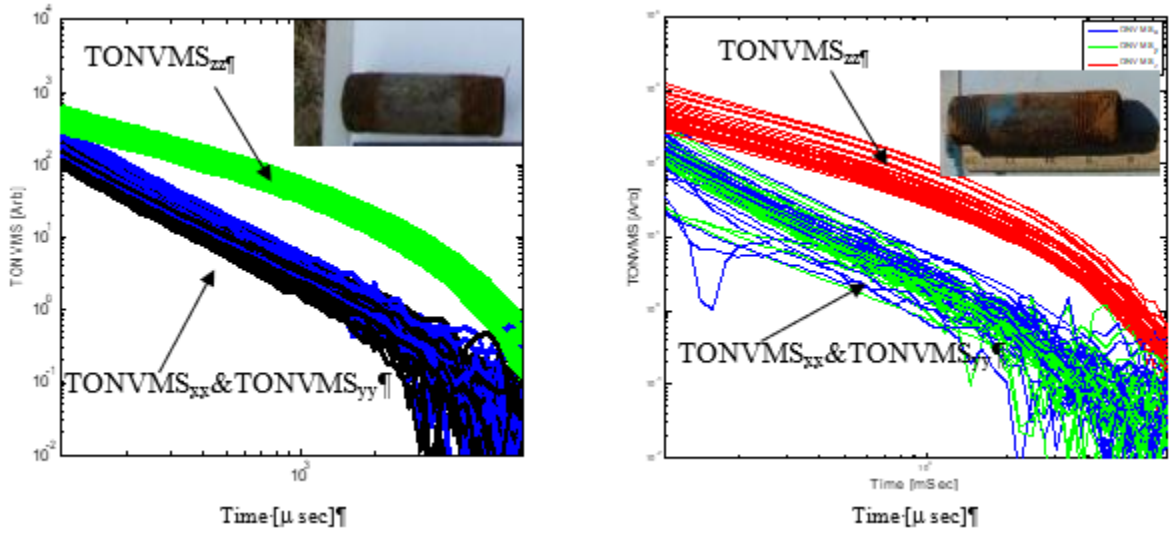

Figure 7. Inverted Total ONVMS Time-decay Profiles for Fort Sill, OK (Left) and Camp Beale, CA (Right) Seeded ISO Targets

2.10 ADVANTAGES AND LIMITATIONS OF THE TECHNOLOGY

Our advanced EMI models are fast, accurate and clutter-tolerant. They provide robust EMI data pre-processing, data inversion, target classification feature parameter estimation, and they provide effective capability to separate UXO from harmless subsurface metallic targets. The methods were adapted to support all advanced multi-axis/transmitter/receiver sensors like TEMTADS [5], the MM [11], the MPV, the 2 × 2 - 3D TEMTADS [19], [20] and the OPTEMA. Over the last decades, our group has implemented a training data selection approach for maximizing classification effectiveness and for selecting the optimal stop-dig point. The main key of our success is the effective use of training data for anomalies ranked within the uncertain category. Using these targets, that are difficult to rank as TOI or non-TOI, substantially helped to increase classification confidence and minimize the number of false positives. To illustrate superior classification performance of our approach compared to other standard techniques, Figure 8 shows comparisons between our results and the results of two other teams for the same Fort Bliss, TX 2x2 TT dataset. The comparison between the ROC curves clearly indicates that our team obtained significantly better classification performance compared to the other two teams. Specifically, we were able to identify about 92% of the clutter items as “No Dig,” whereas Team 1 and Team 2 identified only 13% and 19% of clutter as “No Dig,” respectively.

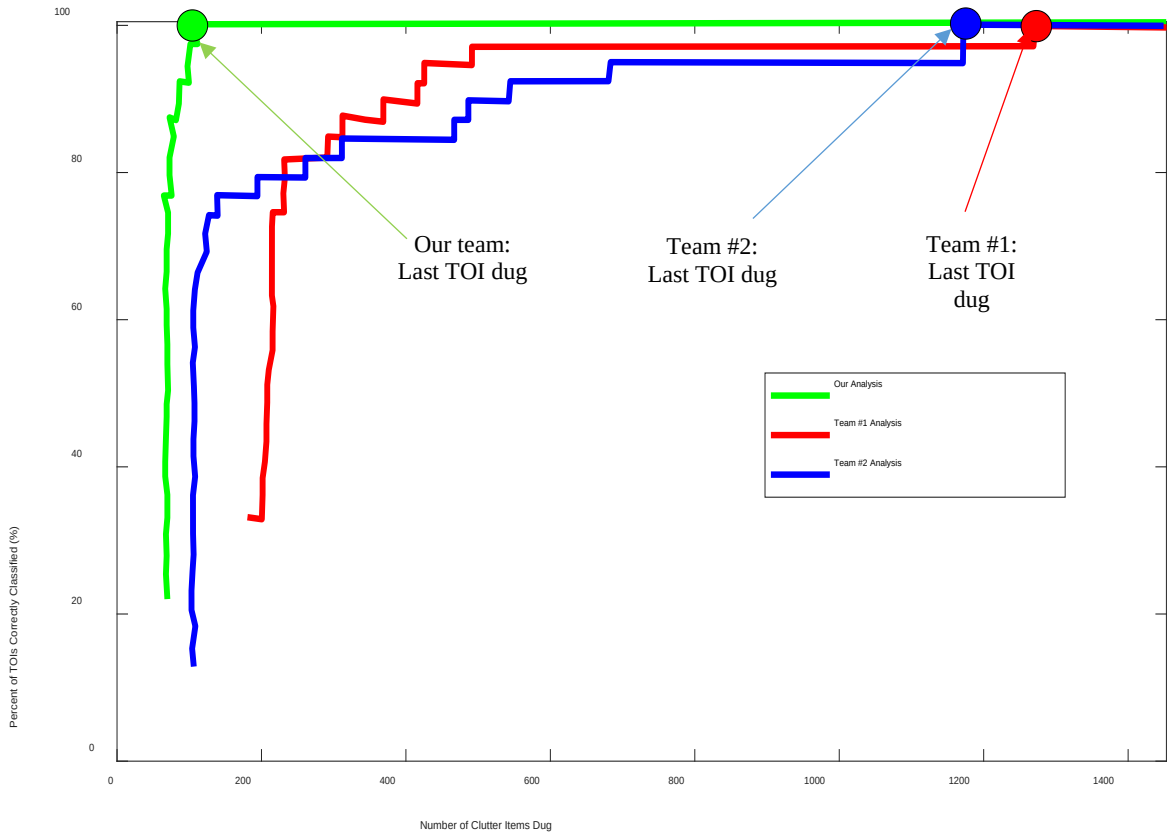

Figure 8. Fort Bliss, TX, 2x2 TT Targets Classification Results in the Form of ROC Curves Obtained by Our Team and Two Other Teams

The methods are applicable for both single- and multiple-target scenarios, and for deep and/or small targets. If sensors provide adequate spatial and temporal diversity data, then the models can classify targets in high density areas. However, the methods can provide limited or no target classification capabilities if the targets responses are not detectable or are masked from other target signals.

2.11 FORT ORD, CA, DATA INVERSION AND CLASSIFICATION SCHEME

The detailed modeling approach of MM Tx and Rx signals using the ONVMS-DE algorithm is described in [19]. The following is a summary of the main steps of our Fort Ord, CA MM data inversion and classification procedure.

Step 1. Data pre-processing: All MM data were pre-processed using data pre-processing and background correction approach described in Section 2.2.

Step 2. Create a MM Multi Static Response (MSR) data matrix: Using procedures described in [19], we constructed the measurement matrix $\bar{\bar{H}}(t_q)$ for each anomaly and used it to create the MM MSR data matrix.

Step 3. Eigenvalue analysis: The JD technique is then applied to the MM MSR data matrix derived in Step 2, which extracts the time-dependent eigenvalues for each anomaly. The eigenvalues for some seeded and native targets are depicted in Figure 9 -Figure 14. The MSR data matrix eigenvalues are intrinsic properties of the targets; each compact 3D metallic target has at least three eigenvalues above the threshold (noise level: low magnitude eigenvalues). For example, Figure 9 shows the eigenvalues extracted for a seeded 155-mm projectile, and Figure 10-Figure 12 show eigenvalues versus time for a 75 mm, small and medium ISOs, 37 mm, 40-mm and 60-mm projectiles. Figure 13 and Figure 14 show eigenvalues versus time for two (multi) targets. The results illustrate that each target has distinguishable eigenvalues and as the number of eigenvalues above the noise threshold increases, and number of responding sources (i.e., target size or number of targets) increases. For an example, the results show that an isolated 155 mm (Figure 9) and 75-mm (Figure 10: top) projectiles have six distinguished eigenvalues above noise level, i.e., two responding sources are required to represent each target's EMI responses accurately. Otherwise, an isolated small and medium ISOs, 35-mm, 37-mm and 40-mm projectiles have only three distinguished eigenvalues above noise levels see Figure 10- Figure 13 (bottom). Thus, one responding source is required to model these targets individually. As the numbers of target increases, the contributions from additional targets appear as additive signals/eigenvalues; see Figure 12, Figure 13 and Figure 14. These eigenvalues are used to discriminate TOIs from clutter by utilizing the MSR eigenvalues time decay shapes. In this project, first we examined the eigenvalues versus time for each case, and then used them to estimate the number of sources and SNR.

Step 4. Extract the total ONVMS for each anomaly: The extrinsic and intrinsic parameters of the targets, including the total ONVMS were derived for all anomalies. Once we completed the JD analysis and estimated SNR for each anomaly, we proceeded to invert all cued MM datasets. The combined ONVMS-DE algorithm, with a maximum of 100 DE iterations, was used to extract the intrinsic and extrinsic parameters of the targets. The algorithm yields the total ONVMS (effective polarizabilities) of the targets, which then are used for classification. By default, all data are inverted under the assumption of containing one, two, and three sources. However, in a case where more than three sources are suspected, the datasets are inverted as four, five and even six sources using the combined DE-ONVMS algorithm. Such multi-target inversion is crucial in the field for cases in which a signal from a UXO is mixed with EMI signals from nearby clutter; see Figure 13 and Figure 14. Note that the two-source inversion code yields three sets of locations and total ONVMS estimates: one for Source 1, one for Source 2, and a combined estimate with Sources 1 and 2 represented by a single object. In the case of 3-target inversion, seven output results are expected: only Source 1, only Source 2, only Source 3, Sources 1 and 2 as a single object, Targets 2 and 3 as a single object, Targets 1 and 3 as a single object, and all three targets acting as a single object. In the general case of n targets, one expects $n(n-1)+1$ sets of ONVMS curves.

The extracted intrinsic (total ONVMS) and extrinsic (locations) inversion results using one, two and three sources are used to cross-validate the inversion and classification results. Figure 15a) shows a comparison between the inverted total ONVMS (effective polarizabilities, blue, black and green lines) using one source model for Fort Ord anomaly #40070 and a library 40 mm (red lines). The one-source inversion yields non-symmetric fast decaying effective polarizabilities illustrating that the source is related to a clutter and not to the TOI; see Figure 15b. The same data were inverted using a two-source inversion.

Figure 16 shows the comparisons between total ONVMS for anomaly #40070 and the 40-mm projectile for the library. The inverted total ONVMS for source 2 out of 2 (Figure 16a) matches very closely to the total ONVMS of the 40 mm-s library signatures. Where else the total ONVMS for the source 1 out 2 (Figure 15b) are non-symmetric and decay rapidly, indicating the source is related to clutter. It can be seen in Figure 12 that the effective polarizabilities for source #1 (left) are smaller (at later time channels) than source #2 (center), and the primary total ONVMS (green line) for the combined source 1 + source 2 matches the total ONVMS of the 40 mm signature with only different values at early time channels.

The extracted total ONVMS from the same data using three-source inversions are depicted in Figure 16. These results show that the total ONVMS for sources 2 of 3 (top, left) coincides with the total ONVMS of the library signature for the 40 mm, and the effective polarizability of the source #1 (Figure 16a) matches the total ONVMS of source #1 in the two-source inversion presented in Figure 15a. Thus, the extracted total ONVMS for Fort Ord anomaly #40070 using one, two and three source inversion illustrate, that: 1) as expected, one-source inversion is not enough to extract high quality total ONVMS from multiple targets with overlapping signals; 2) two-source inversion accurately separates overlapping signals and extract high-quality effective polarizabilities for the unambiguous classification of the target; and 3) three-source inversions further validate two-source inversion results, and in addition assure that there were only two targets in the field of view of the EMI sensor.

As stated above, the combined ONVMS-DE algorithm estimates source locations with respect to the sensor local coordinate system. The extracted locations are used to further increase the confidence of the data inversion and classification results. Table 1 summarizes the inverted locations for source #1, #2 and # 3 using the one, two and three-source inversion approach for the #40070. All estimated locations are estimated from the center of MM system. One-source inversion overestimates source #1 depth, but places is close to source #1 defined in both the two-source and three-source inversions. The estimated locations for sources #1/2 and #1/3 using two- and three-source inversions are identical. This further validates that there were only two potential targets.

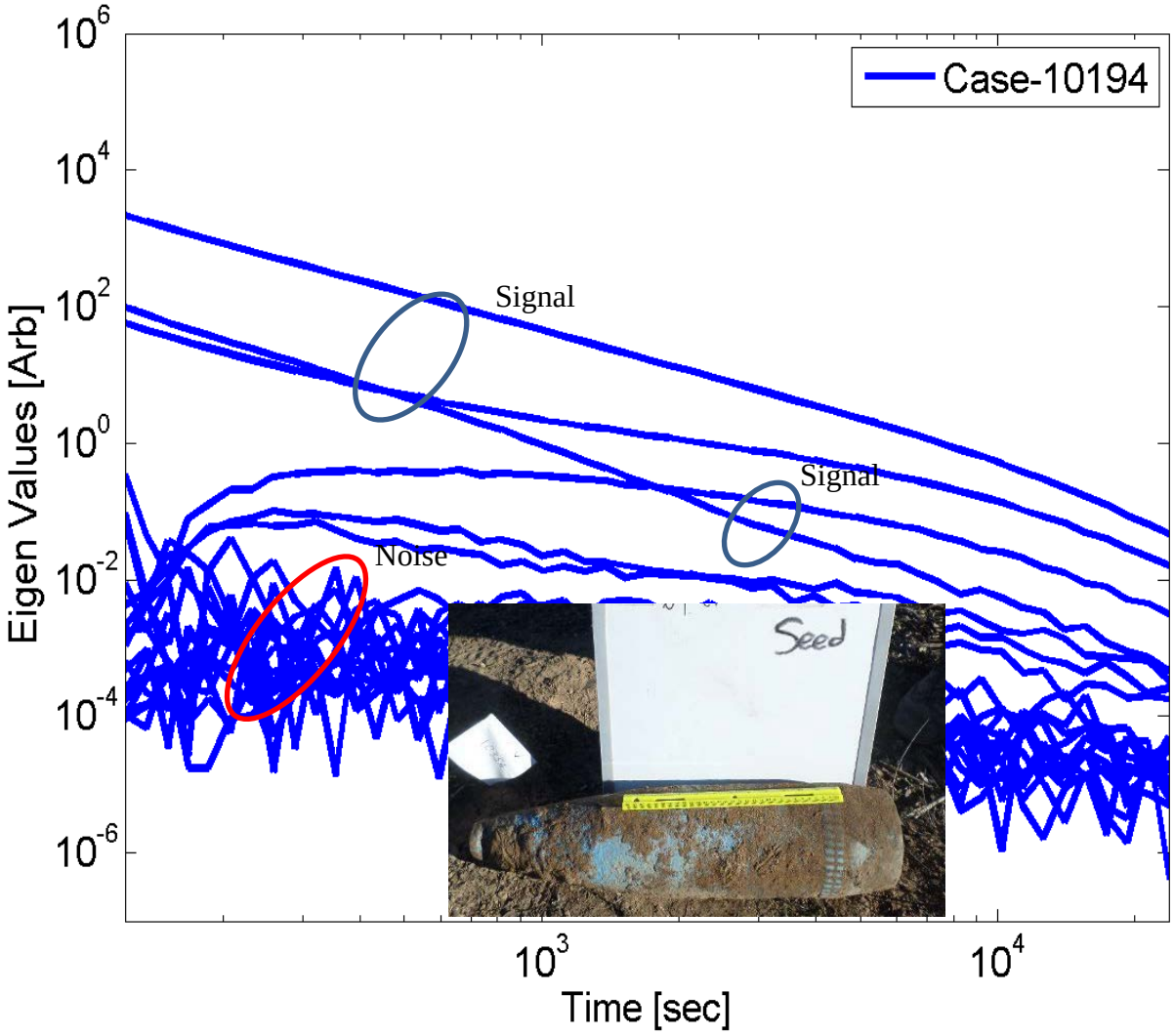

Figure 9. Multi-static Response Matrix Eigenvalues Versus Time for a Seeded 155-mm Projectile

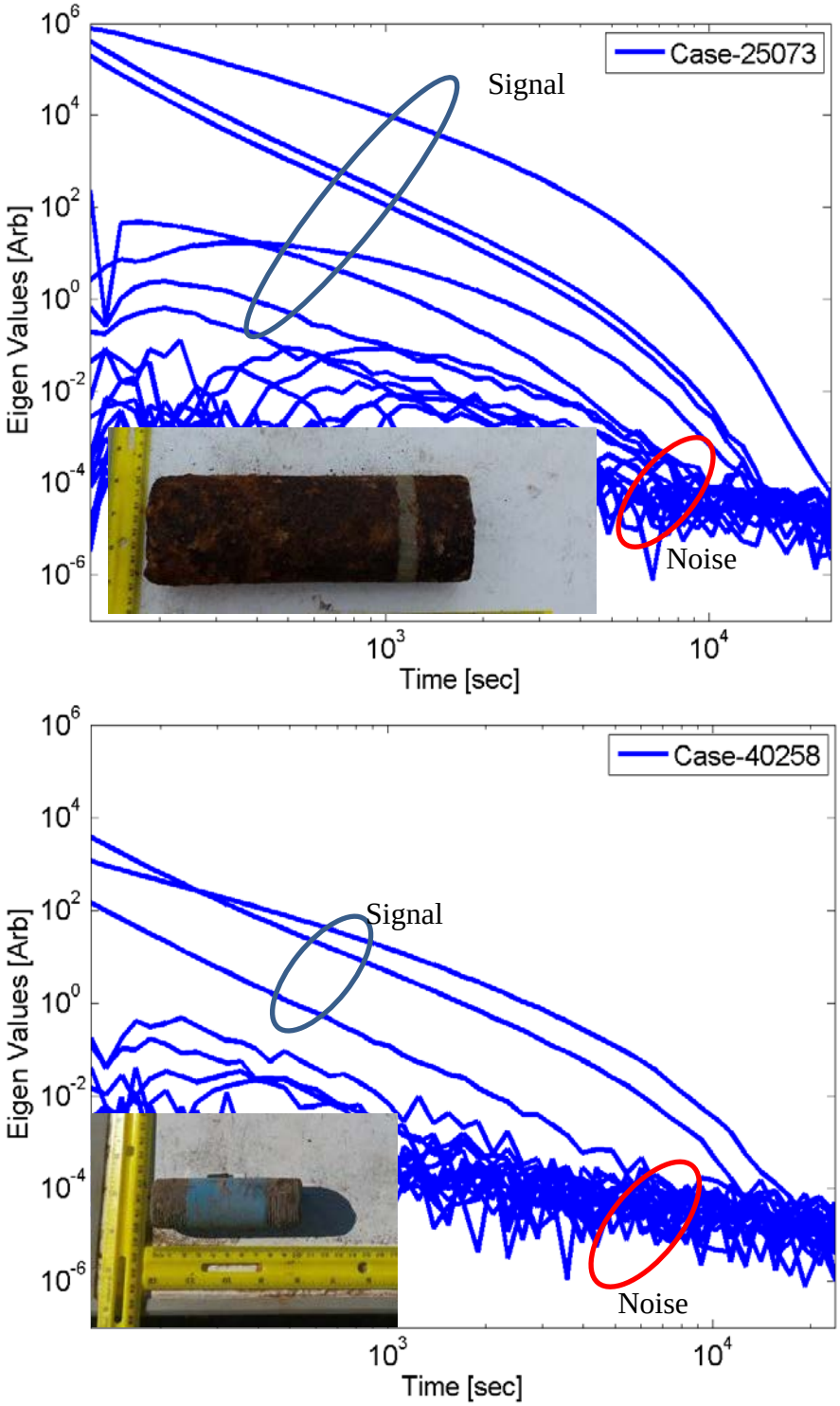

Figure 10. MM Multi-static Response Matrix Eigenvalues Versus Time for a Seeded 75-mm Projectile (Top Figure) and Small ISO (Bottom Figure), Respectively

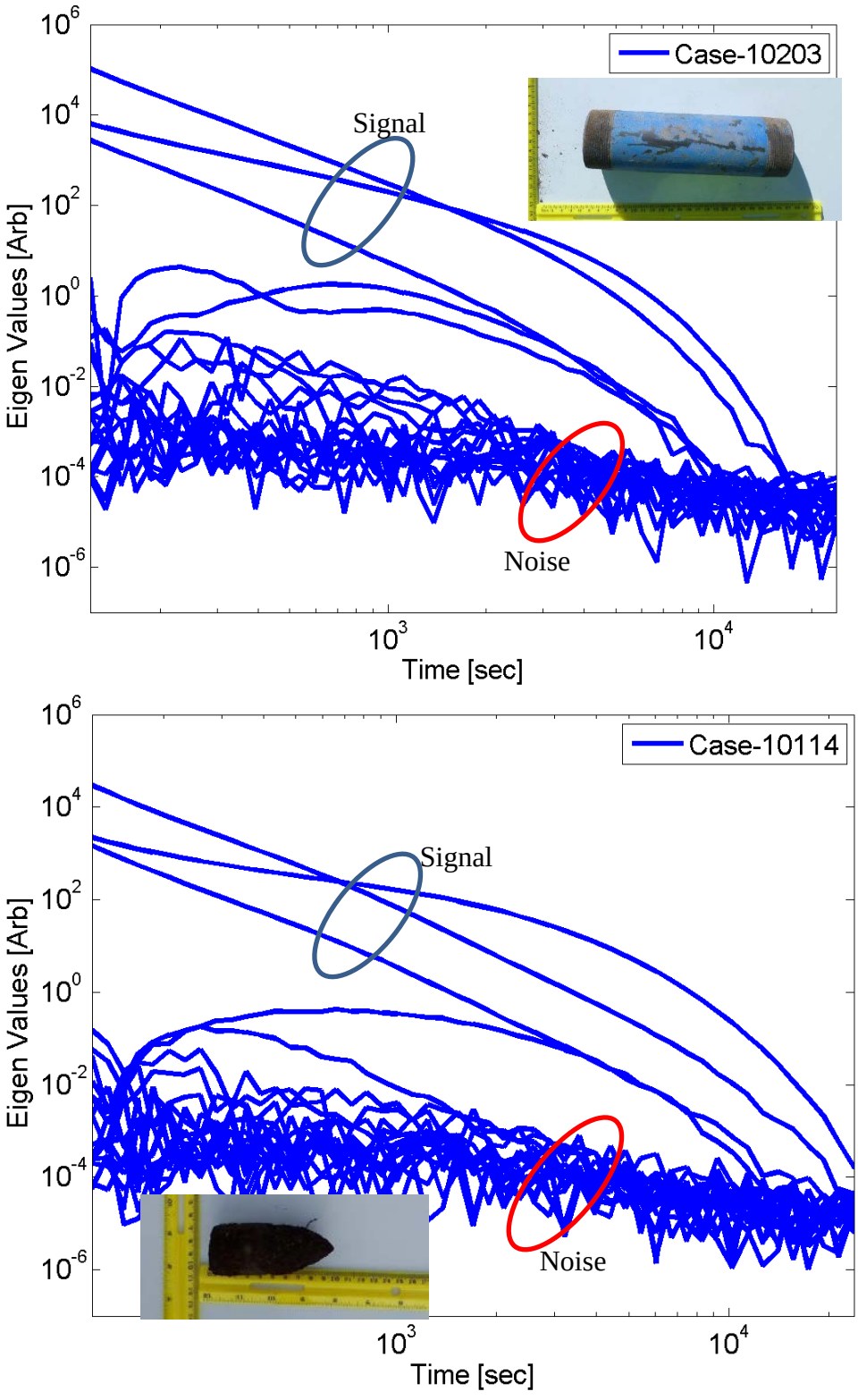

Figure 11. Multi-static Response Matrix Eigenvalues Versus Time for a Seeded Medium ISO (Top Figure) and 37-mm Projectile (Bottom Figure), Respectively

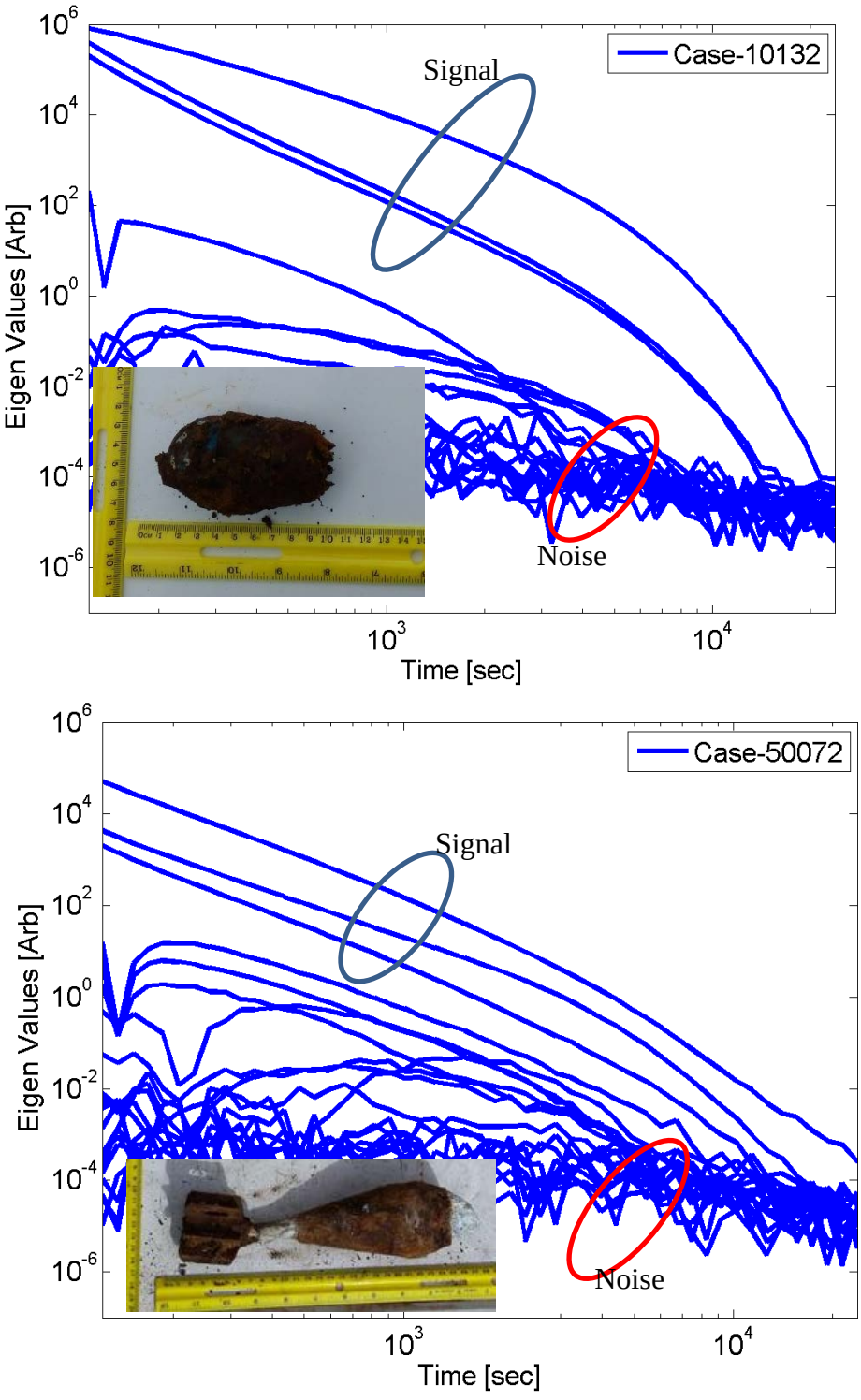

Figure 12. MM Multi-static Response Matrix Eigenvalues Versus Time for a Native 40 mm (Top Figure) and 60 mm (Bottom Figure) Projectiles, Respectively

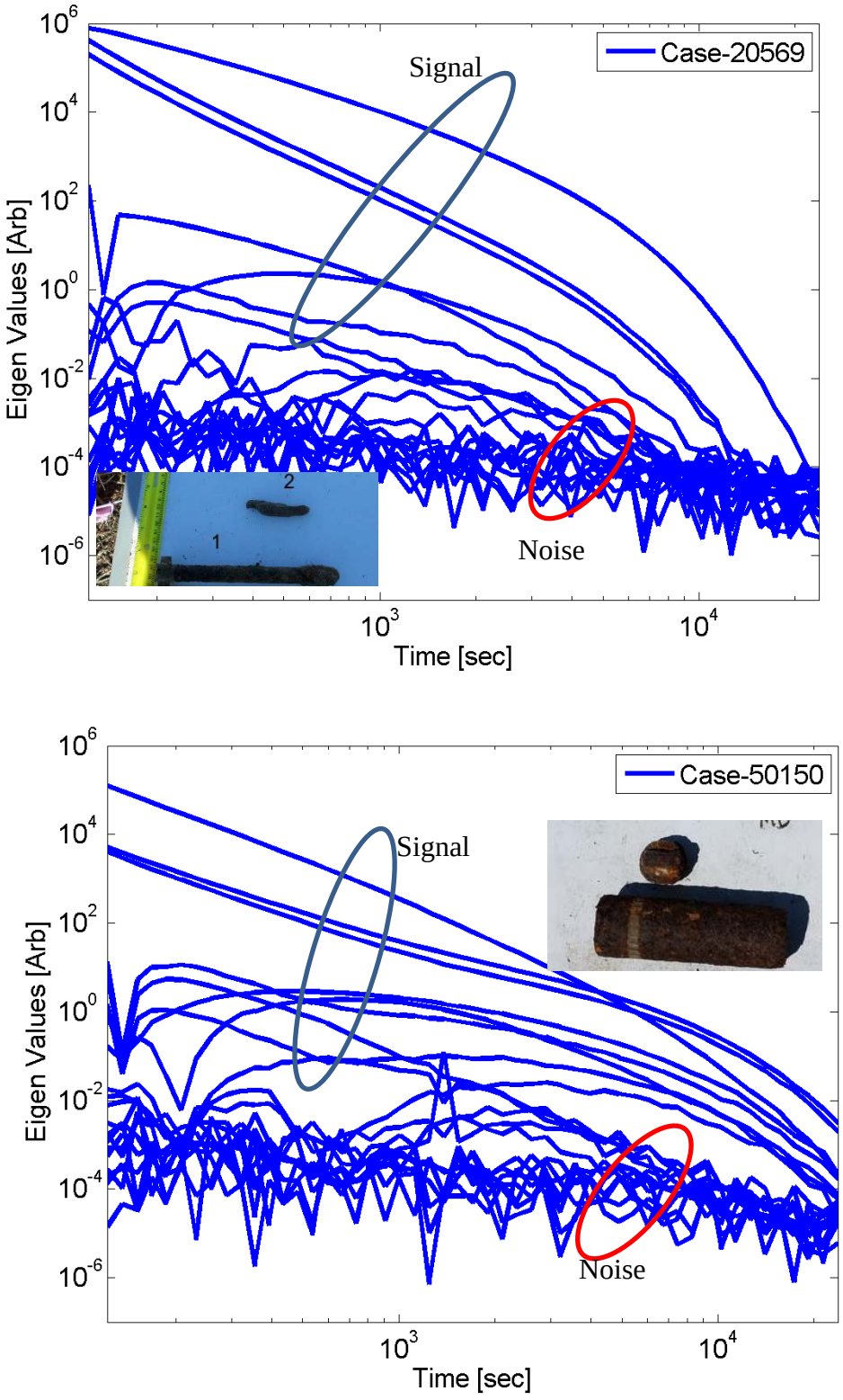

Figure 13. Multi-static Response Matrix Eigenvalues Versus Time for Multi Targets

Top Figure: A native 35-mm projectile and clutter; Bottom Figure: A native 75-mm projectile and clutter.

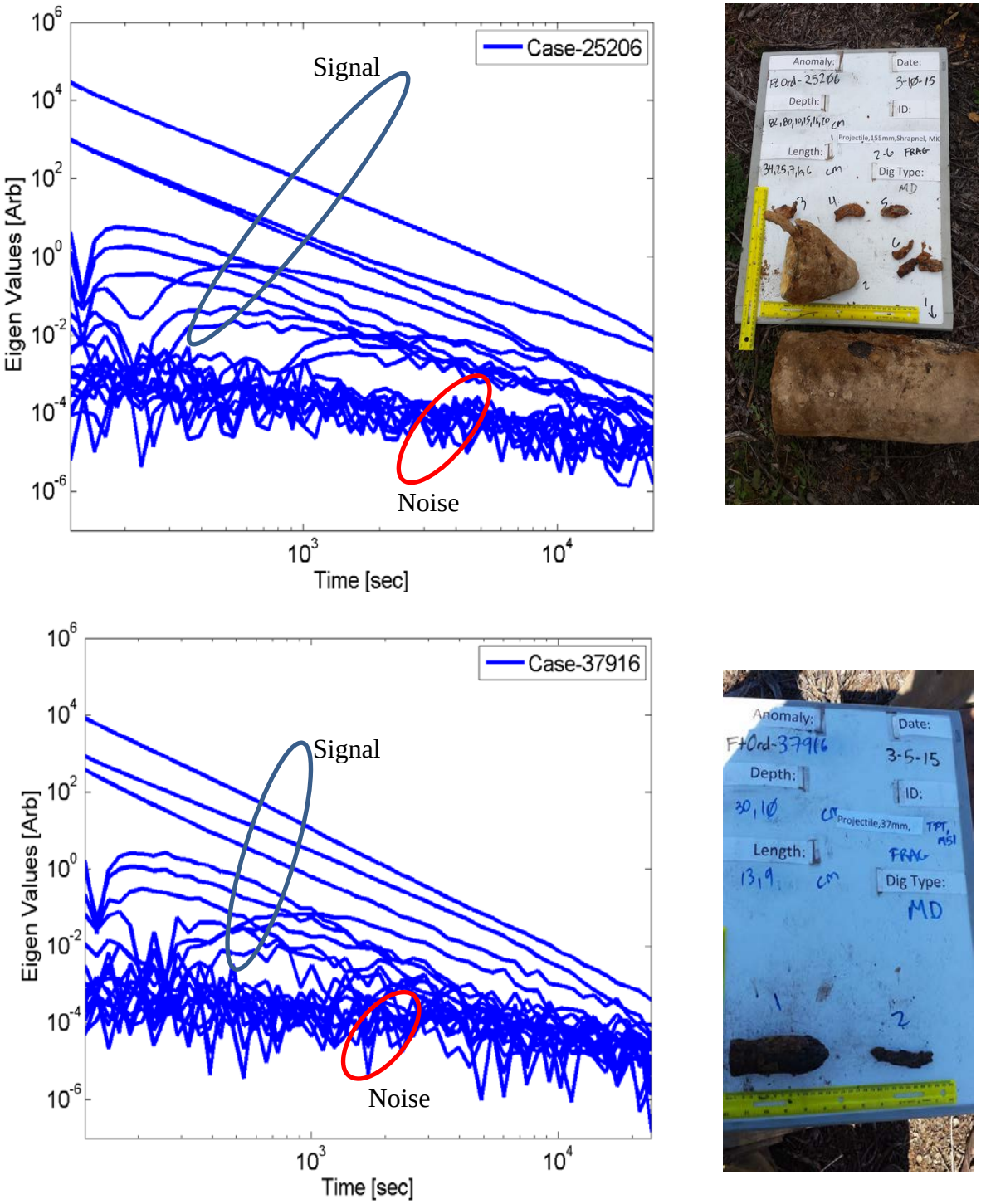

Figure 14. Multi-static Response Matrix Eigenvalues Versus Time for (Top Figure) a Native Deeply Buried 155-mm Projectile and a Set of Shallow Clutters and (Bottom Figure) a Native 37-mm Projectile and Clutter Buried at 30 cm and 10 cm, Respectively

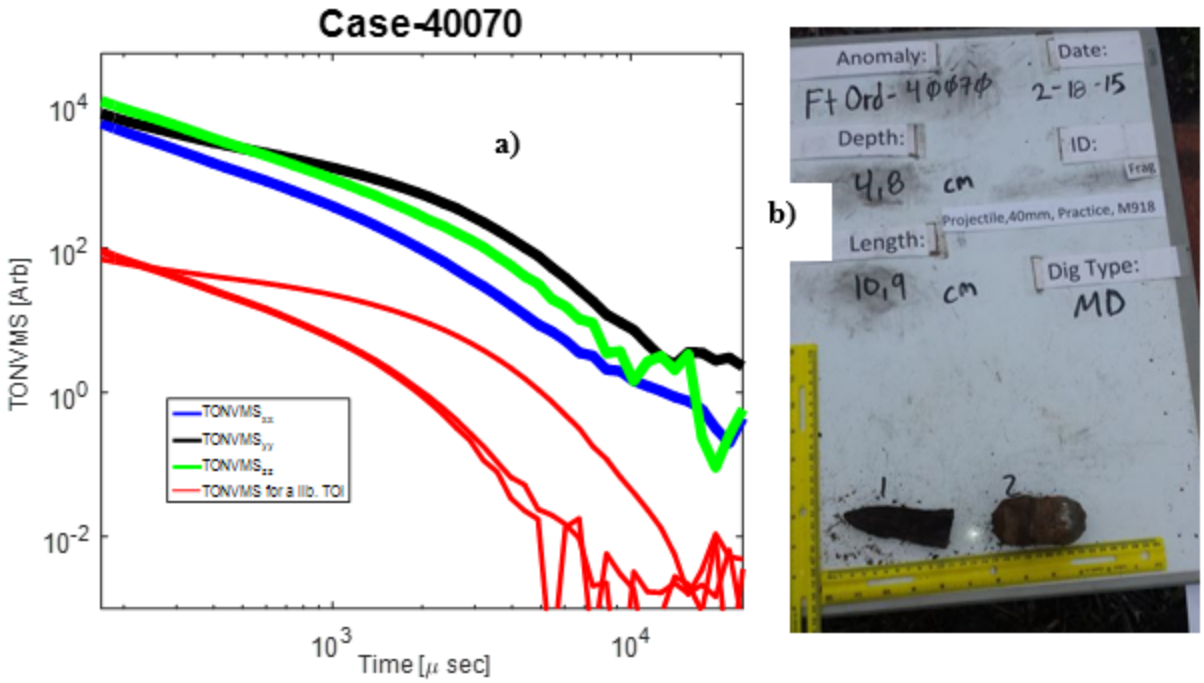

Figure 15. One Source Inversion Result Shows: a) Extracted Total ONVMS (Effective Polarizability) for a Library TOI (Red Lines); and b) Fort Ord Anomaly #40070

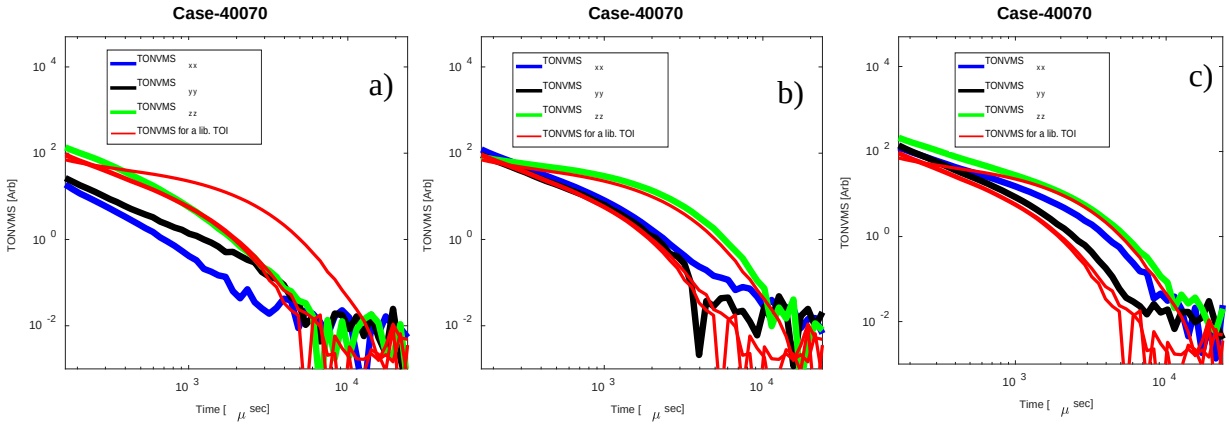

Figure 16. Total ONVMS for Fort Ord Anomaly #40070 Using Two Source Inversion for: a) Source 1/2; b) Source 2/2; c) Source 1+ Source 2

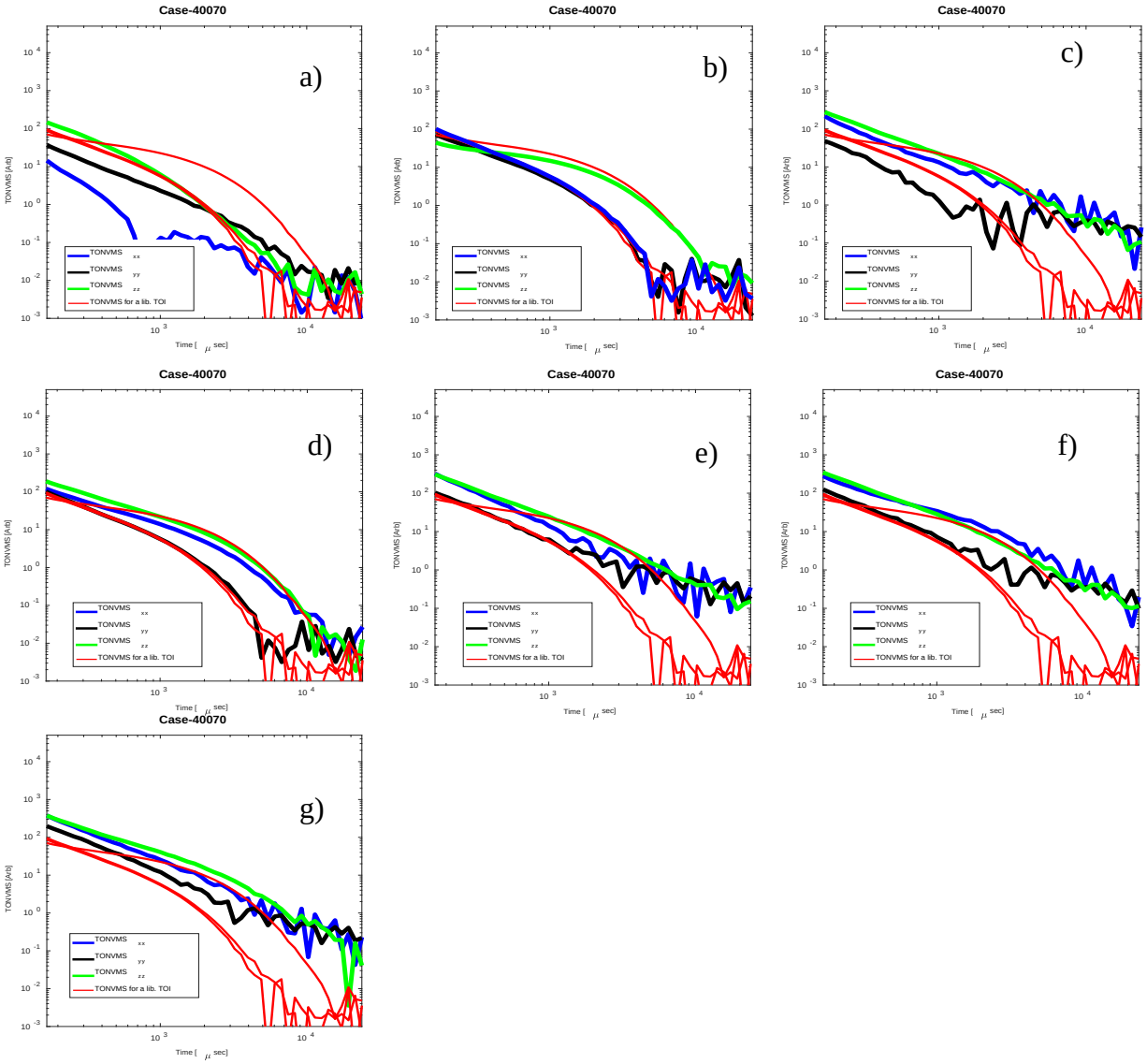

Figure 17. Three Source Inversion for Fort Ord Anomaly #40070

Total ONVMS for : a) Source 1/3; b) Source 2/3; c) Source 3/3; d) Source 1+Source 2 e) Source 1+Source 3; f) Source 2+Source 3; g) Source 1+Source 2+Source 3.

Table 1. Inverted Locations for Fort Ord, CA, Anomaly #40070 Using One, Two and Three Source Inversions

	Source#1 Coordinates [cm]			Source#2 Coordinates [cm]			Source#3 Coordinates [cm]		
Inversion	**x**	**y**	**z**	**x**	**y**	**z**	**x**	**y**	**z**
One-source	17	-2	-53						
Two-source	11.8	-8.8	-3	**9.6**	**-3.1**	**-9.4**			
Three-source	11.5	-8.6	-3.2	**10.3**	**3.6**	**-7.7**	24	-22	-15

Step 5. Request ground truth for selected anomalies: The custom training list, a combination of JD, clustering and ONVMS-DE single-target inversion results, was submitted to the ESTCP office, which then provided the ground truth for training. We used the delivered ground truth to identify the different possible TOI types and their size variations. Figure 18 shows size and shapes some of Fort Ord TOIs.

Figure 18. Fort Ord TOIS, From Left to Right: 20-mm, Small ISO, 37-mm, 35-mm, 40-mm, 60-mm, Medium ISO, 75-mm, 81-mm, 4.2" Mortar, 155-mm Projectiles

Step 6. Create ranked dig list: Based on the ground truth of custom identified training anomalies, and the inverted total ONVMS for each cued data, we created a library for all TOI. All the inverted total ONVMS are seen to show symmetry. Each target has a total ONVMS and features that make it easy to identify: its amplitude at the first-time channel, its decay rate, or the separation between the primary (green lines) and secondary and tertiary (black and blue) components at different time channels. To classify targets accurately, we used a classification approach based on symmetry and time-decay shapes and ranked symmetric targets as TOI's.

Step 7. Submit the dig list to ESTCP: The final prioritized dig list was submitted to IDA for independent scoring. The scored results are presented in subsequent sections.

3.0 PERFORMANCE OBJECTIVES

Under this project we have conducted full UXO classification studies for eleven ESTCP UXO Live Sites including: Spencer Range, TN, Camp Edwards Massachusetts Military Reservation (MMR), MA, Camp Elis, IL, Fort Rucker, AL, New Boston Airforce Station, NH, Southwestern roving Ground, AR, Waikoloa Maneuver Area (WMA), HI, Andersen AF base, Guam, Fort Bliss, TX, West Mesa, NM and Fort Ord, CA. The performance objectives were the same for all eleven sites. To avoid duplications, we provide here only one set of objectives in Table 2.

Table 2. Performance Objectives

Performance Objective	Metric	Data Required	Success Criteria
Maximize correct classification of munitions	Number of targets of interest retained	• Prioritized anomaly lists • Scoring reports from the Institute for Defense Analyses (IDA)	The approach correctly classifies all targets of interest
Maximize correct classification of non-munitions	Number of false alarms eliminated	• Prioritized anomaly lists • Scoring reports from the IDA	Reduction of false alarms by over 75% while retaining all targets of interest
Specification of no-dig threshold	Probability of correct classification and number of false alarms at demonstrator operating point	• Demonstrator-specified threshold • Scoring reports from the IDA	Threshold specified by the demonstrator to achieve the criteria specified above
Minimize the number of anomalies that cannot be analyzed	Number of anomalies that must be classified as "Unable to Analyze"	• Demonstrator target parameters	Reliable target parameters can be estimated for over 95% of anomalies on each sensor's detection list.
Correct estimation of target parameters	Accuracy of estimated target parameters	• Demonstrator target parameters • Results of intrusive investigation	Total ONVMS ± 10% X, Y < 10 cm Z < 5 cm size ± 10%

3.1 OBJECTIVE: MAXIMIZE CORRECT CLASSIFICATION ON MUNITIONS

The effectiveness of the technology for classification of munitions was measured by correct classification of TOIs from non-TOIs with high efficiency.

3.1.1 Metric

Identify all seed items and native TOIs with 99% confidence using advanced EMI classification technology.

3.1.2 Data Requirements

Advanced EMI sensor datasets are required for each anomaly. Custom training datasets (not more than ~10% of entire data) are also required. Ground truth is requested for the custom training datasets and are used to validate the models for the specific site and sensor data. Upon receipt of data, the data processing and analysis is performed to produce target dig-lists which are subsequently scored by IDA.

3.1.3 Success Criteria Evaluation and Results

The objective was considered to be met if all seeded and native UXO items were identified before the Stop-Dig threshold defined by the analyst.

3.2 OBJECTIVE: MAXIMIZE CORRECT CLASSIFICATION OF NON-MUNITIONS

The technology was aimed to minimize the number of false negatives, i.e., maximize correct classification of non-TOI.

3.2.1 Metric

The number of non-TOI targets that can be left in ground with high confidence using the advanced EMI classification technology were compared to the total number of false targets that would be present in the absence of the advanced EMI classification technology.

3.2.2 Data Requirements

This objective required prioritized anomaly lists, which our team generated independently for each sensors dataset, and also required the completed scoring reports from IDA.

3.2.3 Success Criteria Evaluation and Results

The objective was considered to be met if the method eliminated at least 75% targets that do not correspond to targets of interests (TOI) in the classification step.

3.3 OBJECTIVE: SPECIFICATION OF NON-DIG THRESHOLD

This project aimed to provide high-confidence classification approach for UXO site managers. One critical element for minimizing UXO residual risk and providing regulators with acceptable confidence is accurate and reliable Stop-Dig threshold specifications.

3.3.1 Metric

We compared the analyst Stop-Dig threshold point to the point where 100% of munitions were correctly identified.

3.3.2 Data Requirements

To meet this requirement, we required the scoring reports from IDA.

3.3.3 Success Criteria Evaluation and Results

The objective was met if a specific dig list contained all UXO targets placed before the Stop-Dig point and if additional digs (false positives) were requested after all (100%) of the TOIs were correctly identified.

3.4 OBJECTIVE: MINIMIZE NUMBER OF ANOMALIES THAT CANNOT BE ANALYZED

Some anomalies were not classified either because the data were not sufficiently informative – the sensor physically did not provide the data to support classification for a given target at a given depth – or because the data processing was inadequate. The former is a measure of instrument detection performance for all anomalies. The latter is a measure of our classification analyzes quality against the results of other classification analysts.

3.4.1 Metric

The metric for this objective was the number of anomalies that cannot be analyzed by our methods, and the intersection of all anomaly lists among all analysts.

3.4.2 Data Requirements

Each analyst submitted their anomaly list and IDA scored all lists. IDA then returned a list of anomalies that could not be analyzed, which constituted all anomalies that could not be analyzed by any analyst (cannot analyze or failed classification).

3.4.3 Success Criteria Evaluation and Results

The objective was consider met if at least 95% of the selected anomalies were analyzed.

3.5 OBJECTIVE: CORRECT ESTIMATION OF TARGET PARAMETERS

The combined ONVMS-DE algorithm provided intrinsic and extrinsic target parameters. The intrinsic target parameters were used for classification, and extrinsic parameters (locations) utilized for residual risk assessment.

3.5.1 Metric

The classification results depended on how accurately targets intrinsic and extrinsic parameters are estimated.

3.5.2 Data Requirements

This objective was archived by inversion and documentation of targets intrinsic and extrinsic parameters. To validate extracted extrinsic parameters, the results of intrusive investigations were required.

3.5.3 Success Criteria Evaluation and Results

The objective was met if targets intrinsic parameters varied within $\pm$ 10%, and extracted targets X, Y location within $\pm$ 10 cm, and depth within $\pm$ 5 cm.

4.0 SITE DESCRIPTION

In order to evaluate UXO classification technologies, ESTCP launched in 2007 a series of UXO Live Site blind tests taking place in increasingly challenging and complex sites [17], [18]. The first classification study was conducted at the UXO Live Site at the former Camp Sibert in Alabama and used two commercially available first-generation EMI sensors (the EM61-MK2 and the EM-63, both from Geonics, Inc.). At this site, the discrimination test was relatively simple: one had to discriminate large intact 4.2″ mortars from smaller range scrap, shrapnel and cultural debris under site conditions where the anomalies were very well separated.

The second ESTCP UXO Live Site classification study took place in 2009 at Camp San Luis Obispo (SLO) in California and featured a more challenging topography and a wider mix of targets of interest (TOI) [18]. Magnetometers and first-generation EMI sensors (again the Geonics EM61-MK2) were deployed on the site and used in survey mode for an initial screening. Afterwards, two advanced EMI sensing systems—the Berkeley UXO Discriminator (BUD) [4] and the Naval Research Laboratory's TEMTADS array [5]—were used to perform cued interrogation of a number of the detected anomalies. A third advanced system, the Geometrics MM [11], was used in both survey and cued modes for anomaly identification and classification. Among the munitions buried at SLO were 60-mm, 81-mm, and 4.2″ mortars and 2.36″ rockets. Three additional types of munitions were discovered during the course of the demonstration.

The third site chosen by ESTCP was the former Camp Butner in North Carolina. This demonstration was designed to investigate evolving classification methodologies at a site contaminated with small UXO targets, such as 37-mm projectiles [33].

The fourth classification study was conducted in a 10-acre area located at the former Camp Beale, CA within the historical bombing and the Toss Bomb target area using advanced EMI sensors including both handheld devices (MPV-II and 2×2-3D TEMTADS) and cart-based systems (MM). The site was selected because; (1) it is partially wooded, and (2) because it contained a wide variability of mixture of TOIs, including ISO, 37-mm, 60-mm, 81-mm, and 105-mm UXO, as well as fuzes and fuze parts that could be considered TOI on some sites. These two features, plus the magnetically responding soils encountered at the former military camp, are common occurrences in production sites and add a realistic layer of complexity into the classification process, providing additional opportunities to demonstrate the capabilities and limitations of the advanced EMI models at performing classification under a variety of site conditions.

The Fort Sill, OK, UXO Live Site was chosen as fifth classification study site by ESTCP. The main objective of the study was to assess advanced sensors and classification methods under conditions of high anomaly density, and to quantify the limits, if any, of the technology.

Under this project, our team processed advanced EMI data sets collected at eleven different UXO Live Sites. A list of ESTCP UXO Live Site classification studies conducted under this project using the advanced EMI models is summarized in Table 3.

Table 3. ESTCP UXO Live Site Classification Studies

Live Site		Advanced EMI Sensor				
		MM	5x5 TEMTADS	2x2 TEMTADS	MPV	OPTEMA
1	Spencer Range, TN	x	x	x	x	
2	Camp Edwards, MMR, MA	x		x		
3	Camp Ellis, IL	x		x		
4	Ft. Rucker, AL	x				
5	New Boston, NH			x	x	
6	SWPG, AR	x		x		x
7	Waikoloa, HI	x				
8	Andersen AF Base, Guam			x		
9	Fort Bliss, TX			x		
10	West Mesa, NM	x				
11	Fort Ord, CA	x				

4.1 SITE DESCRIPTION

4.1.1 Former Spencer Artillery Range, TN

The Former Spencer Artillery Range was chosen by the ESTCP office to assess the performance of classification technologies in open and wooded areas for advanced EMI sensors operating in both dynamic survey and static cued modes in towed, cart and hand-held configurations (Figure 19). The demonstration was carried out on three areas, including open, dynamic, and wooded areas in a portion of the Munitions Response Site (MRS), see Table 4. The commercial MM and the Naval Research Laboratory (NRL) Time-domain Electromagnetic Multi-Sensor Towed Array Detection System (TEMTADS) 5x5 were used for cued interrogation in an open field area on 1109 anomalies in the towed configuration. The TEMTADS 2x2 array was deployed in cart configuration and the Man Portable Vector (MPV) handheld (HH) sensor were used in cued mode in the wooded area on 694 anomalies. In a dynamic-area of the site, a 1.3-acre area included 355 anomalies, which were used to demonstrate the MM, MPV, and 2x2 TEMATDS array in both: a) survey mode to detect and classify anomalies, and b) cued mode to classify the anomalies they detected for comparison between survey and cued modes.

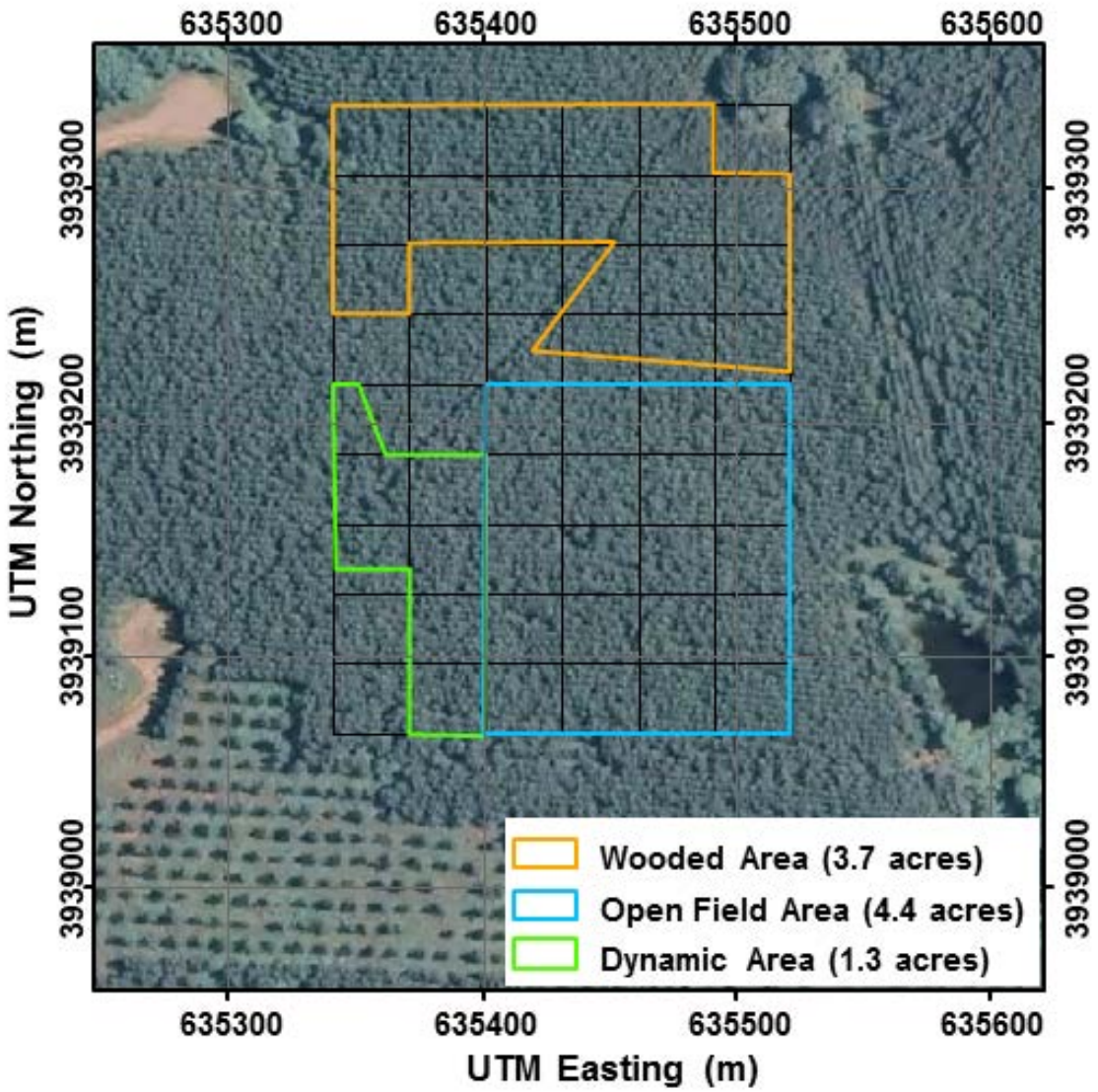

Figure 19. Wooded, Open and Dynamic Areas in a Portion of the Former Spencer Artillery Range MRS

Note: The open field area has been recently cleared of trees, but that is not reflected in the aerial photo.

Table 4. Sites, Targets, Sensors and Survey Modes

#	Area	Number Targets	Sensors	Survey Mode
1	Open	1109	MM TEMTADS 5X5	Cued
2	Dynamic	355	MM, TEMTADS 2X2X3D MPV	Dynamic & Cued
3	Wooded	694	TEMTADS 2X2X3D MPV	Cued

4.1.2 Massachusetts Military Reservations, MA

The Massachusetts Military Reservations (MMR) was chosen by the ESTCP office to establish and quantify capabilities of advanced EMI sensors in areas with high target densities and burial depths, and to identify all MEC targets (whole or partial) that were potential groundwater contamination sources. Located in Cape Cod, Massachusetts, MMR is approximately 200,000-acre site. The demonstration was conducted in two separate, 3-acre areas (northern and southern) of the Central Impact Area (CIA). MM data were only collected in the southern area; TEMTADS data were primarily collected in the northern area, although TEMTADS data were also collected over 300 targets in the southern area to provide an overlap with a portion of the MM targets. An aerial photo of the demonstration area Figure 20.

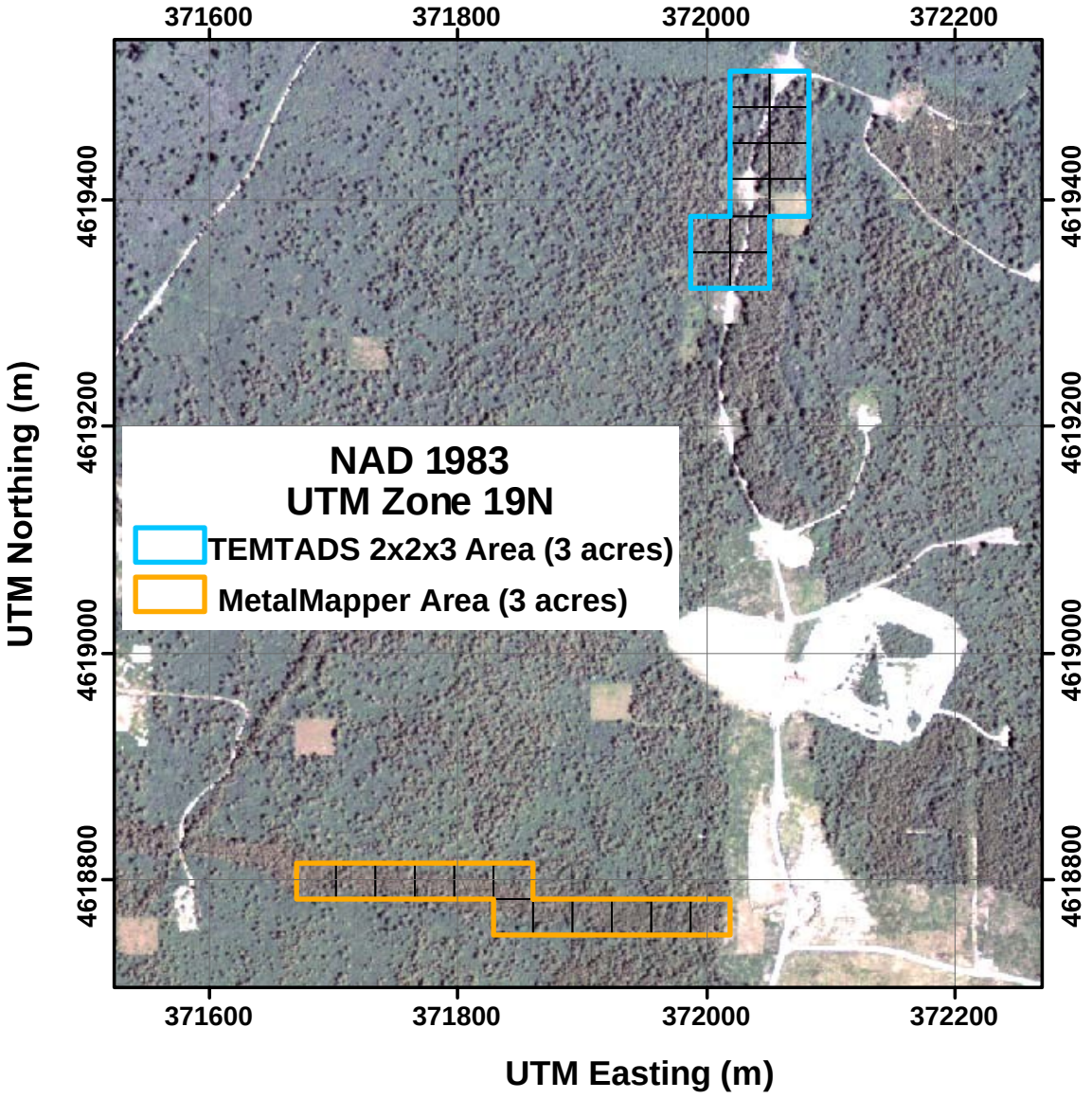

Figure 20. Boundaries of MM and 2x2 TT Demonstration Study Areas at the MMR Site

4.1.3 Former CampEllis, IL

The Former Camp Ellis, whose roughly 17,455 acres located in Fulton County, between the towns of Ipava and Table Grove in western Illinois, was chosen by ESTCP as a UXO Live Site classification site because of very high anomaly density, which was estimated from a geophysical transect survey (see Figure 21).

Figure 21. Former Camp Ellis ETCP UXO Live Site Classification Study Area with Geophysical Anomaly Density

Most of the land areas of the Former Camp Ellis are used for farming, though some parts of the former site also are used as pastureland, and a few wooded areas exist in the northern portion. The historical records indicated that rocket, rifle, and hand grenades munitions were used on the site. The demonstration was conducted in 5-acre area located within and around the high-density target area (Figure 21), using advanced EMI sensors including the cart-based (2 × 2-3D TEMTADS) and towed systems (MM devices).

4.1.4 Fort Rucker, AL

This site was selected as one in a series of sites for ESTCP UXO Live Site classification demonstration to demonstrate the capabilities and limitations of the classification process on a variety of site conditions. Most of the site consists of well-maintained grassy areas with few trees (see Figure 22). The wooded areas generally lack significant undergrowth and are easily accessible. Access is open to military personnel and the general public. Although warning signs of dangers of potential MEC are prominently displayed, the site continues to be heavily used as a golf course.

Figure 22. An Aerial Photo of the ESTCP UXO Live Site Classification Site Located at Fort Rucker, AL

4.1.5 New Boston Air Force Station, NH

The New Boston Air Force Station (NBAFS) is a 2,826-acre site located within the towns of New Boston, Amherst, and Mont Vernon, New Hampshire. It was chosen as one in a series of sites for demonstration of the classification process. Particularly, the site was chosen because it presented the opportunity to demonstrate UXO classification performance against 20-mm projectiles and high anomaly densities. The ESTCP study was conducted on a subset of the 115-acre MU705 shooting fields, located in the northwestern portion of NBAFS, directly southeast of Joe English Hill. MU705 is a moderately sloped area with portions heavily forested with dense brush (see Figure 23). Advanced EMI data were collected within approximately 10 acres of open field and portions of the woods using cart-based 2x2 TEMATDS and hand-held MPV sensors.

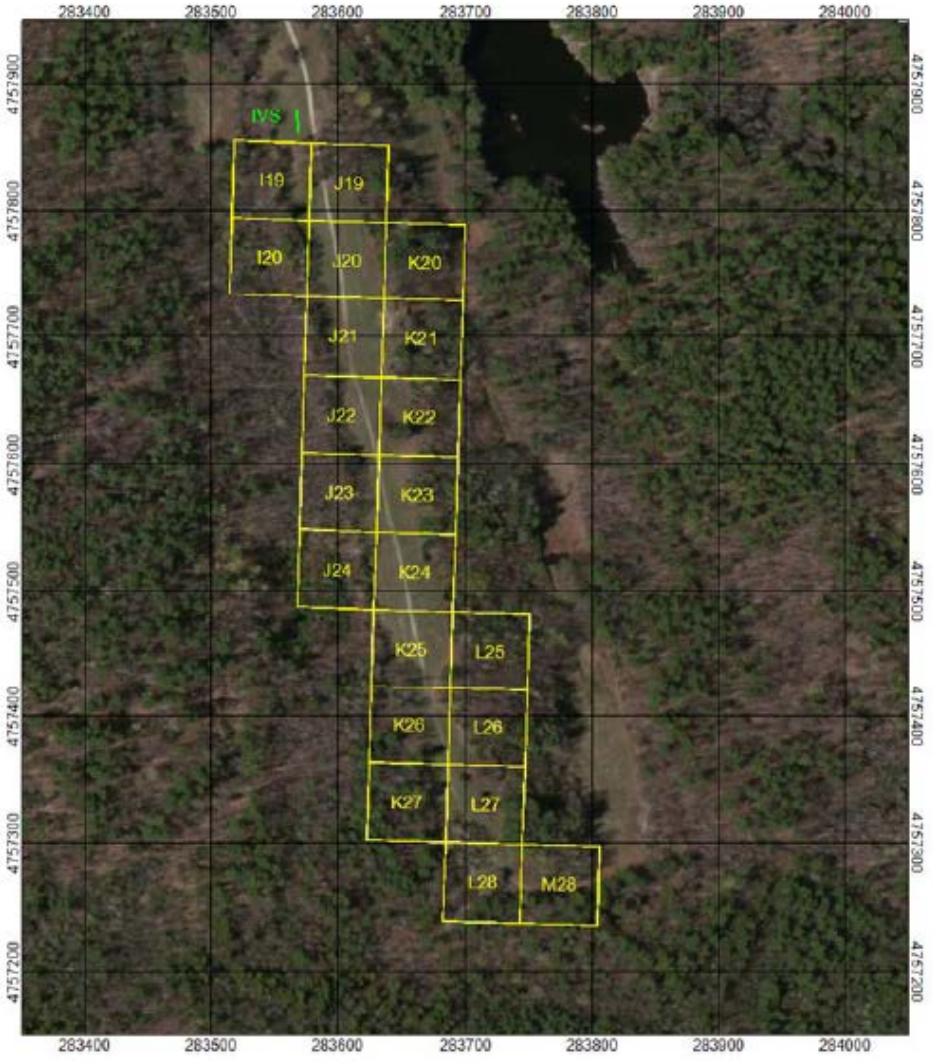

Figure 23. ESTCP Demonstration Area MU705, Located within the New Boston Air Force Station, NH

4.1.6 Former Southwestern Proving Ground, AR

The former SWPG, approximately 50,077 acre in extent, is located near Hope, AR, and was chosen by ESTCP as a demonstration and validation site for the classification process. This ESTCP UXO Live Site classification demonstration was performed on Recovery Field 15 (RF 15) of SWPG, Figure 24. The site was selected for demonstration because it was expected to contain a wide variability of mixture of TOIs: 20-mm, 37-mm, 40-mm, 57-mm, 75-mm, 76-mm, 90-mm, 105-mm, 120-mm, and 155-mm projectiles and 81 mm mortars, in high concentrations. These features increase the site's complexity and are similar to conditions encountered on production sites.

Figure 24. Boundary of the ESTCP UXO Live Site Classification Area Located at the Former Southwestern Proving Ground, AK

4.1.7 Waikoloa Maneuver Area, HI

The Former Waikoloa Maneuver Area (WMA), is located on the northwest side of the Big Island of Hawaii between Waikoloa Village and Waimea, and was chosen as one of series of sites for demonstration of the advanced classification process. The demonstration was using the MM system deployed over three areas of interests: TO20 Area A, TO20 Area B, and TO17. A map of the demonstration area and area of interests is shown in Figure 25. The site terrain and high magnetic susceptibility soil were the main features used to select WMA for the classification demonstration.

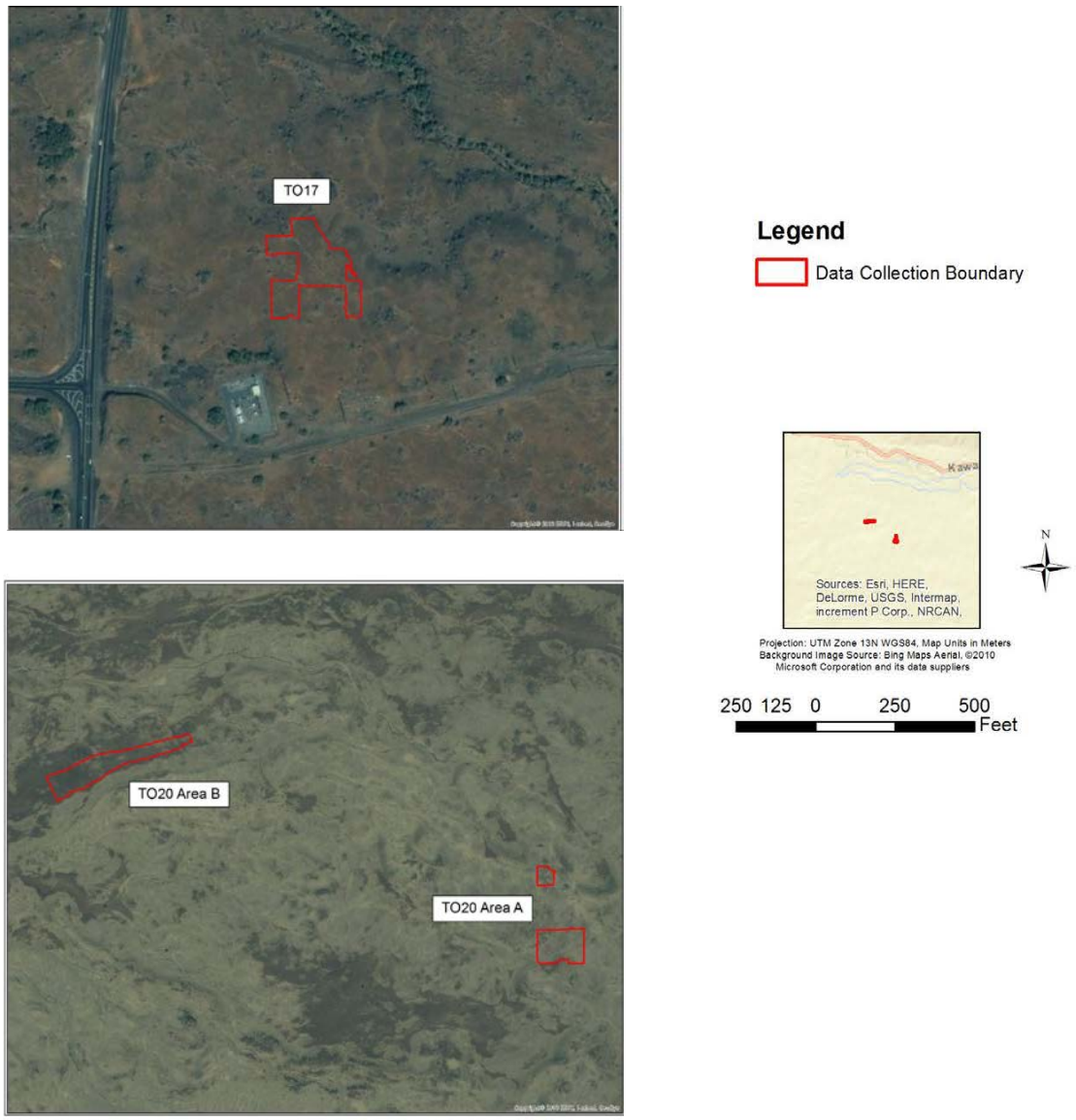

Figure 25. ESTCP Data Collection Boundaries at WMA, HI

4.1.8 Andersen Air Force Base, Guam

The Andersen AFB UXO Live Site was chosen by ESTCP to assess performance of advanced EMI sensors and classification methods in an industrial zone. The ESTCP study was performed in the North Ramp Parking (NRP) area of Andersen AFB, Figure 26. The NRP area is undergoing a munitions and explosives of concern (MEC) removal action in advance of military construction (MILCON) activities. MEC are known or suspected to be present at various sites on Guam as a result of WWII battles and subsequent military activities. As a requirement of the MILCON program, sites such as the NRP area that have a moderate to high probability of encountering MEC require a removal action in advance of construction. The NRP area site provides opportunities to demonstrate the capabilities and limitations of the geophysical classification process on a MILCON area which contain utilities, previous infrastructure, and potential MEC.

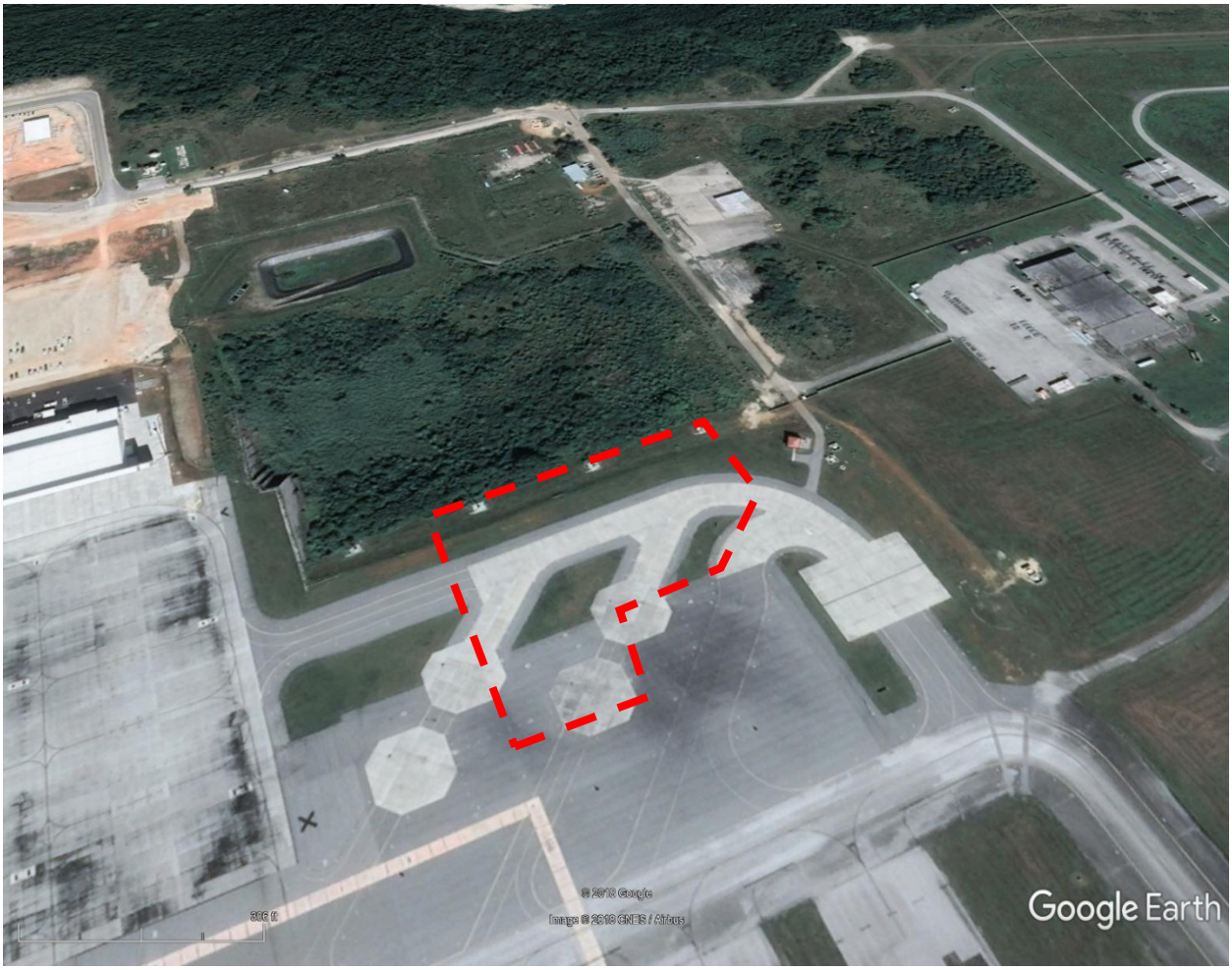

Figure 26. Boundary of Demonstration Area at NRP, Andersen AFB, Guam

4.1.9 Fort Bliss, TX

Fort Bliss, that is located in Dona Ana and Otero counties in New Mexico, and El Paso County in Texas. The site was chosen as one in a series of sites for demonstration of the munitions classification process. The ESTCP demonstration was conducted on a 5 acre subset of the closed Castner Range MRS, Figure 27. This site was selected for demonstration because of rough terrain and proximity of the study area to an alluvial fan containing ferrous rocks. These features increase the complexity of the site, and represent characteristics likely to be encountered on production sites.

Figure 27. ESTCP Classification Demonstration Area at Castner Range, Ft. Bliss, TX

4.1.10 West Mesa, NM

The former Kirtland Air Force Base precision bombing range MRS in West Mesa, which encompasses approximately 1,252 acres in Bernalillo County, near Albuquerque, New Mexico was chosen as an ESTCP UXO Live Site classification study sites, Figure 28. The study was conducted on a 10 acre subset of the new demolition bombing site within the high- or medium anomaly density target areas. This site was chosen to demonstrate applicability of the advanced geophysical classification approach for remedial design/ remedial action, and to minimize the number of intrusive investigations by characterizing targets as UXO and non-UXO. In addition, since the site is near to a municipal airport, and major traffic thoroughfare (see Figure 28), there was high interest for correctly characterizing UXO as M38-A2 100-lb practice bombs verses AN-M30 100-lb general purpose high explosive bombs, because the accurate classification could allow for intrusive investigation of targets without closing down the airport and disrupting traffic.

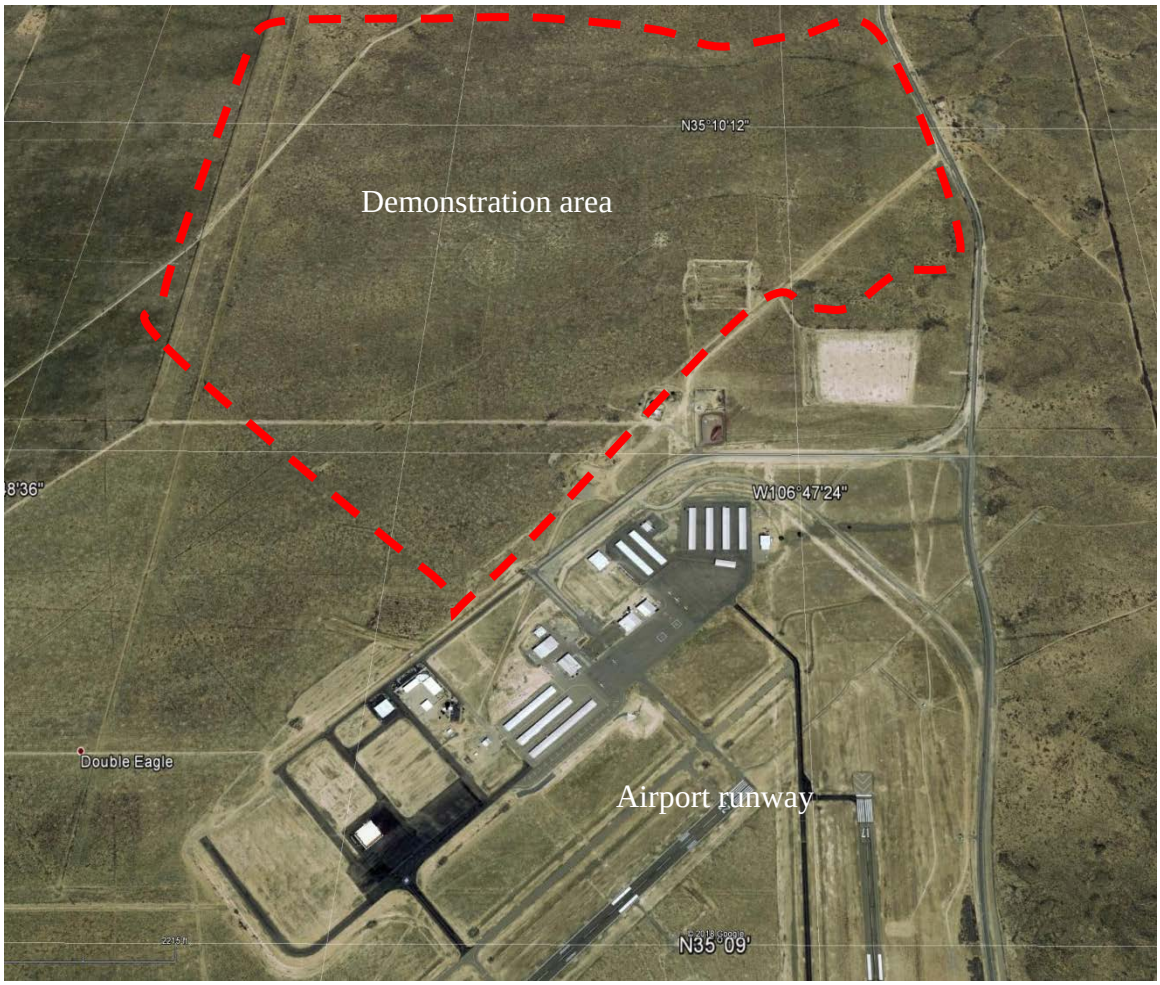

Figure 28. Boundary of ESTCP Live Site Area at the Former Kirtland AFB Precision Bombing Range, West Mesa, NM

4.1.11 Former Fort Ord, CA

The Former Fort Ord, which is a closed installation located in Monterey County, CA, was chosen as one in a series of ESTCP Live Sites for demonstration of the munitions classification process. The site was selected for demonstration because it has an ongoing munitions response program managed by the U.S. Army Corps of Engineers (USACE) Sacramento District, on behalf of the Fort Ord Base Realignment and Closure (BRAC) Office. The site vegetation, challenging terrain, and a wide variability of mixture of TOIs in high concentrations increase site complexity for classification and are similar to conditions encountered on actual production sites. The ESTCP demonstration was conducted within a 5 acre subset of Units 11 and 12, which are within the 476 acre Impact Area Munitions Response Area (MRA), Figure 29.

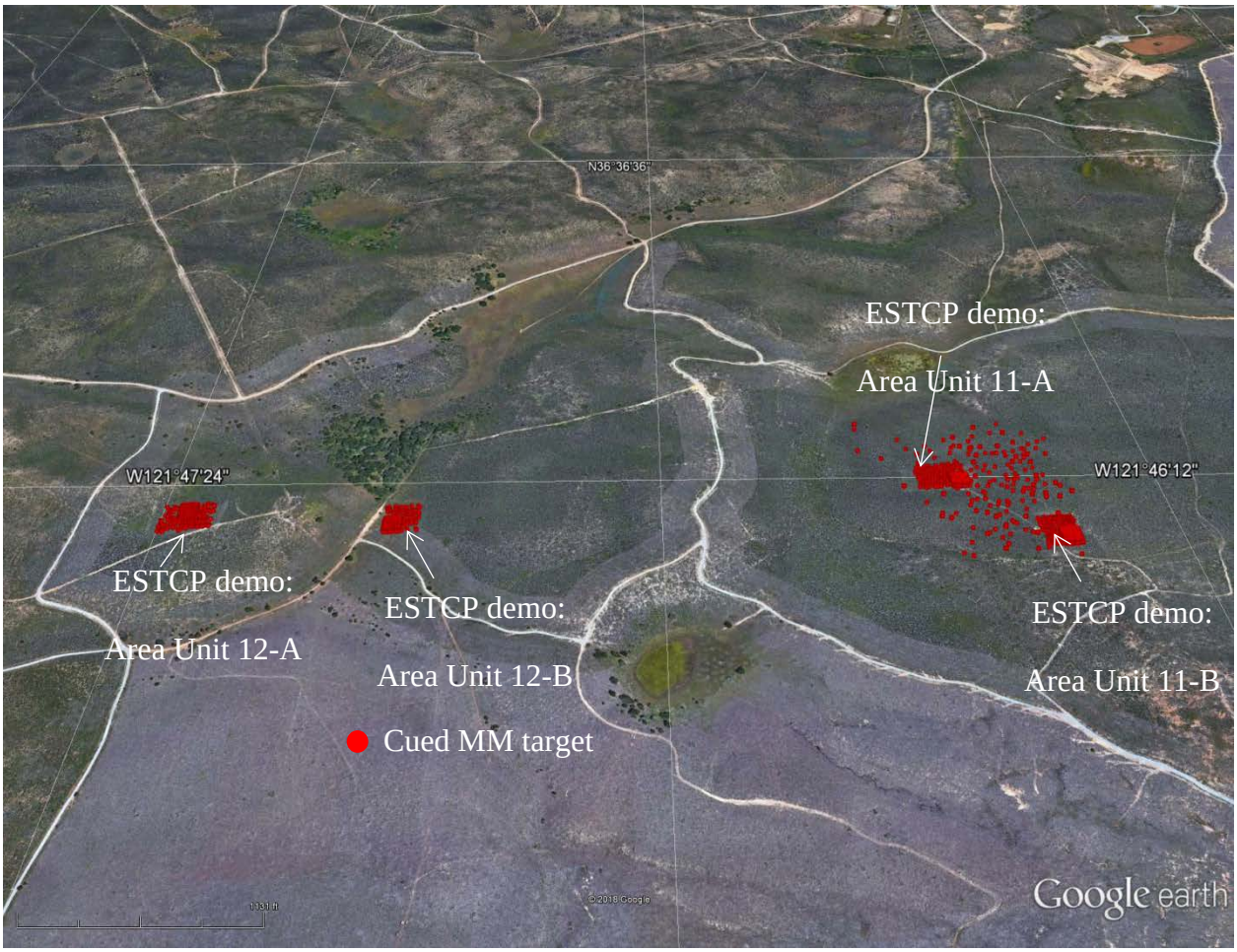

Figure 29. Locations of Cued MM Anomalies During ESTCP UXO Live Site at Units 11 and 12 in the Impact MRA, Former Fort Ord, CA

4.2 BRIEF SITE HISTORY

4.2.1 Spencer Artillery Range, TN

The Former Spencer Artillery Range, established in 1941, is 30,618-acre site and located in Spencer/Van Buren County, TN. Originally the site was intended as a firing range for heavy artillery, but it was utilized by other units, including infantry. The land returned to the original twenty-five leaseholders in the summer of 1946. Several surface decontamination sweeps were completed on portions of the former range in the 1950s. Since then, numerous tracts of land have been sold and/or subdivided, significantly increasing the number of property owners from the original twenty-five to several hundred landowners today. The ESTCP demonstration was conducted in a portion of the MRS (Figure 19). The site was selected for demonstrations because it is partially wooded and contains a wide range of munitions, such as 37-mm, 75-mm, 76-mm, 105-mm, and 155-mm projectiles.

4.2.2 Massachusetts Military Reservations, MA

Massachusetts Military Reservations is an approximately 200,000-acre site in western Cape Cod, Massachusetts. Portions of MMR were used by the military beginning in the early 1900s. The central impact area has been established as an area for artillery and mortars from the late 1930s until 1997. During the late 1940s, the CIA also contained Navy air-to-ground rocket ranges that utilized 2.25-inch rockets. Various types of munitions, including 37-mm, 40-mm, 75-mm, 90-mm, 105-mm, and 155-mm artillery projectiles and 50-mm, 60-mm, 70-mm, 81-mm, 3-inch, and 4.2 inch mortars, have been fired into the CIA. These munitions include high explosive (HE) charges designed to explode upon impact, and practice or “inert” rounds which do not contain an HE charge but may contain a spotting charge designed to emit smoke upon impact. The ESTCP pilot studies were conducted in two separate, 3-acre areas (northern and southern) of the CIA, (Figure 20).

4.2.3 Camp Ellis, IL

Camp Ellis is located between the towns of Ipava and Table Grove in western Illinois. The camp area covers approximately 17,455 acres, and the terrain of the former facility varies. The site was selected for a training camp in early 1942 by the War Department. Construction began on the camp in September 1942 and continued through the winter. Most of the area to be appropriated was farmland, although it included the small village of Bernadotte. The completed camp had more than 2,300 buildings, 1,100 of which were coal-heated barracks.

Camp Ellis trained a wide variety of soldiers during the World War II at different small arms ranges, including four 1,000-inch courses, a transition range, combat ranges, a target pistol range, a submachine-gun course, a miniature anti-aircraft range, two infiltration courses, two bazooka and rifle grenade ranges, and two live hand grenade courts. It also had a small “German Village” to train troops in the detection of land mines and booby traps. Training at Camp Ellis reached its full capacity in June 1944. Upon completion of their training, units were dispatched to the European and Pacific theaters. In January 1945, the engineer group stationed at the Camp Ellis was disbanded, and other units trained at the camp soon followed. The camp, however, remained open with the primary mission of guarding Prisoners of War. The ESTCP pilot studies were conducted on a subsection (see Figure 21).

4.2.4 Ft. Rucker, AL

Fort Rucker, which is approximately 58,000 acres in size, is located in Dale County, in the southeastern corner of Alabama near the city of Enterprise. The site was used by the US Army as an anti-tank rocket/grenade range from 1942 to 1951. About 38 acres of 52 acres of the MRS has been converted to a golf course and is used by installation personal and general public. The remaining approximately 14 acres of the MRS is easily accessible wooded area.

4.2.5 New Boston Air Force Station, NH

The New Boston Air Force Station (NBAFS) was established in the fall of 1941 after the Federal Government acquired the 2,826 acres of land comprising the current configuration of NBAFS. This land was used as an active bombing range in support of Grenier Field at nearby Manchester, NH, until 1956. On 1 October 1959, the 6594th Instrumentation Squadron was activated at NBAFS. The squadron was assigned to the 6594th Aerospace Test Wing at Sunnyvale, California, and was a tenant of the 2235th Air Base Group, Grenier Field, where administrative and support facilities were maintained. Satellite support operations began on 1 April 1960, using van-mounted equipment while permanent buildings were being constructed. By the summer of 1964, dual-satellite tracking, telemetry, and command capabilities were operating in permanent facilities at NBAFS. In March 1972, it was announced that Grenier Field would close in September of that year. All support facilities including supply, transportation, fire protection, and civil engineering were moved to NBAFS. On 1 October 1979, the 6594th Instrumentation Squadron was re-designated as Detachment 2, Air Force Satellite Control Facility (AFSCF), Air Force Systems Command. On 1 October 1987, Detachment 2, AFSCF was re-designated as Detachment 2, 2nd Satellite Tracking Group and ownership was transferred from Air Force Systems Command to Air Force Space Command (AFSPC). On 1 November 1991, Detachment 2, 2nd Satellite Tracking Group was re-designated as the 23rd Space Operations Squadron. NBAFS currently provides launch, operation, and on orbit support for more than 170 DoD satellites. In addition to bombing activities, training and maneuver activities were performed on the property from 1956 until 2002, when the range officially closed. Unserviceable tanks, trucks, and half-tracks were used as strafing targets for machine guns, 20 mm cannons, and rockets.

4.2.6 SWPG, AR

The SWPG was established in 1941 and used as a U.S. Army testing center for artillery and air bombs. It also hosted an air field for bomber and fighter planes. This site is 50,780 acres in extent, and was designed for testing wide variety munitions including 250-pound and 500-pound bombs; mines; 60-mm and 81-mm mortars; hand and rifle grenades; 20-mm, 37-mm, 40-mm, 75-mm, 76-mm, 90-mm, 105-mm, and 155-mm projectiles; and small rockets. Although a majority of the rounds tested were inert/ballast, fillers also included high explosives, white phosphorous and smoke mixtures. No chemical material was tested. The SWPG was closed as soon as World War II ended in 1945. The government returned the lands back to the public. The airport complex was transferred to the city of Hope, AR, who in 1947 made it the Hope Municipal Airport. Upon closure, subsequent range clearances were performed for surface contamination, with Certificates of Clearance being issued in 1947 and 1948 delineating specific areas as “surface use only.” In the early 1950s additional range clearances were performed by Army Corps of Engineers clearance teams, with a final Certificate of Clearance being issued 16 March 1954. This ESTCP UXO Live Site classification demonstration was performed on Recovery Field 15 (RF 15) of SWPG.

4.2.7 Waikoloa, HI

The 100,000 acre Waikoloa maneuver area was acquired by the Navy in 1943 and used as a military training camp and artillery range for 50,000 troops from 1943 to 1945. More than 100 different types of munitions have used on the site, including mortars, projectiles, hand grenades, rockets, land mines, and Japanese ordnance. Two surface clean-up activities were done in 1946 and 1954. The 1946 clean-up was done after the departure of the military. The 1954 clean-up followed an accidental detonation of a dud fuse or shell killing two civilians and seriously injuring three others. Munitions and explosives continue to be discovered at the Former WMA. To date more than 1,800 MEC items, 117,000 pounds of military debris, and 149,000 pounds of munitions debris (MD) have been cleared from 22,600 acres of the former WMA. The demonstration was conducted in grids selected from pre-existing areas of interest at the site.

4.2.8 Andersen AF Base, Guam

Andersen Air Force Base (AFB) is operational since the 1940's. The main purpose of this 20,000-acre site has been to provide support for Strategic Air Command operations. During WWII, Andersen AFB served as a large forward operating base for U.S. military operations. The base continues to support strategic operations in the region, and serves as a staging base for activities in Asia and the South Pacific. The site was invaded by the Japanese military in December 1941 and lasted until 1944 when the United States military liberated Guam. The Battle of Guam began on July 21, 1944 with American troops landing on the western side of the island. After several weeks of heavy fighting, Japanese forces officially surrendered on August 10, 1944. The heavy military activity on Guam caused a variety of American and Japanese war time remnants, including MEC, to be distributed throughout the island. The results of the MEC distribution have resulted in the investigation and removal of MEC in a systematic process under the military construction program.

4.2.9 Castner Range Fort Bliss, TX

The Castner Range at Fort Bliss, TX, as a training area first was acquired in 1926 and initially encompassed 3,500 acres. Additional land was acquired by 1939, bringing the range to 8,328 acres. Castner Range was heavily used for small arms firing courses and artillery firing and impact areas from 1926 until 1966 when ordnance use at Castner Range was discontinued. In 1972, the Department of the Army declared Castner Range surplus to its needs, and began to transfer parcels to non- DoD entities. Many isolated clearance operations have been conducted on Castner Range. Approximately 1,244–1,321 acres east of U.S. Highway 54 have been cleared of UXO and have been transferred; however, the remaining 7,007 acres of the Closed Castner Range MRS have not been transferred and remain in the Army's control.

4.2.10 West Mesa, NM

The former Kirtland Air Force Base Precision Bombing Ranges were established in the early part of World War II, when the U.S. leased approximately 10,345 acres of land from the City of Albuquerque. The land was owned by the State of New Mexico and the Santa Fe Pacific Railroad and leased to the City of Albuquerque, who in turn, subleased it to the U.S. Government.

This acreage, along with 4,790 acres transferred from the Department of the Interior, was leased for building precision bombing ranges. Documentation and munitions-related items found on site indicate that the ordnance used for training consisted of 100-lb sand-filled bombs and 100-lb concrete bombs, both with M1A1 spotting charges and aircraft flares. In addition, specific munitions debris was found in the new Demolition area, which indicates the use of High-Explosives (HE) bombs. In 1996, during the construction of a road in the New Demolition Area, near the Double Eagle II Airport, a 100-lb HE bomb was found intact and subsequently detonated by Kirtland AFB Explosive Ordnance Disposal (EOD) personnel. Currently, the West Mesa is largely empty rangeland. The City of Albuquerque operates the Albuquerque Shooting Range, the Albuquerque/Bernalillo County Water Utility Authority Soil Amendment Facility, and the Double Eagle II Airport, which is a small airstrip for private planes. Eclipse Aviation is currently building manufacturing facilities southeast of the Double Eagle II Airport.

4.2.11 Fort Ord, CA

The Fort Ord, CA site was established as an artillery training field for the US army by the US department of war right after the American entry into World War I, in 1917. The area was known as the Gigling Reservation, U.S. Field Artillery Area, Presidio of Monterrey and Gigling Field Artillery Range. Despite a great demobilization of the U.S. Armed Forces during the inter-war years of the 1920s and 1930s, by 1933, the artillery field became Camp Ord. At the beginning primarily, the site was used for horse cavalry units training camp until the military began to mechanize and train mobile combat units such as tanks, armored personnel carrier and movable artillery. By 1940, the 23-year-old Camp Ord was expanded to 2,000 acres. In August 1940, it was re-designated Camp Ord and the 7th Infantry Division was reactivated, becoming the first major unit to occupy the post. In 1941, Camp Ord became Fort Ord. Between 1947 and 1975, Fort Ord functioned as a basic training center. After 1975, the 7th Infantry Division was based at Fort Ord. In 1991, Fort Ord was slated for closure and by 1993 the majority of the soldiers were reassigned to other Army posts. Fort Ord was officially closed in September 1994. There are no active Army units stationed at the former Fort Ord.

4.3 SITE GEOLOGY

4.3.1 Spencer Range, TN

The Former Spencer Artillery Range is underlain by Pennsylvanian era sandstone, shale, siltstone, and conglomerate. The rocks in this area consist of Pennsylvanian marine deposits of sandstone, shale, coal, and limestone. Bedrock is observed at the surface in some areas of the site. Where covered with soil, depth to bedrock generally ranges from approximately 2 feet to 6 feet below ground surface. The soil types on site include the Gilpin silt loam, Hartsells loam, Lonewood silt loam, and Udorthents-Mine Pits complex. The site-specific soil and geology did not influence on the data quality.

4.3.2 Massachusetts Military Reservation, MA

The geology of western Cape Cod comprises glacial sediments deposited during the retreat of the Wisconsin stage of glaciation. Three extensive sedimentary units dominate the regional geology; the Buzzards Bay Moraine, the Sandwich Moraine, and the Mashpee Pitted Plain.

These moraines form hummocky ridges. The MPP, which consists of fine- to coarse-grained sands forming a broad outwash plain, lies south and east of the two moraines. Underlying the Mashpee pitted plain are fine-grained, glaciolacustrine sediments and basal till at the base of the unconsolidated sediments. Overall, the MMR soil is comprised of fine to coarse sand and gravel, with discontinuous and continuous clays and silts. The study area at MMR area was generally rugged, with many large, deep craters and a considerable amount of roughly cut brush. The MMR soil and geology did not affect the application of advanced EMI systems.

4.3.3 Camp Ellis, IL

The former camp Ellis consists of three geological units: shallow soil, glacial till, and bedrock [41]. The youngest of these units is the shallow soil, followed by the underlying glacial till, and then by bedrock, which is at greater depths. All three of these soil types consist primarily of silt, with some clay. The underlying glacial till is between 6 to 15 meters in thickness and is composed of a mixture of sand, silt, clay, and gravel. The bedrock in the area is composed of sedimentary rocks, which are primarily shale, sandstone, and limestone. The shallow soils at the demonstration site are comprised of: Ipava Silt Loam, 0 to 2 percent slopes; Sable Silty clay loam, 0-2 percent slopes and Greenbush silt loam, 2 to 5 percent slopes. Several small streams flow in the vicinity of the Area A MRS; however, none of them cross the UXO Live Site demonstration area. The site-specific soil, geology, and hydrogeology did not present a problem to the EMI technologies during this demonstration.

4.3.4 Fort Rucker, AL

Fort Rucker lies in the East Gulf Coastal Plain physiographic section, with sedimentary origins dating to the Cretaceous, Tertiary, and Quaternary ages. Fort Rucker soils overlie the Buhrstone Escarpment, a formation held up by Early Tertiary shale and sandstone. Geologic formations that outcrop on Fort Rucker are Tertiary to Holocene in age and include the Tuscahoma Sand, Hatchetigbee and Tallahatta Formations, Lisbon Formation, Residuum, Alluvial High Terrace Deposits, and Low Terrace Deposits. These formations strike east-west, dipping to the south at a rate of 15 to 40 feet per mile. The data analysis showed that the site-specific soil responses were negligible.

4.3.5 New Boston AF Station, NH

NBAFS is located on highly folded metasedimentary rocks, which are structurally related to the Merrimack Syncline. This syncline complex trends northeast and exhibits highly folded sections due to east-west oriented compressive forces. The site is situated on the Lower Devonian Littleton Formation, which consist of slightly to moderately metamorphosed rock. A gray, micaceous quartzite is the predominant rock type, with lesser amounts of gray, coarse mica schist. Bedrock underlying NBAFS is highly fractured in the upper sections due to structural compression and folding. A thin veneer of Pleistocene and recent glacial alluvium consisting of boulders, gravel, sand, and silt covers most areas on the installation. Alluvium is generally thickest in the low-lying areas and valley bottoms. The NAFS soil and geology did not produce any noticeable EMI response.

4.3.6 SWPG, AR

The Southwestern site has very flat topography. The sedimentary deposits, that are mainly poorly consolidated deposits of clay, sand, silt, limestone, and lignite of Tertiary age, are found in the area. The data showed that the site has negligible soils responses.

4.3.7 Waikoloa, HI

The former maneuver area is characterized by a generally smooth to rocky, sloping land surface of consistent grade, marked by numerous cinder cones along the volcanic rift zones that are now covered with grassland vegetation and cut by widely spaced erosional gullies. The WMA is surrounded by three of the five volcanoes that comprise the Island of Hawaii. On the north are the Kohala Mountains, the oldest volcanic feature on the island; on the east is Mauna Kea; and on the southwest are the Hualalai Cone and Crater. Coastal land bounds the former maneuver area from the south onto the west. The former WMA extends inland from near sea level to approximately 6,000 feet above mean sea level. Bedrock is at a depth approximately 10 to 40 inches below ground in most locations but deeper in the upper reaches of the maneuver area. The bedrocks and soils have high iron contests which forms the magnetic geology at the WMA. The soil's magnetic susceptibility, which varies spatially across the site, produced significant and variable background soil responses at Waikoloa and caused additional challenges to estimating targets parameters from advanced EMI sensors data sets.

4.3.8 Andersen AF Base, Guam

Andersen AF Base in Guam consists of an undulating limestone plateau and a volcanic basement rocks. The volcanic rocks on the island are of Eocene and Oligocene age and comprise the Facpi Formation and Alutom Formation. Near the base, the volcanic basement rocks of Alutom Formation are almost entirely overlain by a limestone plateau. Northern Guam, near the AAF base geology comprises most of the bedrock, which is the principal aquifer rock, but it is exposed on the plateau surface only in the interior of island where it occupies 18% of the surface. The studies have showed that there were no or negligible background EMI soil responses.

4.3.9 Castner Fort Bliss, TX

The Fort Bliss Castner range is situated over a structural basin filled with Quaternary-aged sediments derived from the Hueco Mountains. The basin is called the Hueco Bolson and consists of a thick sequence of layered fluvial, alluvial fan, evaporite, and eolian sediments. The Hueco Mountains reside along the eastern edge of the MRS. Outcrops in the Hueco Mountains are primarily of Pennsylvanian and Permian-aged limestone. The Hueco Bolson consists of unconsolidated to slightly consolidated deposits composed of fine- to medium-grained sand with interbedded lenses of clay, silt, gravel, and caliche. The sediments have a maximum thickness of 9,000 feet. However, the bottom part of the Hueco Bolson is primarily clay and silt. Relatively small deposits of Castner Limestone containing diabase (or dolerite) dikes and sills are in the central portion of the site. This area can be characterized as having potential magnetic geology. However, the EMI data collected at the ESTCP demonstration site did not experience any interference from the geology in the area.

4.3.10 West Mesa, NM

The West Mesa is characterized by basaltic volcanic soil and rock, with much of the surface soils being derived from windblown sand and dust originating from sand dunes to the southwest. Rock is exposed in large sections of the eastern portions of the site, located east of Atrisco Vista Boulevard. The soils west of Atrisco Vista Boulevard in the vicinity of Munitions Response Site N-2 / New Demolition Area are light in color, calcareous, low in organic matter and consist of grain sizes ranging from loamy sands to clays. Soil consistency ranges from soft to extremely hard. Most of the ground surface is covered with vegetation; however, some portions are bare. No significant EMI soil responses were observed in the ESTC demonstration area.

4.3.11 Fort Ord, CA

Fort Ord is within the Coast Ranges Geomorphic Province. The region consists of northwest-trending mountain ranges, broad basins, and elongated valleys generally paralleling the major geologic structures. In the Coast Ranges, older, consolidated rocks are characteristically exposed in the mountains but are buried beneath younger, unconsolidated alluvial fan and fluvial sediments in the valleys and lowlands. In the coastal lowlands, these younger sediments commonly inter-finger with marine deposits. Fort Ord geology contains: Mesozoic granite and metamorphic rocks; Miocene marine sedimentary rocks of the Monterey Formation; Upper Miocene to lower Pliocene marine sandstone of the Santa Margarita Formation. Although, marine sandstone usually has high iron concentrations, our studies showed that Fort Ord soil did not have a noticeable impact on the EMI sensor data.

4.4 MUNITIONS CONTAMINATION

Suspected munitions present at the ESTCP UXO Live Sites are listed in the sub-sections below.

4.4.1 Spencer Range, TN

Suspected munitions at the Spencer Range, TN, demonstration site were:

- 37-mm, 75-mm, 76-mm, 105-mm, and 155-mm projectiles

4.4.2 MMR, MA

Suspected munitions at the MMR demonstration site were:

- 5-inch, 7-inch, 8-inch, 14.5-mm, 20-mm, 30-mm, 37-mm, 75-mm, 90-mm, 105-mm, 155-mm, and 175-mm projectiles
- 60-mm, 81-mm, and 4.2-inch mortars
- 2.36-inch, 2.75-inch, and 3.5-inch rockets

4.4.3 Former Camp Ellis, IL

Suspected munitions at the former Camp Ellis, IL, demonstration site were:

- 2.36-inch practice rockets
- Rocket, rifle, and hand grenades

4.4.4 Fort Rucker, AL

Suspected munitions at the Fort Rucker, AL, demonstration site were:

- 2.36-inch rocket, rifle, and fragmentation grenades
- 3.5-inch practice rockets

4.4.5 New Boston Air Force Station, NH

Suspected munitions at the NBAFS demonstration site were:

- 20-mm projectiles
- 2.25-inch and 5-inch practice rockets
- 5-inch high explosive (HE) rockets
- 3-lb, 4.5-lb, 100-lb, 500-lb, and 1,000 lb- practice bombs
- 100-lb general purpose HE bombs
- 325-lb and 350-lb HE depth bombs
- M69 incendiary bombs
- M46 photoflash bombs

4.4.6 Southwestern, AR

Suspected munitions at the SWPG Demonstration site were:

- 20-mm, 37-mm, 40-mm, 57-mm, 75-mm, 76-mm, 90-mm, 105-mm, 120-mm, and 155-mm projectiles
- 81-mm mortars

4.4.7 Waikoloa, HI

Suspected munitions at the Waikoloa demonstration site were:

- 60-mm and 80-mm high explosive mortars
- 75-mm, 105-mm, and 155-mm projectiles
- 2.36-inch rocket propelled anti-tank rounds

- US MK II hand grenades
- Rockets
- M1 anti-tank land mines
- Japanese ordnance

4.4.8 Andersen Air Force Base, Guam

Suspected munitions present at the Andersen Air Force Base demonstration site were:

- MK II Hand Grenades
- 20-mm, 105-mm, 155-mm, 5-inch, and 6-inch projectiles
- 60-mm and 81-mm mortars
- 100-lb bombs

4.4.9 Fort Bliss, TX

Suspected munitions at the Castner, Fort Bliss demonstration site were:

- 37-mm, 75-mm, 105-mm, 155-mm, and 240-mm HE projectiles
- 155-mm shrapnel projectiles
- 37-mm, 75-mm, and 8-inch armor piercing projectiles
- 60-mm and 81-mm mortars

4.4.10 West Mesa, NM

Suspected munitions at the West Mesa, NM, demonstration site were:

- 100-lb, sand-filled and 100-lb concrete bombs;
- M1A1 spotting charges and aircraft flares;
- AN-M30 100-lb general purpose high-Explosives (HE) bombs

4.4.11 Fort Ord, CA

Suspected munitions at the Fort Ord, CA, Demonstration Site were:

- 20-mm, 35-mm, 37-mm, 40-mm, 57-mm, 60-mm, 75-mm, 90-mm, 105-mm, and 155-mm projectiles

5.0 TEST DESIGN

The only required test at the ESTCP UXO Live Sites entailed collecting target characterization training data. This activity included the use of a calibration pit, where the data-collection team made a series of static measurements of example targets at several depths and attitudes in order to; (1) cross-check models, (2) confirm Tx and Rx polarity for the sensors, and (3) characterize and validate target signatures in the UXO classification Library.

5.1 SITE PREPARATION

N/A

Page Intentionally Left Blank

6.0 DATA ANALYSIS AND PRODUCTS

The detailed descriptions of cued and dynamic data analysis and products for the Spencer Range, TN, Camp Edwards Massachusetts Military Reservation (MMR), MA, Camp Elis, IL, Fort Rucker, AL, New Boston Airforce Station, NH, Southwestern Proving Ground, AR, Waikoloa Maneuver Area (WMA), HI, Andersen AF base, Guam, Fort Bliss, TX, West Mesa, NM and Fort Ord, CA UXO Live Site are given in [42]-[52]. To avoid duplications, we provide below only main steps of advanced EMI data preprocessing, inversion and targets classification approaches. These steps are applicable for 5x5 TEMTADS, MM, MPV-TD, 2x2-3D TEMTADS and OPTEMA systems operating in both cued and dynamic modes.

6.1 EMI DATA INVERSION AND CLASSIFICATION STEPS

The discrimination process comprises three sequential tasks: data collection, data inversion, and classification. Each EMI sensor produces unique datasets and requires different modeling schemes. The detailed data modeling approach of advanced EMI sensors' Tx and Rx signals using the ONVMS-DE algorithm is described in [19]. This approach includes a three-step process including: (1) data pre-processing, (2) creation of the MSR data matrix, (3) the eigenvalue analysis. These steps are described below.

Step 1. Data pre-processing. This initial step is used to convert all data files into a uniform data format and remove background effects in the data as described in [21].

Step 2. Create MSR data matrix. During this second step, we use the measurement bi-static data set for each anomaly and create the MSR data matrix.

Step 3. Eigenvalue analysis. The third step establishes the target feature parameters used for initial target classification and ranking. The JD technique is applied to the created MSR data matrix to extract the time-dependent eigenvalues for each anomaly.

Step 4. Data inversion. The effective magnetic polarizations (i.e., total ONVMS) are extracted for each anomaly using the combined ONVMS-DE for one, two and three sources [38].

Step 5. Choosing training targets list. Our classification approach is based on custom training data. At the first stage of the process a semi-supervised clustering technique is used for identifying potential site-specific TOIs. Training target selection is achieved as follows:

(a) The intrinsic features ($M_{zz}(t_1)$, $M_{zz}(t_n)/M_{zz}(t_1)$) of targets are selected from the extracted total ONVMS; *n* is chosen based on feature separation. EMI datasets of all anomalies, corresponding to single-and multi-object inversions, are produced.

(b) Initial clustering is performed, and associated ground truth is requested, for all targets whose features are located closest to the corresponding cluster centroid with TOI-like ONVMS features.

(c) Clusters containing at least one TOI are identified, and a smaller domain is selected within the feature space for further interrogation. In addition to the statistical clustering algorithm, ONVMS time decay curves are inspected for each anomaly. The TONVMS time decay shapes and symmetries are used to further validate or modify the custom training anomaly list. Anomalies with significantly asymmetric TONVMS are removed from the training list; anomalies with fast decay but symmetric profiles are added to the training list for which the ground truth are requested.

(d) Additional clustering is performed within the selected domain, and those targets with features closest to the corresponding cluster centroids evaluated via collection of intrusive ground truth. The clusters with at least one identified UXO are marked as *suspicious* and analyzed further.

(e) All targets whose features (based on multi-object inversion and library matching) fall inside any of the *suspicious* clusters are used to train the statistical classifier and the library-matching procedure.

Step 6. Targets classification. Once target classification feature parameters are clustered and site-specific ground truth is obtained for training targets, all anomalies are classified as following:

(a) Probability density functions are created for single- and multi-target scenarios;

(b) All unknown targets are scored based on the probability density functions;

(c) Dig Lists are produced for both single-and multi-object cases and compared to each other to find similarities and differences;

(d) Total ONVMS results are analyzed using library matching and visual inspection of all anomalies;

(e) A set of anomalies is identified and, if necessary, additional training datasets are requested. The new information is incorporated into the classification model and all items are re-scored;

(f) Based on the previous steps, a classification threshold is selected defining the Stop-Dig point and a final dig list is produced.

During this project our classification approach was tested on eleven ESTCP UXO Live Site classification demonstrations sites conducted at the Spencer Range, TN, Camp Edwards Massachusetts Military Reservation (MMR), MA, Camp Elis, IL, Fort Rucker, AL, New Boston Airforce Station, NH, Southwestern Proving Ground, AR, Waikoloa Maneuver Area (WMA), HI, Andersen AF base, Guam, Fort Bliss, TX, West Mesa, NM and Fort Ord, CA. The classification results at these sites clearly showed that our team obtained significantly better classification results than the other teams [21].

6.2 DATA PRODUCTS

The main product of advanced EMI classification is a prioritized dig list which was scored against ground truth. Throughout this project we have developed and documented robust data pre-processing, background correction, data inversion, training data selection, classification parameters selection and classification approaches. Each step of the classification process has been documented and successfully applied to datasets collected during ESTCP UXO Live Site classification studies. While the prioritized dig list is the primary product produced by the advanced classification process, there are also many other data products provided, such as intrinsic and extrinsic parameters of targets, site-specific target signature libraries, MSR data eigenvalues, mismatch functions between modeled and actual data, anomaly detection, and subsurface 3D maps. These products and their associated graphical visualizations are used to measure advanced classification performance against required site-specific objectives, gain regulators acceptance and communicate with public.

7.0 PERFORMANCE ASSESSMENT

In this section, we assess the performance of the advanced classification approach against the performance objectives of Table 2. In order to demonstrate detection and classification effectiveness of the advanced EMI model, we will discuss performance results from all eleven UXO Live Sites.

7.1 CORRECT CLASSIFICATION OF MUNITIONS

One of the main goals of advanced EMI classification technology is to detect and identify all seeded and native TOI. Under this project, we used the extracted total ONVMS to establish classification features. Both statistical classification algorithms and expert judgment were applied to distinguish TOIs from clutters. Data from three instruments including the MM, 2×2-3D TEMTADS, and MPV-II were analyzed independently. For each sensor, custom training datasets (using not more than ~10% of entire data) were utilized. The ground truth derived from the custom training datasets were used to validate the models for each specific site and sensor, and to identify which type of TOIs were present at the site. The goal was considered to be met if an optimal Stop-Dig threshold was determined, i.e., all seeded and native UXO items were identified below the analyst-specified Stop-Dig threshold. The results are described below.

7.1.1 Results for Spencer Range, TN

The ESTCP demonstration was carried out on three areas; open, dynamic, and wooded areas in a portion of the MRS. In the open area, cued data were collected over 1,109 anomalies using the commercial MM and the Naval Research Laboratory (NRL) Time-domain Electromagnetic Multi-sensor Towed Array Detection System (TEMTADS) 5x5. Cued data sets from 694 anomalies were collected in the wooded area using the TEMTADS 2x2 man-portable system and the Man Portable Vector (MPV) handheld (HH) sensor. In the dynamic area of the site, 354 anomalies were used to demonstrate the MM, MPV, and 2x2 TEMATDS array in both: (a) dynamic mode to identify and classify anomalies; and (b) cued mode to classify the anomalies they detect for comparisons between dynamic and cued modes.

A multi-step process was utilized. First, data were pre-processed using a multi-static response (MSR) data matrix eigenvalue approach [19]. Next, for each anomaly, extrinsic features (locations and orientations) and intrinsic features (total ONVMS, i.e., effective polarizabilities) were calculated using the combined ONVMS-DE algorithm for one, two and three sources. Next, the extracted total ONVMS features were clustered using the attributes of both size and decay, facilitating the creation of custom training lists. Finally, using ground truth of the identified training anomalies, all Former Spencer Artillery Range anomalies were classified as either a Target of Interest (TOI) or clutter, and prioritized dig lists were created and submitted to ESTCP for independent ranking.

We processed all MM, 2x2 TEMTADS and MPV data sets using the same data inversion and classification steps as outlined in [42] for the 5x5 TEMTADS system. The comparisons between total polarizabilities extracted from the datasets from these three systems, collected on common anomalies in the Spencer Range dynamic area, are depicted in Figure 30. These comparisons show that the extracted total ONVMS are sensor-independent, and that they are intrinsic properties of the object. The extracted total ONVMS for all Spencer Range MM, 2x2 TEMATDS and MPV TOI anomalies are shown in [42].

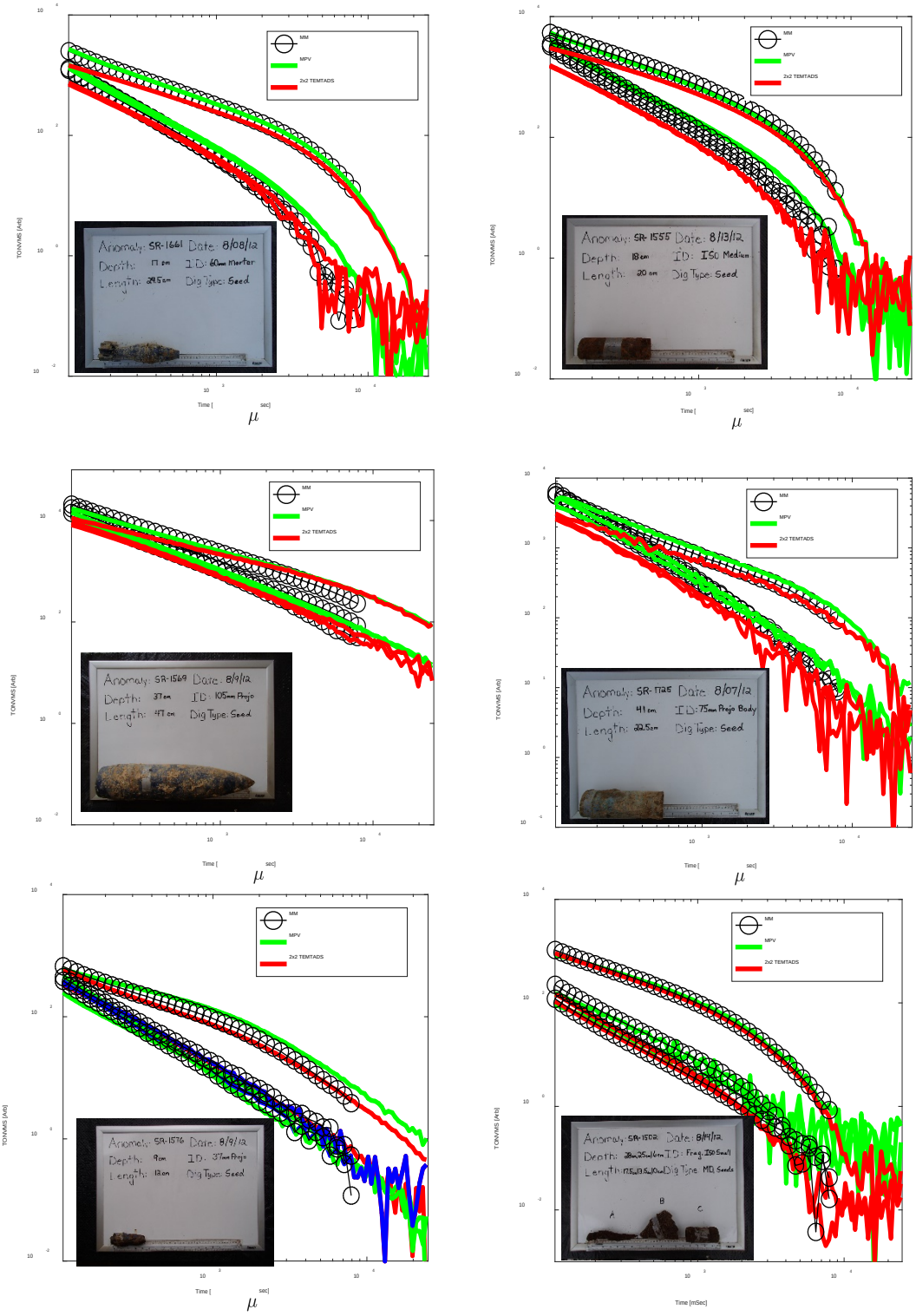

Figure 30. Comparisons Between Effective Polarizabilities Extracted from MM, MPV and 2x2 TEMTADS Data for a 60 mm Mortar (SR-1661), Small (SR-1502) and Medium (SR-1555) Size ISOs, 105 mm (SR-1569), 75 mm (SR-1725) and 37 mm (SR-1576) Projectiles

The final prioritized dig lists were created for each data set independently and submitted to IDA for scoring. The independent scored results in the form of a receiver operating characteristic (ROC) curve is depicted in Figure 31 for the 5x5 TEMATDS sensor. The result shows that of the 33 targets that were dug for training, 20 targets were not TOIs (representing a shift along the *x*-axis) and 13 were TOIs (representing a shift along the *y*-axis). In addition, there were 9 "can't analyze" anomalies. The results show that all TOIs were ranked as "Dig" before the dig-stop point and 92% of "non-TOIs" were ranked correctly as "No-Dig".

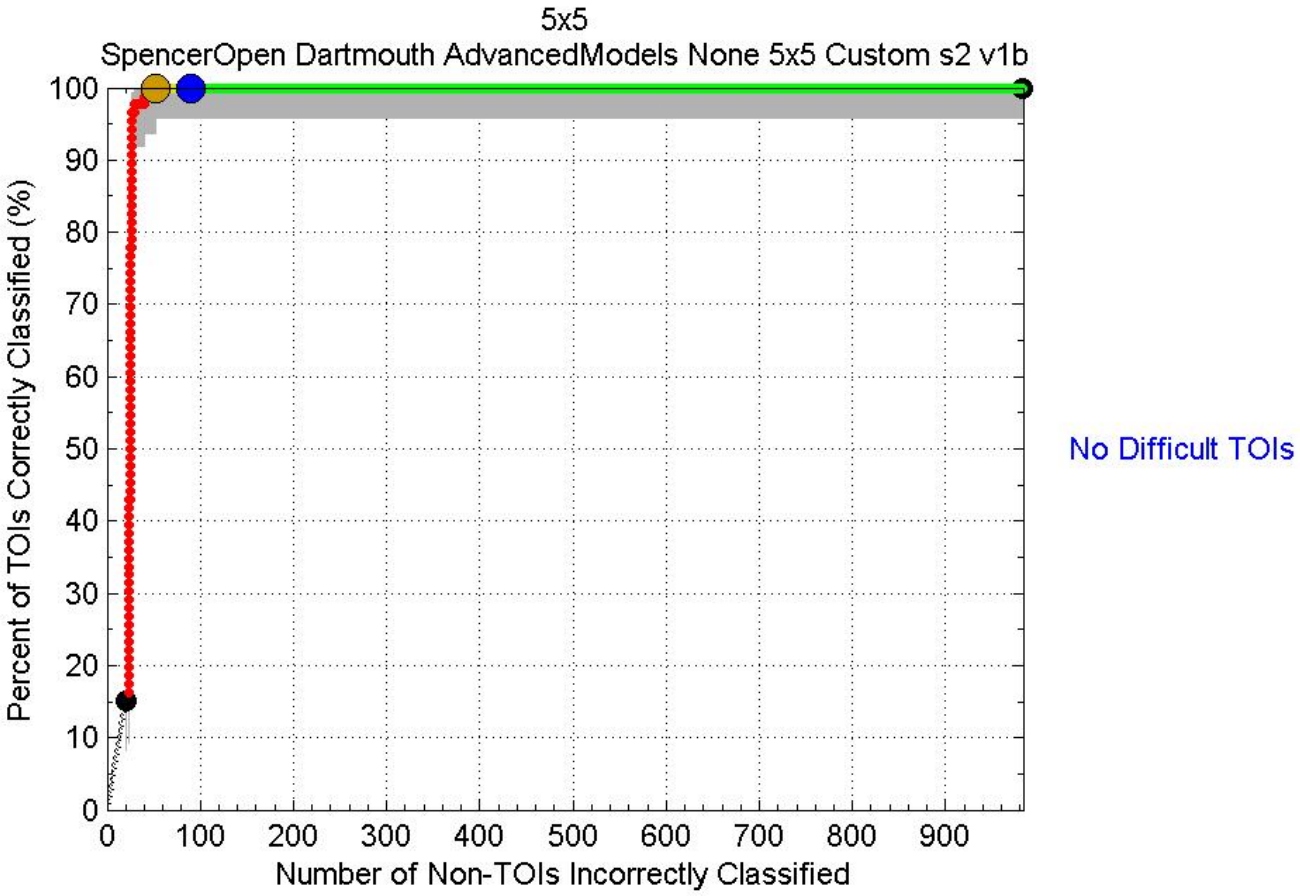

Figure 31. ROC Curve for the Spencer Artillery Range 5x5 TEMTADS Data

The ROC curve for the MM system in open field is shown in Figure 32. The result shows that all TOIs were ranked as "Dig" before the Stop-Dig point (see the dark blue dot in Figure 32) and 90% of clutters were ranked correctly as "No-Dig".

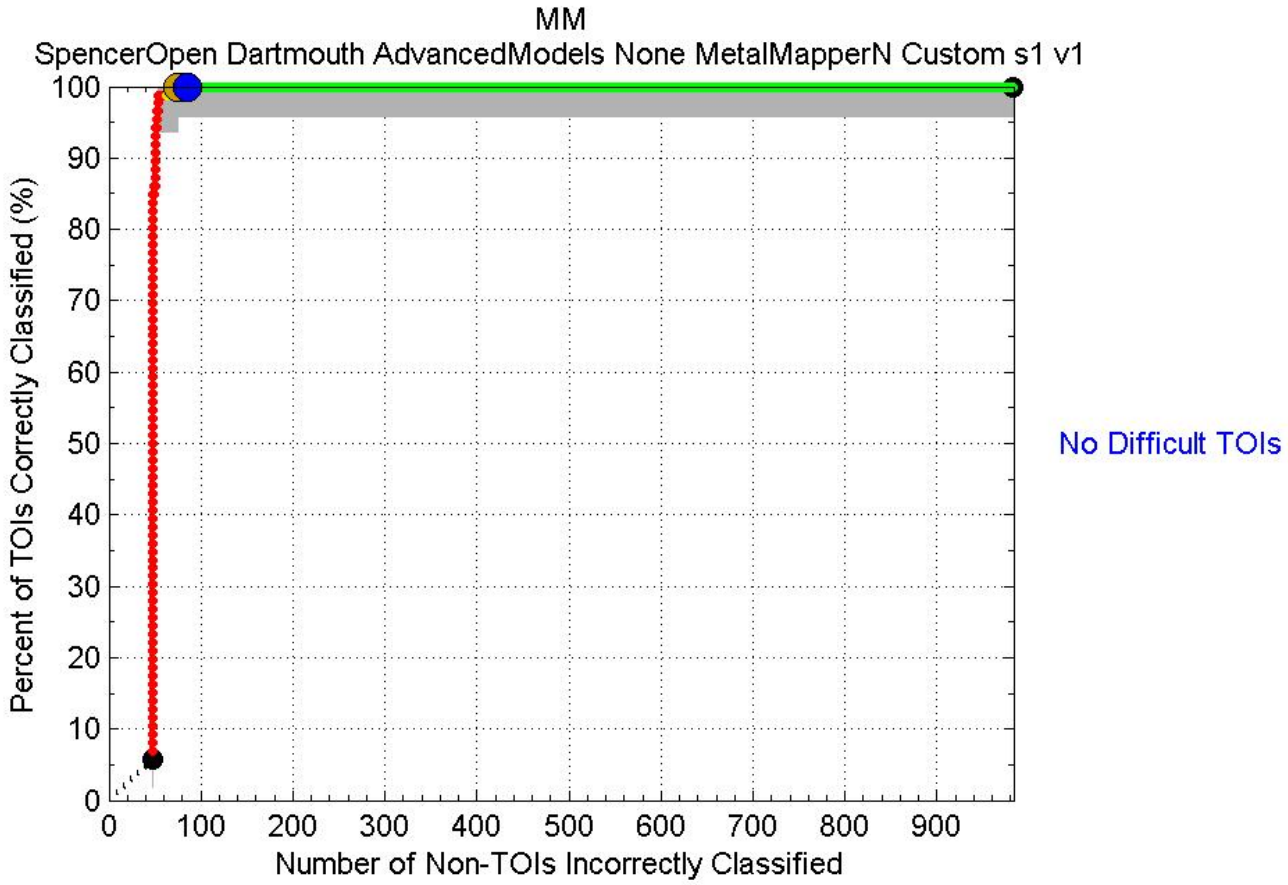

Figure 32. ROC Curve for the MM Data in the Spencer Artillery Range Open Area

Similarly, classification results for MM, MPV and 2x2 TEMTADS in forms of ROC curves from the Spencer artillery range dynamic area are depicted on Figure 33. There were 355 anomalies in total. Both MM and 2x2 TEMTADS data were collected over all 355 anomalies, and out of 355 anomalies, MPV data were collected for 287 anomalies. The 68 anomalies for which data were not collected were categorized as "Can't analyze" MPV anomalies (and appear as a shift along the *x*-axis, see ROC for MPV in Figure 33). Classification features were extracted for all anomalies. Using the inverted features each anomaly was classified as either clutter or TOI. The study shows that there were no false negatives, all 23 TOI were identified correctly from each system data set. 86% of MM and 90% 2x2 TEMTADS of non-TOI anomalies were classified correctly as clutters. Although with 11 false positives and 68 "Can't analyze" only 252 MPV anomalies with clutter were not dug, i.e., ~70% of non-TOI (332) were left in the ground, (see Figure 33).

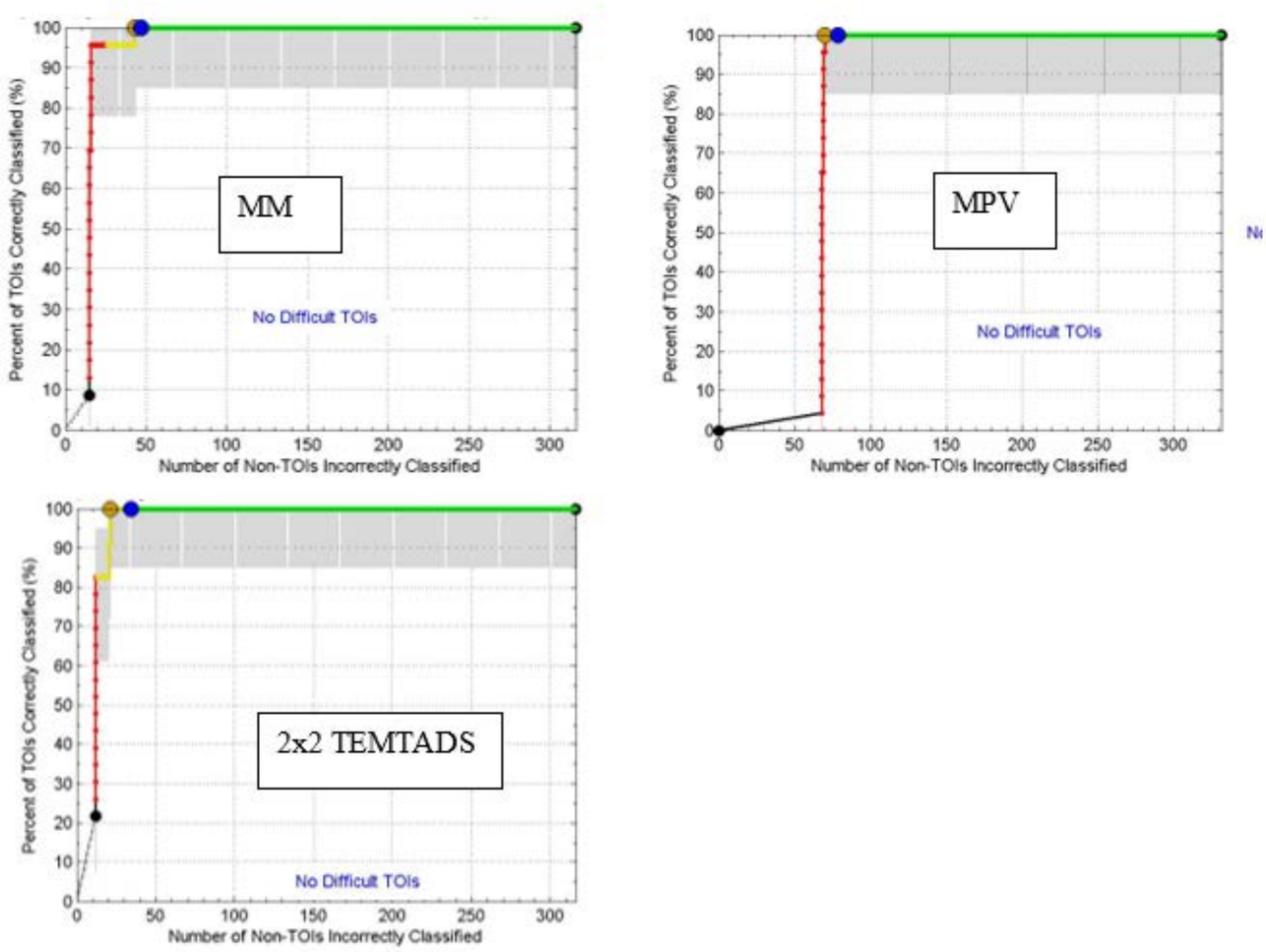

Figure 33. ROC Curves for MM, MPV and 2x2 TEMTADS Anomalies from the Spencer Range Dynamic Area

Classification Results for MPV and 2x2 TEMTADS Anomalies in Spencer Artillery Range Wooded Area

To assess classification performance in a challenging area, the classification studies were conducted for 2x2 TEMADS and MPV data sets, which were collected in the Former Spencer Artillery Range wooded area over 692 anomalies. Again, first the classification features were extracted from each sensor's dataset independently, using the ONVMS-DE inversion results. The inverted total ONVMS were then analyzed using the data processing scheme outlined in [42], and a set of targets were selected for training and submitted to the ESTCP office. The 2x2 TEMTADS data analyst chose 53 anomalies for training. Fourteen out of 53 were TOI. The MPV data analyst requested 38 anomalies for training; ten out of 38 were TOIs. In addition, there were three MPV anomalies for which data were not collected, and subsequently ranked as "Can't analyze." The ground truth for the training targets were received (see black dot on Figure 34) and used to rank anomalies as TOI or clutter. The ranked lists were submitted to IDA for scoring. The results are shown on Figure 34. There were 71 TOI. Both 2x2 TEMTADS and MPV analysts identified independently all TOIs except one small ISO target labeled as #2355. The classification efficiency and rejection rates are summarized in Table 5.

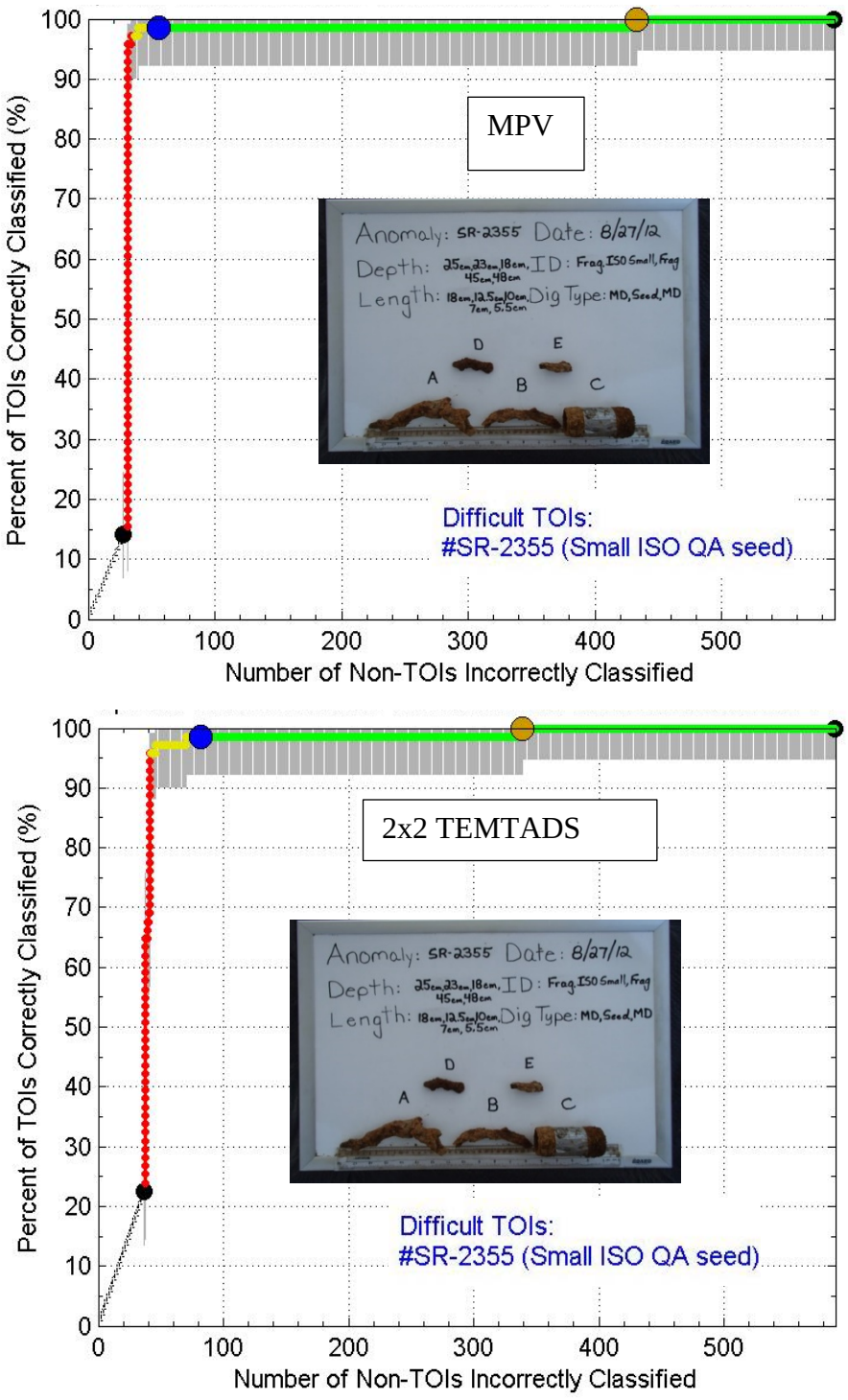

Figure 34. ROC Curves for MPV and 2x2 TEMTADS Anomalies in Spencer Range Wooded Area

Table 5. Efficiency and False Positive Rejections Rates for 2x2 TEMTADS and MPV System in Spencer Range Wooded Area

Data Set		Detection Efficiency	False Positive Rejection Rate
2x2 TEMTADS	At dig stop point	98.6%	91%
	With all TOI classified	100%	26.25%
MPV	At dig stop point	98.6%	86%
	With all TOI classified	100%	41%

Spencer Range, TN Missed TOI, Retrospective Analysis

As seen in Figure 34, both 2x2 TEMTADS and MPV data analysts misclassified the same anomaly #2355. To understand why this target was missed we did a retrospective analysis. The ground truth showed that the misclassified anomaly consisted five metallic objects, four clutters and one TOI, a small ISO (see Figure 34). Data were processed using one, two and three sources inversion code. The inverted primary, secondary and tertiary effective polarizabilities for anomaly # 2355 from 2x2 TEMTADS data set are show in Appendix D, in [42] as a shaded graph. The result shows that the extracted secondary and tertiary polarizabilities are non-symmetric at early times. This early time gate non-symmetric feature, which is caused by a small piece of clutter, misled the analyst and anomaly was ranked as "No-Dig". To further understand the cause of this misclassification, Figure 35 shows the inverted total ONMVS from the three-source inversion from MPV data. As seen, the inverted total ONVMS for a three-source inversion does not match the total ONVMS of a library small ISO. We then re-analyzed the data assuming four, five, and six target sources. Four- and five-target inversion did not show a significant improvement in classification, but the six-target inversion, depicted on Figure 36 shows that the total ONVMS of the fifth target coincides with that of the ISO projectile in the library. Thus, the model could accurately classify a small ISO surrounded by clutter.

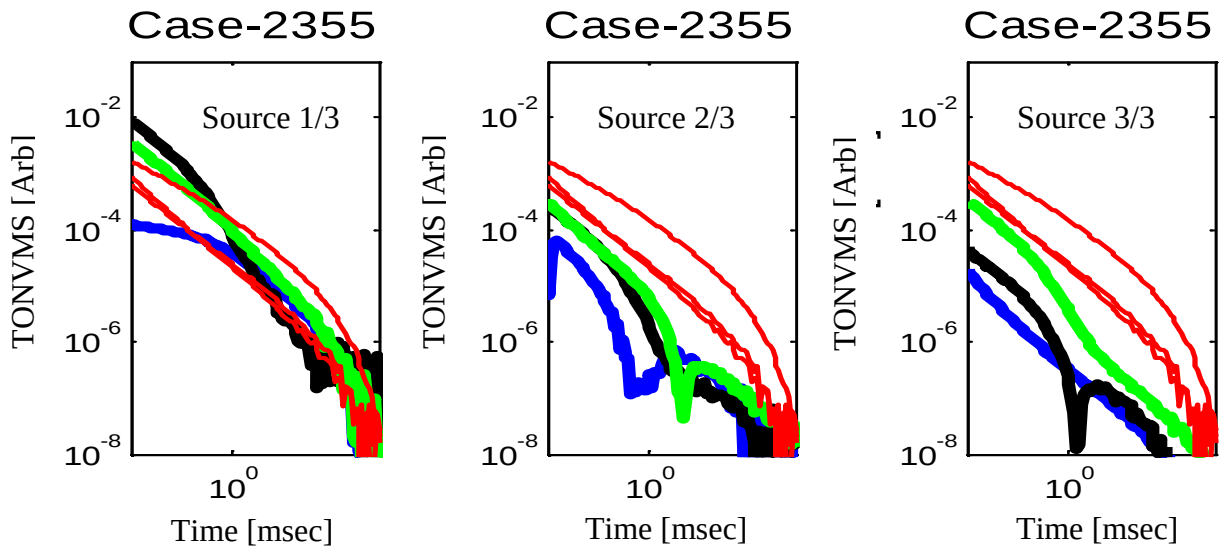

Figure 35. Time-dependent Total ONVMS Inverted from MPV-II Data for the Spencer Range Anomaly #2355 using Three-target Inversion

Red lines are total ONVMS for a library small ISO, green is primary, black secondary, and blue tertiary total ONVMS for anomaly #2355.

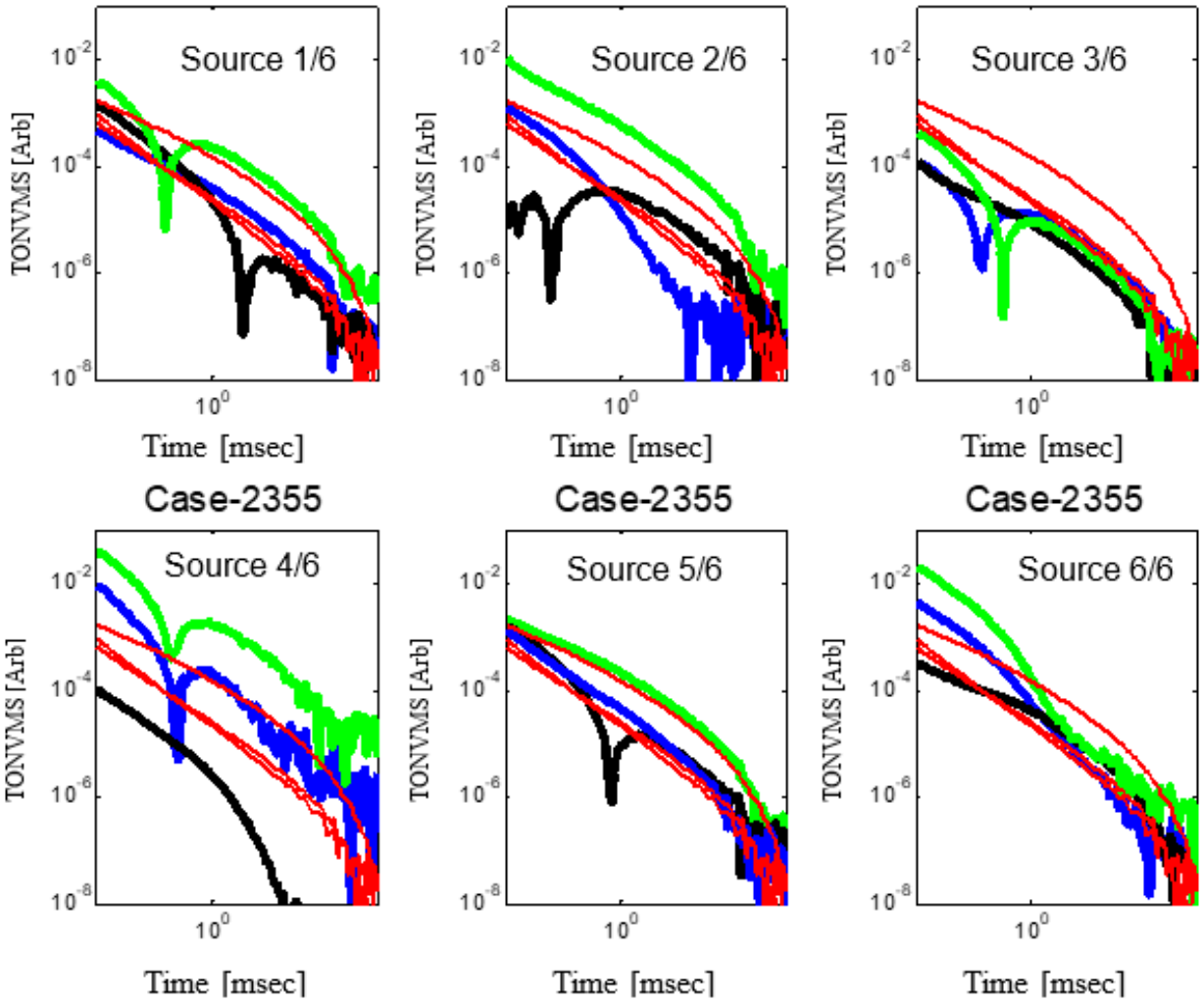

Figure 36. Six-target Inversion Results: Time-dependent Total ONVMS, Inverted from MPV-II Data, for Spencer Range Anomaly #2355

Red lines are the total ONVMS for a library small ISO, green is primary, black is secondary, and blue is tertiary total ONVMS for #2355.

7.1.2 Massachusetts Military Reservation, MA

The classification studies at the MMR site was conducted in two separate, 3 acre areas (northern and southern) of the Central Impact Area (CIA). MM data were only collected in the southern area; TEMTADS data were primarily collected in the northern area. In addition, TEMTADS data were also collected over 300 targets in the southern area to provide an overlap with a portion of the MM targets, see Figure 20.

The data sets were processed and dig lists were created for each sensor independently using advanced EMI models outlined in [19], [21], [42]-[52]. The final dig lists were submitted to the IDA for independent scoring. The scored results in the form of the ROC curve are shown in Figure 37 and Figure 38 for 2x2 TEMTADS and MM systems, respectively.

The result clearly shows that advanced EMI sensing and classification technologies are applicable for MMR site active UXO sites, which is a very highly contaminated and cluttered site. This high-density area included approximately 800 anomalies per/acre in the demonstration area. The results on the Figure 37 show that the 2x2 TMETADS system is able to leave at least 86% and 78% of clutter items in the ground to correctly classify 95% and 100% TOIs, respectively.

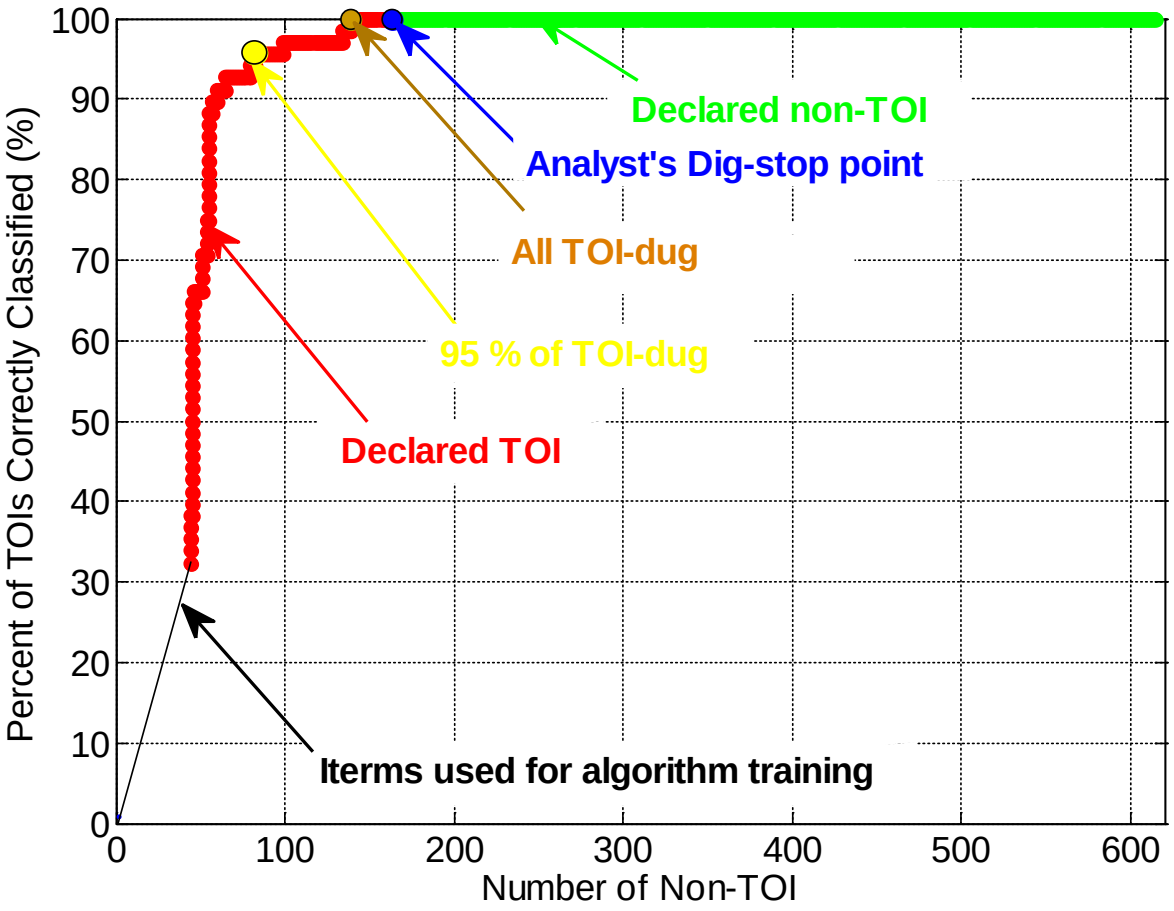

Figure 37. ROC Curve for the MMR 2x2 TEMTADS Data

Similarly, the independent scored results depicted in Figure 38 show that the Metal Mapper sensor and advanced models can be used at the highly cluttered MMR UXO sites. Namely, the results show that of the 65 targets that were dug for training, 52 targets were not TOI (shift along *x*-axis) and 13 were (shift along *y*-axis); all TOI targets were ranked as "Dig," except one native 81-mm projectile. Thus, the technology provides the ability to leave at least 88% and 67% of clutter items in the ground to correctly classify 95% and 100% TOIs, respectively.

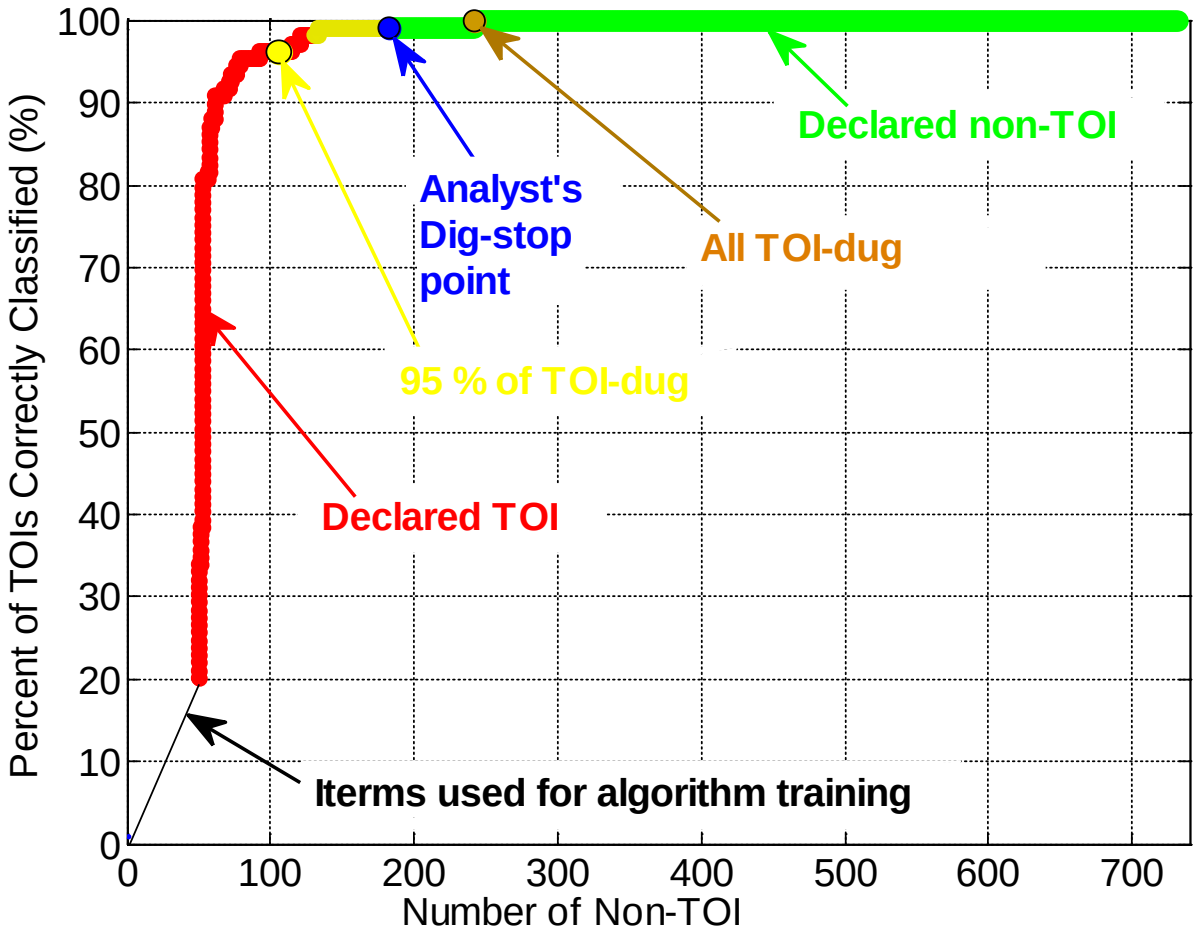

Figure 38. ROC Curve for the MMR MM Data

To compare the performance of two separate systems at highly cluttered UXO Live Sites, cued data were collected using both the MM and the 2x2 TEMATDS systems over the same 300 anomalies in the southern grids. A comparison of the classification performance between MM and 2x2 TEMATDS obtained by our team is shown in Figure 39. The comparison shows that the classification results are nearly identical, which leads to conclusion that either sensor can be used effectively at this highly cluttered site.

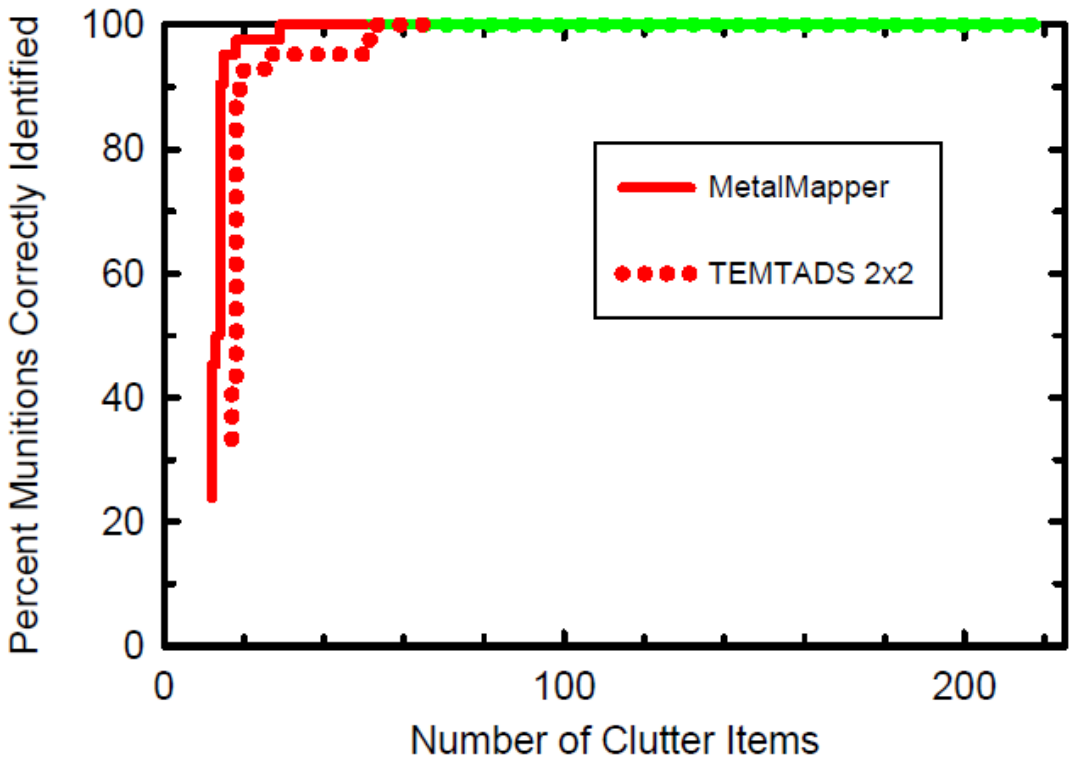

Figure 39. ROC Curves of MM and 2x2 TEMTADS Systems Develop for the Same Set of Anomalies

7.1.3 Camp Ellis, IL

The ESTCP demonstration at Camp Ellis was conducted over a 5 acre area located within and around a very high density target area, (Figure 21). Data were collected using MM and 2x2 TEMATDS systems. All TOIs, except one, were correctly classified. Namely, both systems missed the same TOI, anomaly #EL-941, a rifle grenade at 19 cm depth. Retrospective analysis showed: (a) there were a limited number of rifle grenades in each dataset (MM and TEMTADS datasets had only three and two rifle grenades, respectively); (b) the mis-classified EM-941 grenade was missing part of the head mechanism, and had different size and shape than other rifle grenades in the data sets; and (c) the inverted classification features for EL-941 were more closely matched the non-TOI rocket motors. These specific conditions made this anomaly particularly challenging for the analysists. The classification results in form of ROC curves are shown in Figure 40 and Figure 41 for MM and 2x2 TEMATDS systems, respectively. At the Stop-Dig point 12% of non-TOI were dug for the MM and 16% were dug for the TEMTADS 2x2. The actual reductions of clutter items at the point where all TOIs for MM and TEMTADS datasets were found was 82.5% and 63%, respectively. The slightly different classification result for MM and TEMTADS datasets at the point of finding all TOI illustrates the needs of having classification features in our library for various size and shape rifle grenades.

Retrospective Analysis for Camp Ellis, IL

Both MM and TEMTADS data classification analysts missed the same TOI, anomaly #EL-941, placed at 19 cm depth.

MM Data Set

There were only three rifle grenades within the Camp Ellis MM anomalies (EL-33, EL-132 and EL-941), see Figure 42. These targets have different sizes, forms and compositions. As a result, these anomalies produced varying total ONVMS (effective polarizabilities), which made it difficult for the analyst to rank EL-941 anomaly as "Dig." Figure 43 shows extracted total ONVMS (effective polarizability) for EL-33, EL-132 and EL-941. The comparisons between effective polarizabilities for these three rifle grenades illustrate that EL-33 produced significantly different polarizabilities than EL-132 and EL-941 anomalies, and there is a good correlation between primary polarizabilities for EL-132 and EL-941 anomalies, which helped the classification algorithm to keep EL-941 anomaly close to the "Stop-Dig" point. However, significant separation between secondary/tertiary polarizabilities for these targets confused the MM data analyst. As a result, the anomaly EL-941 was ranked as "non-TOI" and placed after the "Stop-Dig" point.

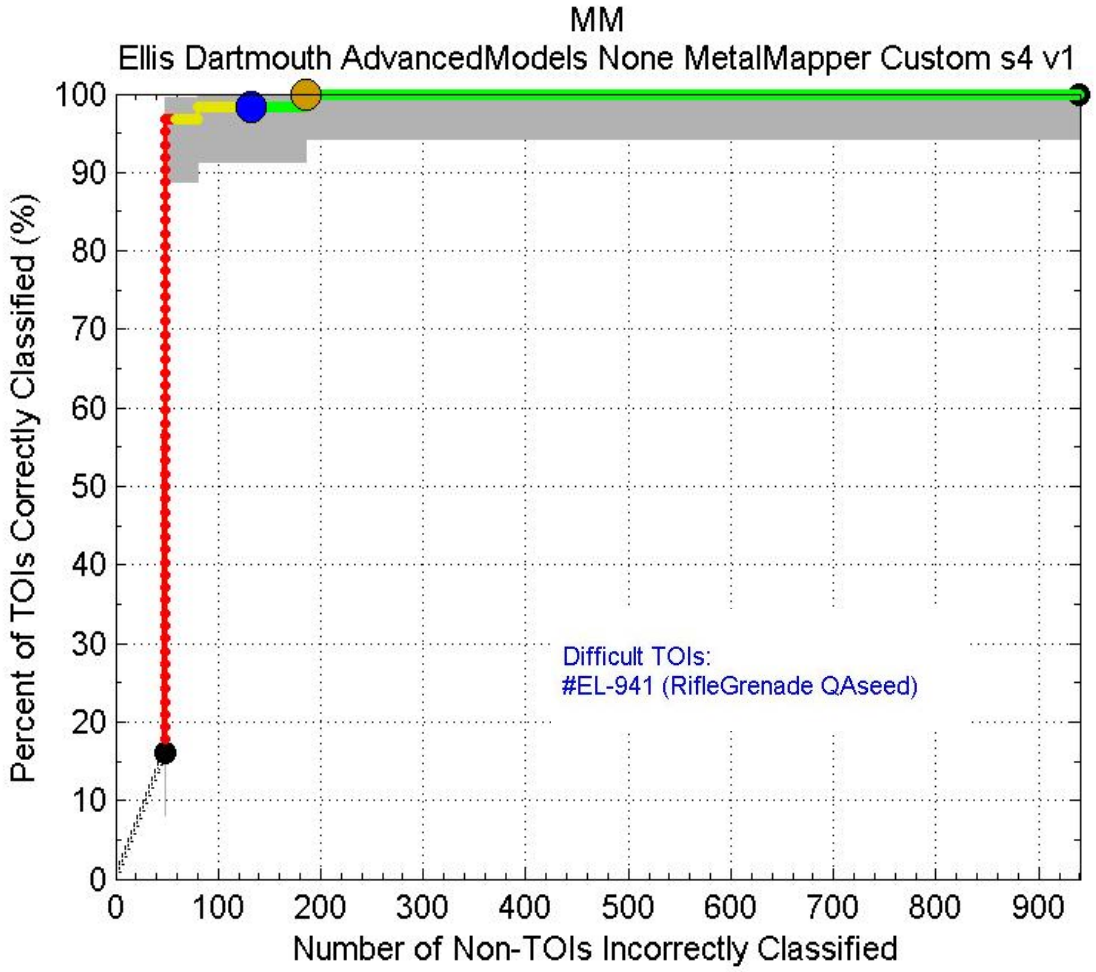

Figure 40. ROC Curve for the Camp Ellis MM Data

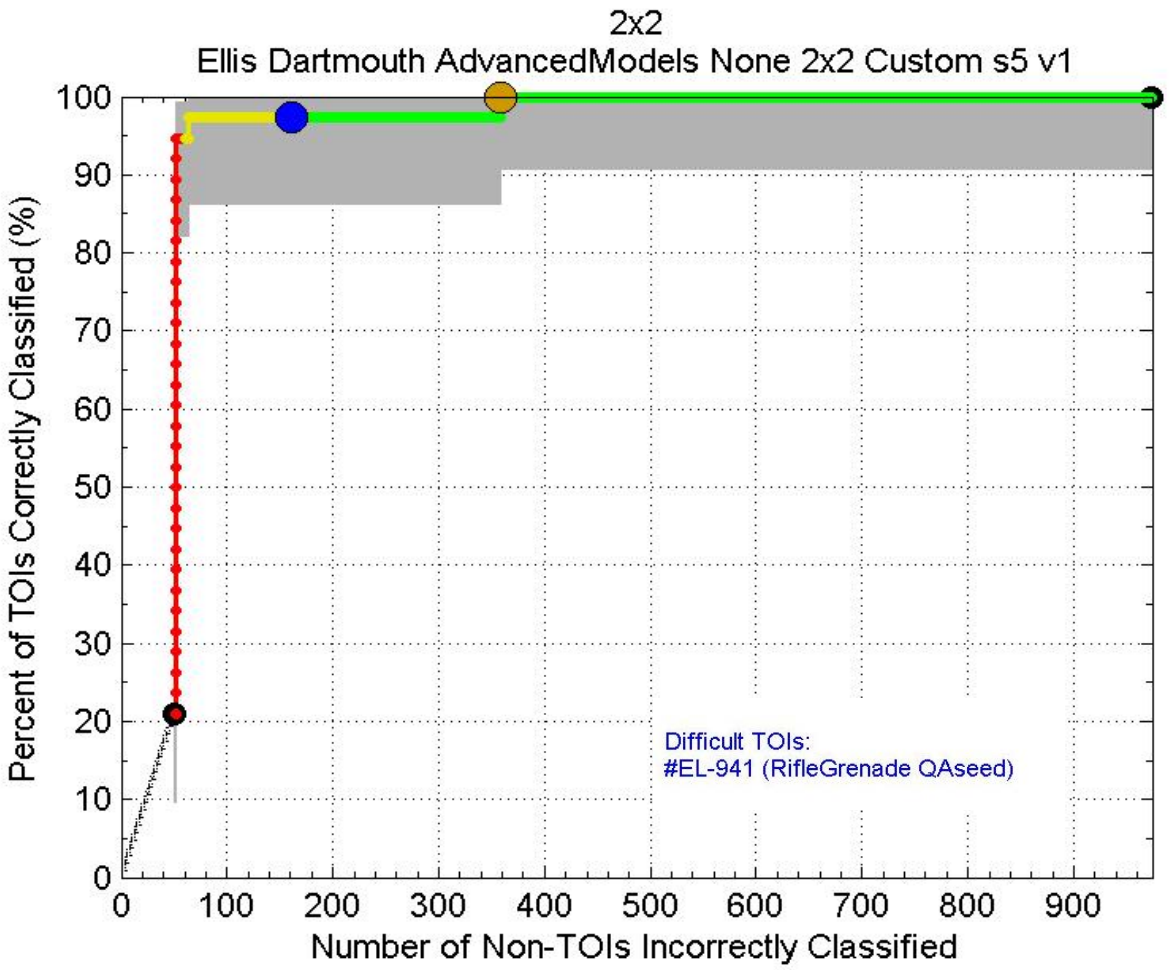

Figure 41. ROC Curve for the Camp Ellis 2x2 TEMTADS Data

Figure 42. Ground Truth Photos for Camp Ellis MM Anomalies (Left to Right) #EL-33, EL-132 and EL-941

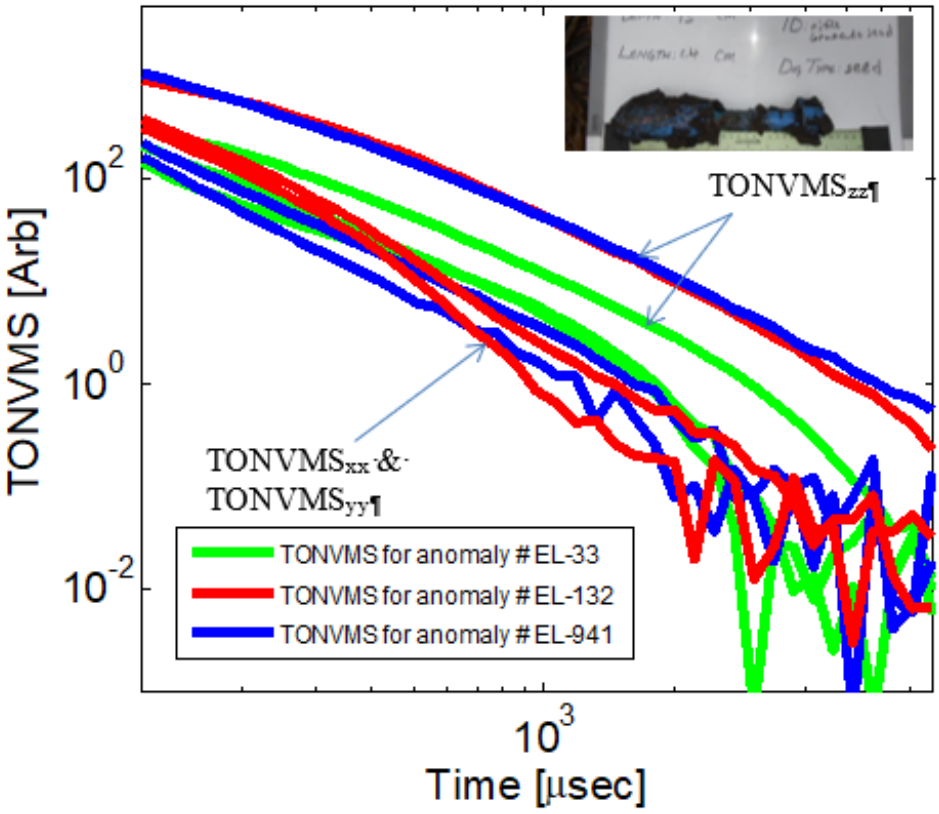

Figure 43. Inverted Total ONVMS Time-decay Profiles for Camp Ellis Seeded Rifle Grenades

TEMTADS Data Set

The TEMTADS data analyst missed the same EL-941 target. There were only two rifle grenades in the Camp Ellis TEMTADS anomalies (EL-319 and EL-941) list, see Figure 44. These targets had the same form, but different sizes (23cm and 20cm). Comparisons between extracted effective polarizabilities for EL-319 and EL-941 anomalies are depicted in Figure 45. The results show significant differences between polarizabilities for these two rifle grenades. Because of these discrepancies, as well as the limited number of rifle grenades in our library, the EL-941 anomaly was placed after the "Stop-Dig" point. In addition, it is worth noting that the TEMTADS analysts moved EL-941 anomaly form position 213 in the ranked Dig List (#s2-v2 Figure 46) to position 412 in the Final Dig List (S5-V1, Figure 41). This change in position of the rifle grenade in the Dig List is significant because it shows that the operator marked it a clutter. We believe that including more rifle grenades, with different sizes, shapes and compositions, in our library could have placed EL-941 anomaly before the final "Stop-Dig" point.

Figure 44. Ground Truth Photos for Camp Ellis TEMTADS Anomalies #EL-319 and #EL-941

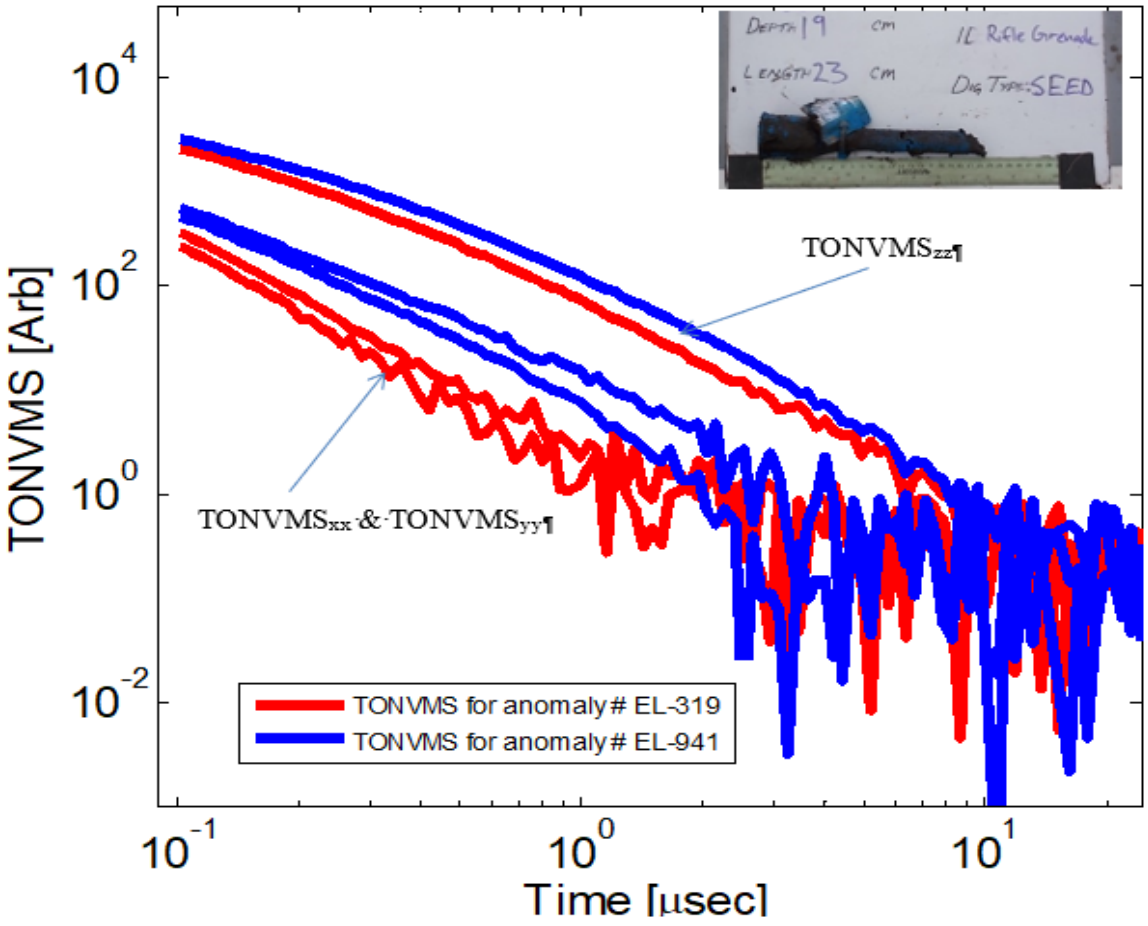

Figure 45. Inverted Total ONVMS Time-decay Profiles for the Camp Ellis Seeded Rifle Grenades, 2x2 TEMTADS Data Set

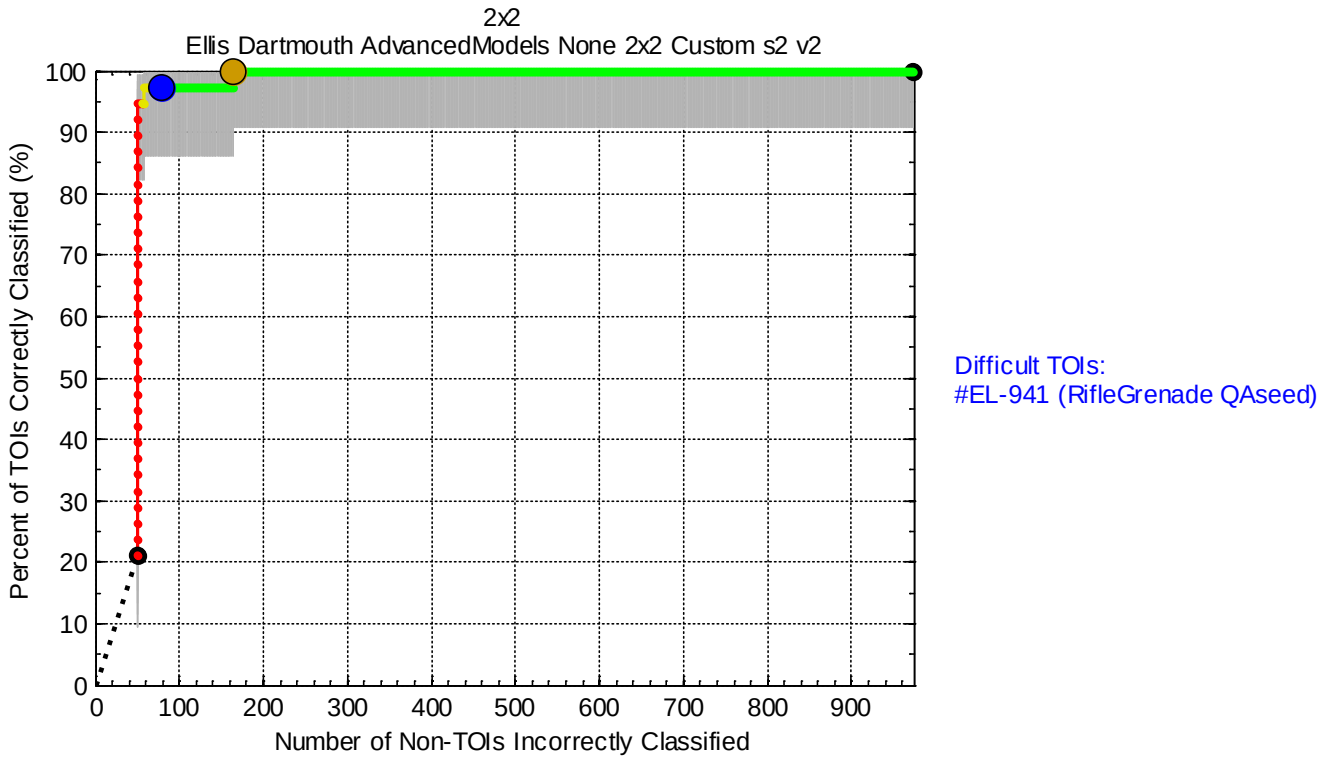

Figure 46. S2-V2 ROC Curve for the Camp Ellis 2x2 TEMTADS Data

7.1.4 Fort Rucker, AL

The ESTCP UXO Live Site classification demonstration at Fort Rucker, AL was conducted on well-maintained grassy areas with few trees (Figure 22), using both MM and 2x2 TEMTADS systems. Our team processed and classified the MM dataset using the advanced EMI approaches, see [45]. All TOIS were correctly classified, however due to similarities between TOI (2.36" and 3.5" rocket motors) and their associated frag (fins, slugs, cone), the algorithm did not correctly classify 75% of the non-TOI. Actual percent reductions of clutter items at the "Stop-Dig" point was only 43%. Although our advanced classification methods were able to correctly identity all TOIs, the comparisons between costs for advanced classification and an old flag/dig approaches indicates that at this highly contaminated UXO site it will be more cost effective to use the old "Flag and Dig" approach than using advanced classification. The independently scored results in the form of a ROC curve is shown in Figure 47. The result shows that of the 20 targets that were dug for training, 8 targets were not TOI (shift along *x*-axis) and 12 were TOI (shift along *y*-axis); all TOI targets were ranked as "Dig."

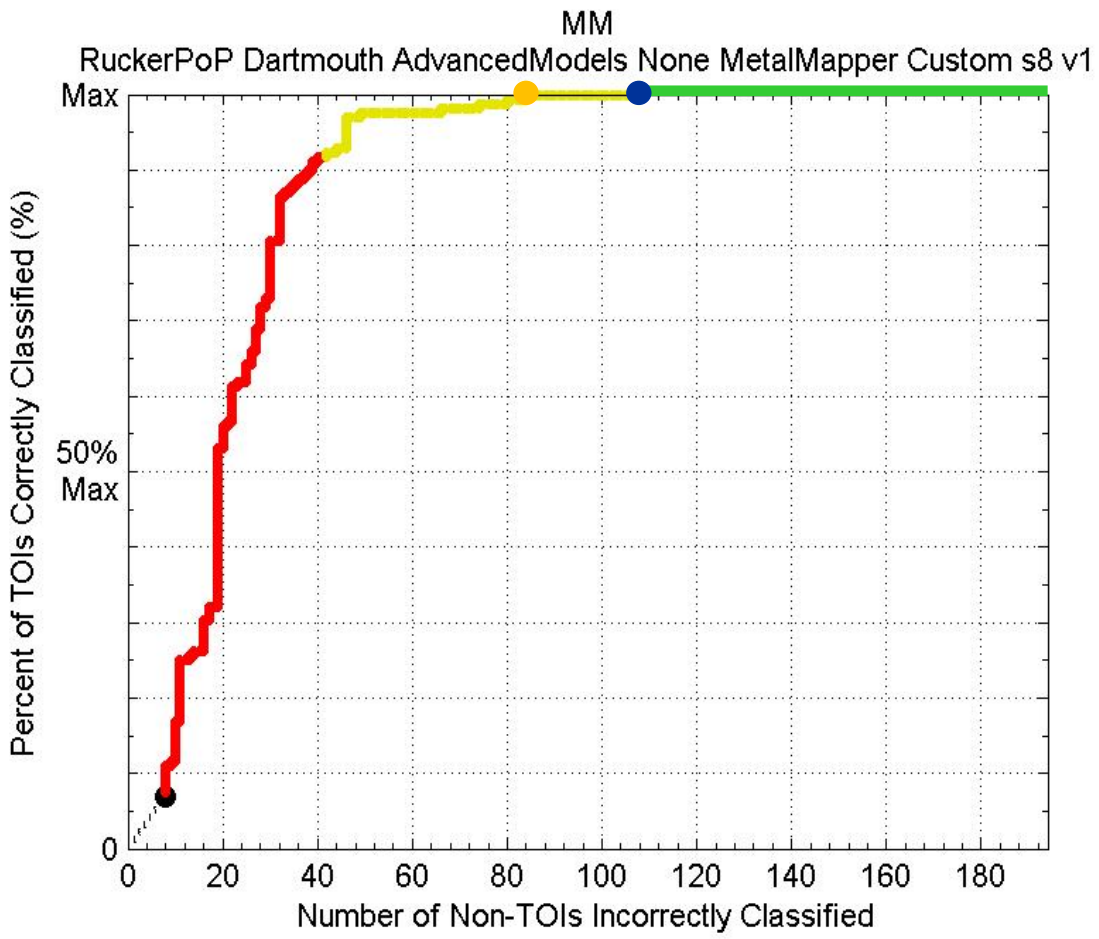

Figure 47. ROC Curve for the Camp Rucker MM Data

7.1.5 New Boston AF Station, NH

This classification study at New Boston Air Force Station was conducted on a subset of a 115 acre size MU705 Shooting Fields, which is a moderately sloped area with portions heavily forested with dense brush (Figure 23). The intrusive investigation of NBAFS anomalies showed that about 70% of anomalies were TOIs. Furthermore, ground truth analysis revealed, that forty-eight out of seventy-eight anomalies were 20-mm projectiles but were ranked as munition debris by the ESTCP office, because they were found below the pre-defined 15cm detection depth. Due to particular high-density TOI contamination at the NBASF site, the classification algorithm was able to reject about 55% (or 62.5% if forty-eight anomalies are counted as TOIs) false positives. A comparison of costs for WRT's advanced classification approach versus a traditional flag/dig method indicates that at this site it will be more cost effective to use a "Flag and Dig" approach than advanced classification. The partial ROC curve obtained via our advanced EMI models is shown in Figure 48. The results show that there were 10 "Can't Analyze" anomalies (solid black line), and in the first stage 134 out of 150 MPV anomalies were ranked as "Dig." Out of 134 excavated anomalies, 57 were non-TOIs.

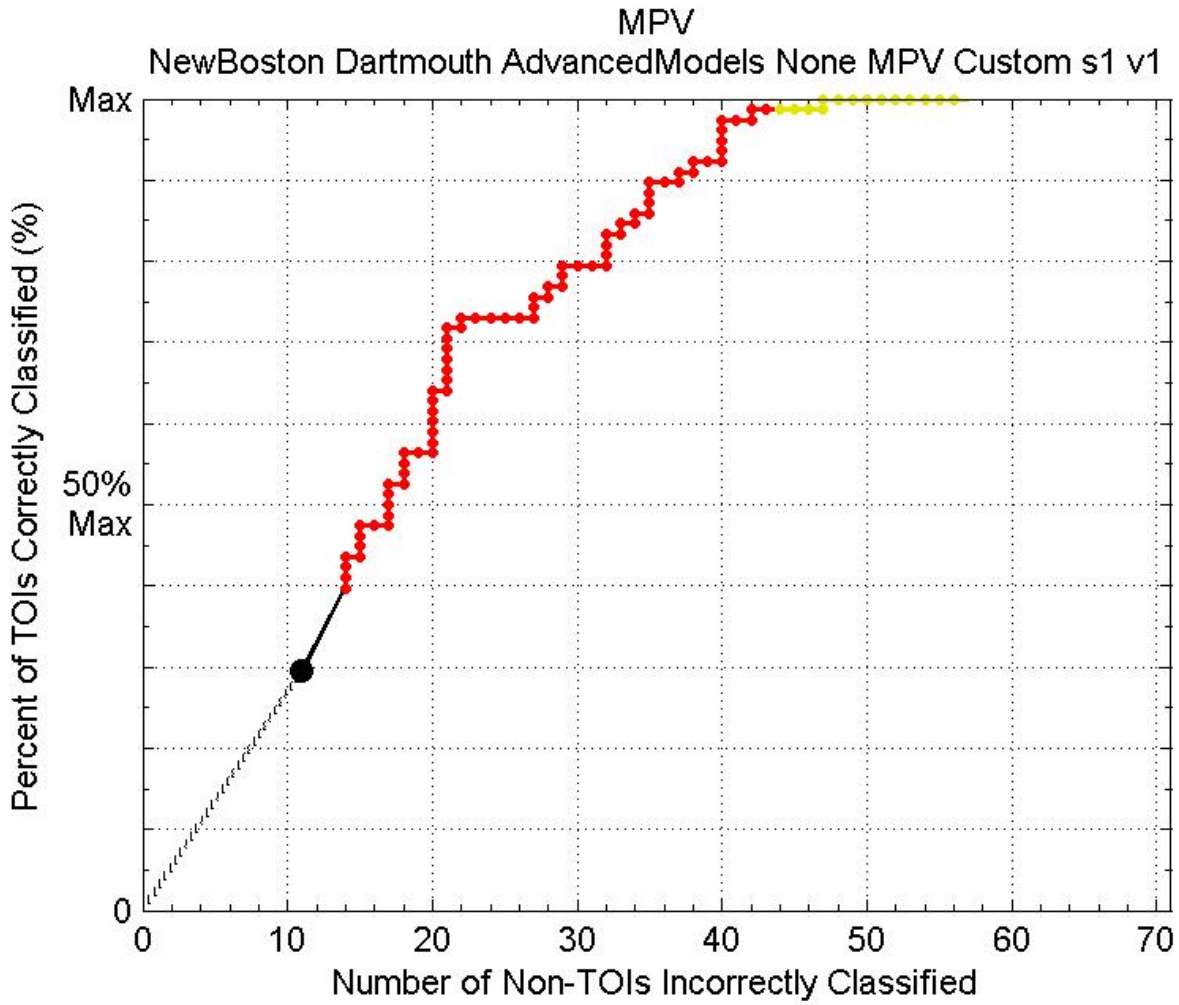

Figure 48. ROC Curve for the NBAFS MPV Data

7.1.6 SWPG, AR

The ESTCP UXO Live Site classification demonstration was performed on Recovery Field 15 (RF 15) of SWPG, Figure 24. The data were collected in cued mode using the both 2x2 TEMTADS and MM systems. Using advanced EMI models, all targets were classified as TOI or clutter, and the final prioritized dig lists were created independently and submitted to ESTCP for independent ranking. The independent scored results are shown in Figure 49 and Figure 50. The studies showed that our classification approaches were able to successfully mark all TOIs as "Dig" before the "Stop-Dig" point with a reduction in false alarms of 92.5% and 94% for the 2x2 TEMTADS and MM, respectively.

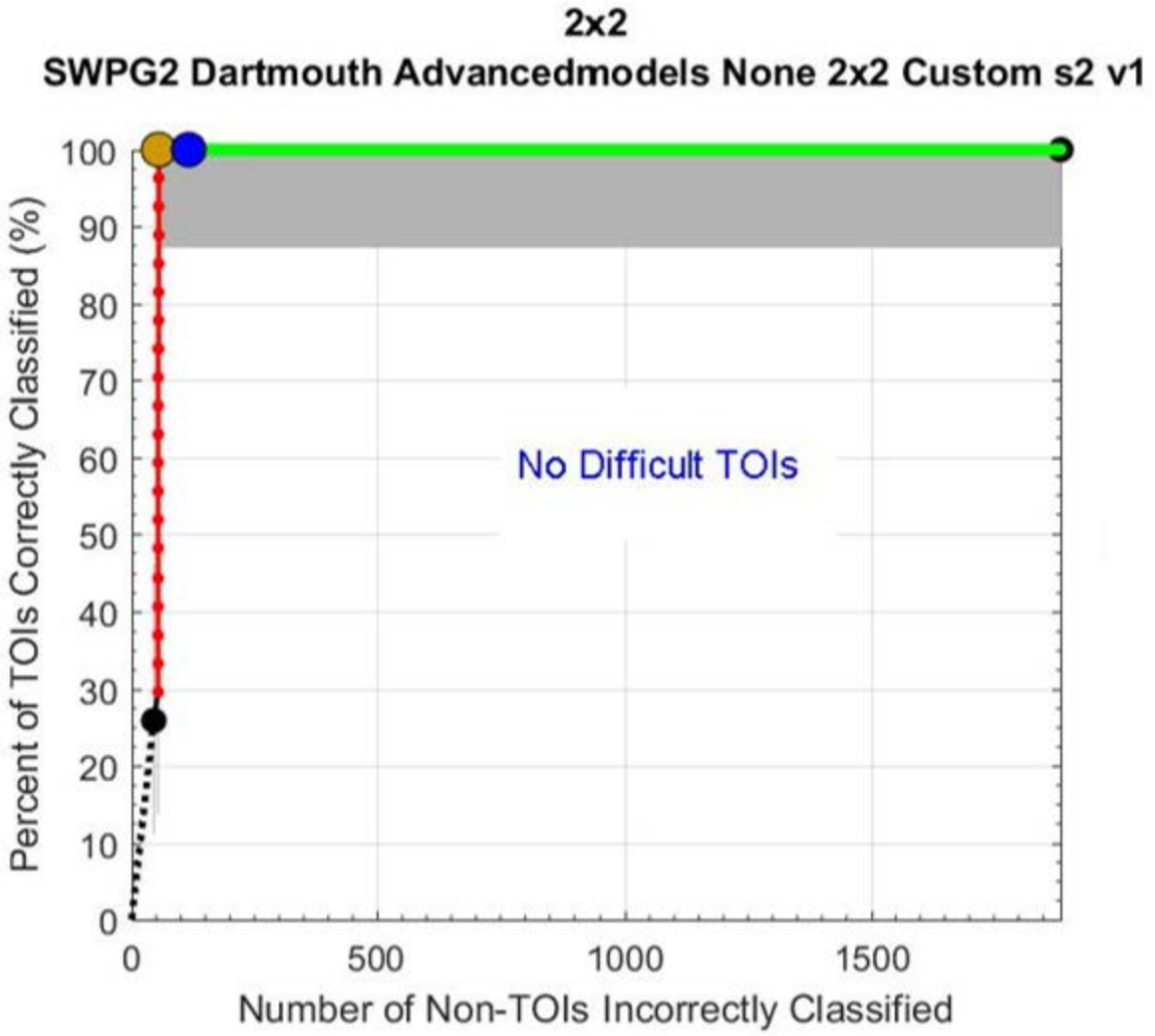

Figure 49. ROC Curve for the SWPG 2x2 TEMTADS Data

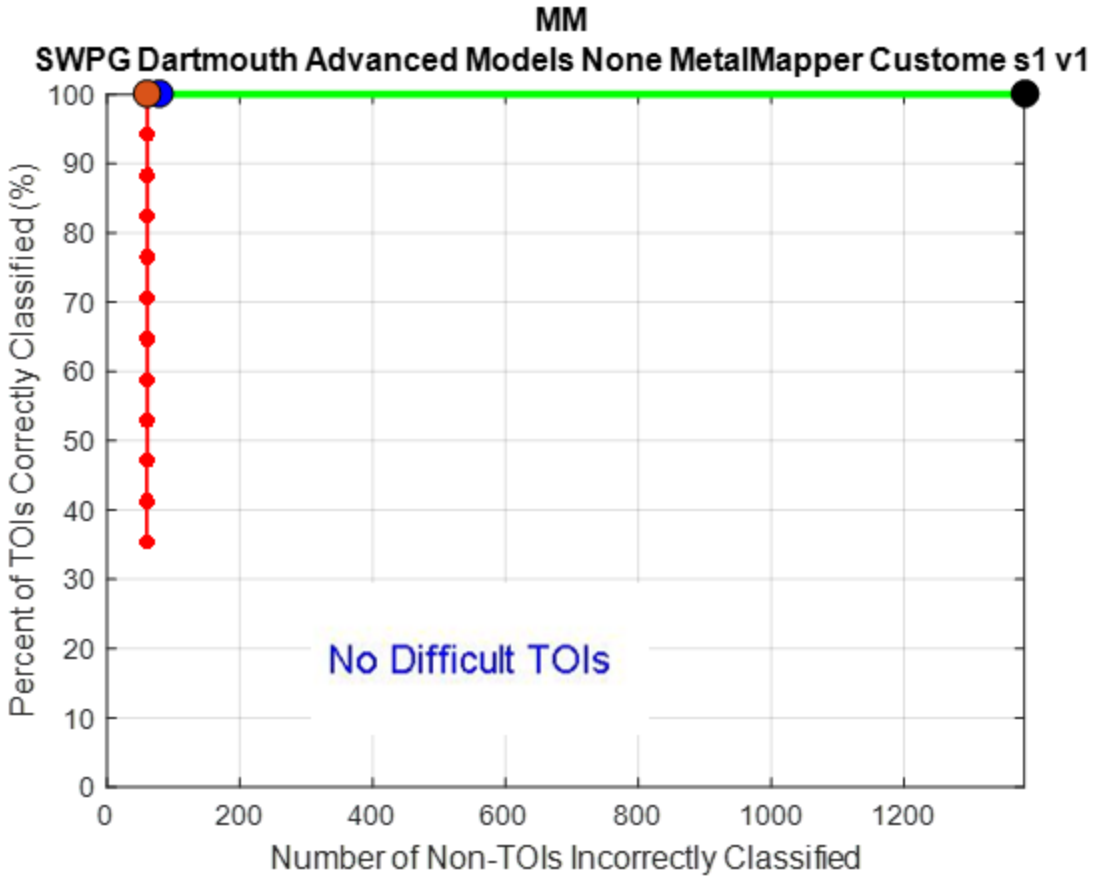

Figure 50. ROC Curve for the SWPG 2x2 MM Data

7.1.7 Waikoloa Maneuver Area, HI

This demonstration was conducted over three areas of interests at the Waikoloa Maneuver Area, HI: T20Area A, TO20 Area B, and TO17, using the MM system. A map of the demonstration area and area of interests is shown in Figure 25. The data were processed, and all targets were classified as TOI and clutter using the advanced EMI models. The prioritized dig list was generated and submitted to the ESTCP office and scored against the ground truth from the intrusive investigation. WMA classification studies showed that the advanced models are able to separate targets responses from magnetic soil responses without any difficulties when the distance between target and sensor was less than 30 cm. However, two seed items were incorrectly classified as nonhazardous clutter. Failure analysis (see next section) indicated that the incorrect classification was due to the combination of lateral offset, strong geological background responses, and breakdown of one of the receiver cubes. Namely, misclassification of one of the two targets was due to significant (43 cm) offset between the MM data collection point and the actual location of the seed. The second incorrect classification appeared to be a result of combination of: (a) the large offset (27.9 cm) between the MM center and the seed target; and (b) the complete failure of one MM receiver cube (Rx#0) adjacent to the actual seed target. We believe that having a robust in-field or off-line quality check step could guide an operator to place the sensor close to the anomaly, collect high quality data, and avoid these misclassifications in challenging sites, such as WMA.

The Figure 51 shows the final scored ROC curve. The result shows that all TOI targets were ranked as “Dig” except one small ISO and one 60mm mortar, which laterally were offset more or about than 30 cm from the center of MM sensor. The result clearly shows that advanced EMI sensing and classification technologies can be applied to active and challenge UXO sites, which in addition to man-made clutter also consists of magnetic soils. In addition, these studies show that even when targets are buried in a highly susceptible magnetic soil, the technology provides the ability to leave at least 80% of clutter items in the ground if the lateral offset between the center of the sensor and the acquired target is less than 30 cm.

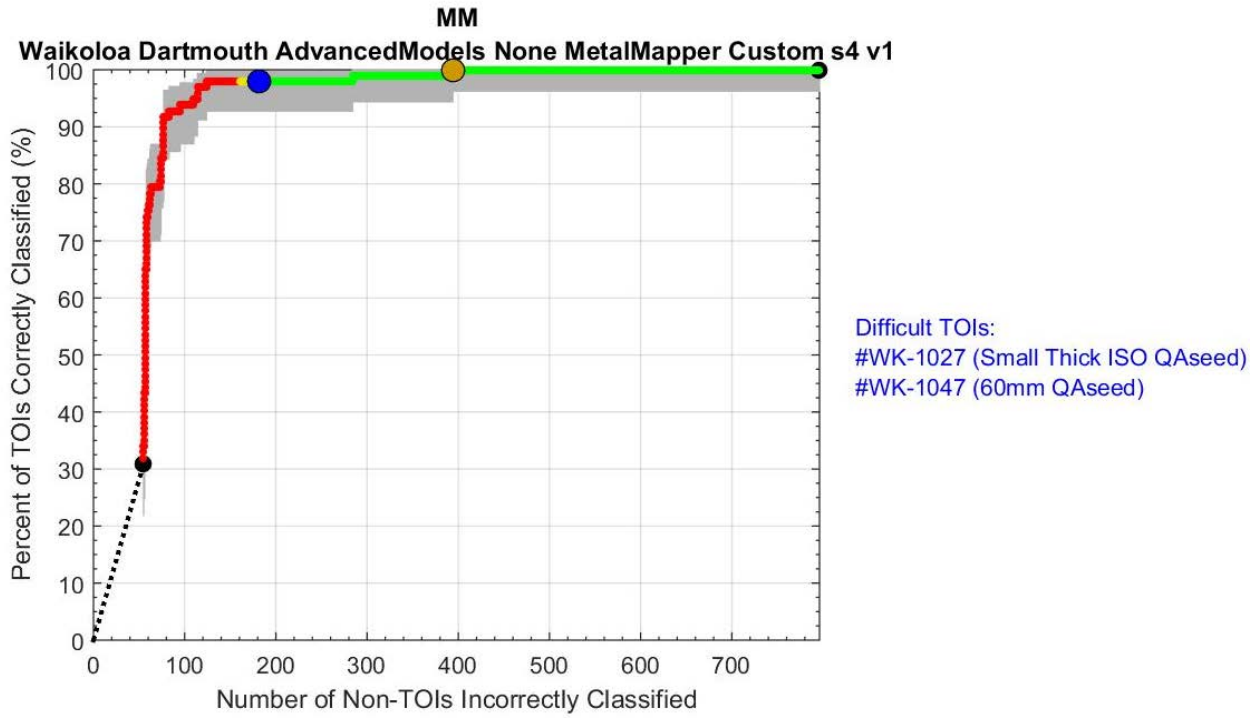

Figure 51. ROC Curve for the WMA, HI, MM Data

WMA Root Cause Analysis

To understand the cause of mis-classifying two TOIs, we re-examined the classification procedures for all WMA anomalies. Classification studies were conducted at three areas, including T017 and T20-A and T020-B. The T017 and T020 areas were chosen to understand how lava flows under the sites introduce an effect on the geological background responses and subsequent target classifications. The T017 site is near the coast and the lava flow underlying it is considerable younger than the lava flow underlying the two T020 sites. Both of the missed TOIs were in area T017. To assess geological background responses, we analyzed the largest eigenvalues versus time for soils in these areas when the sensor was placed on the ground. The results in Figure 52 show that the geological background response for the T017 area is higher than background responses for area T020A and T020B. Typically, high background responses degrade the data and cause mis-classifications, particularly when the lateral offset of the target is more than approximately 30cm from the center of the sensor.

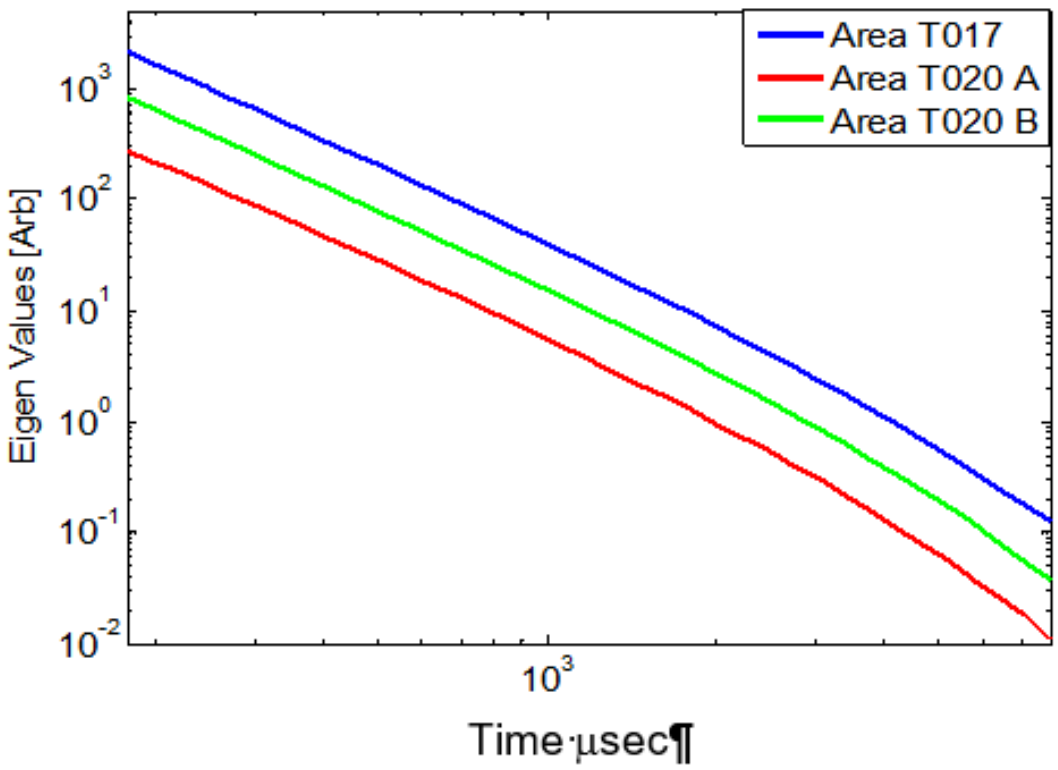

Figure 52. Eigenvalues Versus Time for Three WMATest Areas: T017, T020 A and T020 B

In addition to geological background noise, the malfunction of the EMI sensor significantly effects target classification as well, particularly when the failed sensor is in close proximity to the target. Unfortunately, during the WMA MM data collection one of the receivers failed completely. Namely, all three components of Rx#0 did not work properly, and the responses measured by receiver Rx#0 were not included in the data inversion and processing. The inverted total ONVMS (effective polarizabilities) and eigenvalues for the mis-classified small ISO (anomaly #1027) and 60mm mortar (anomaly #1047) are depicted on Figure 52. The inverted effective polarizabilities for the anomaly #1027 shows some symmetry but its magnitude is much smaller than the library ISO target (Figure 7). Also, the plot of eigenvalues versus time show that there is a significant soil response as well (see the eigenvalues linear decay in the log-log plot of Figure 52). To better understand why the inverted effective polarizabilities for anomaly #1027 do not match the effective polarizabilities for small ISO target in the library, we checked the distance between the center of the MM sensor and dug target location. The analysis shows that for the anomaly #1027, the center of the sensor was located 27.9 cm from the target. Since this offset is less than 30 cm, the extracted classification parameters should have been robust and closely correlated with the effective polarizabilities for a library signature for the small ISO target. However, after further investigation it was found that the closest Rx sensor to the target was the failed Rx#0 sensor. This and the dominant ground responses in other sensors caused the algorithm to mis-classify this small target. We believe that positioning the center of the sensor closer to the anomaly, or having properly working Rx adjacent to the target, could have avoided this misclassification.

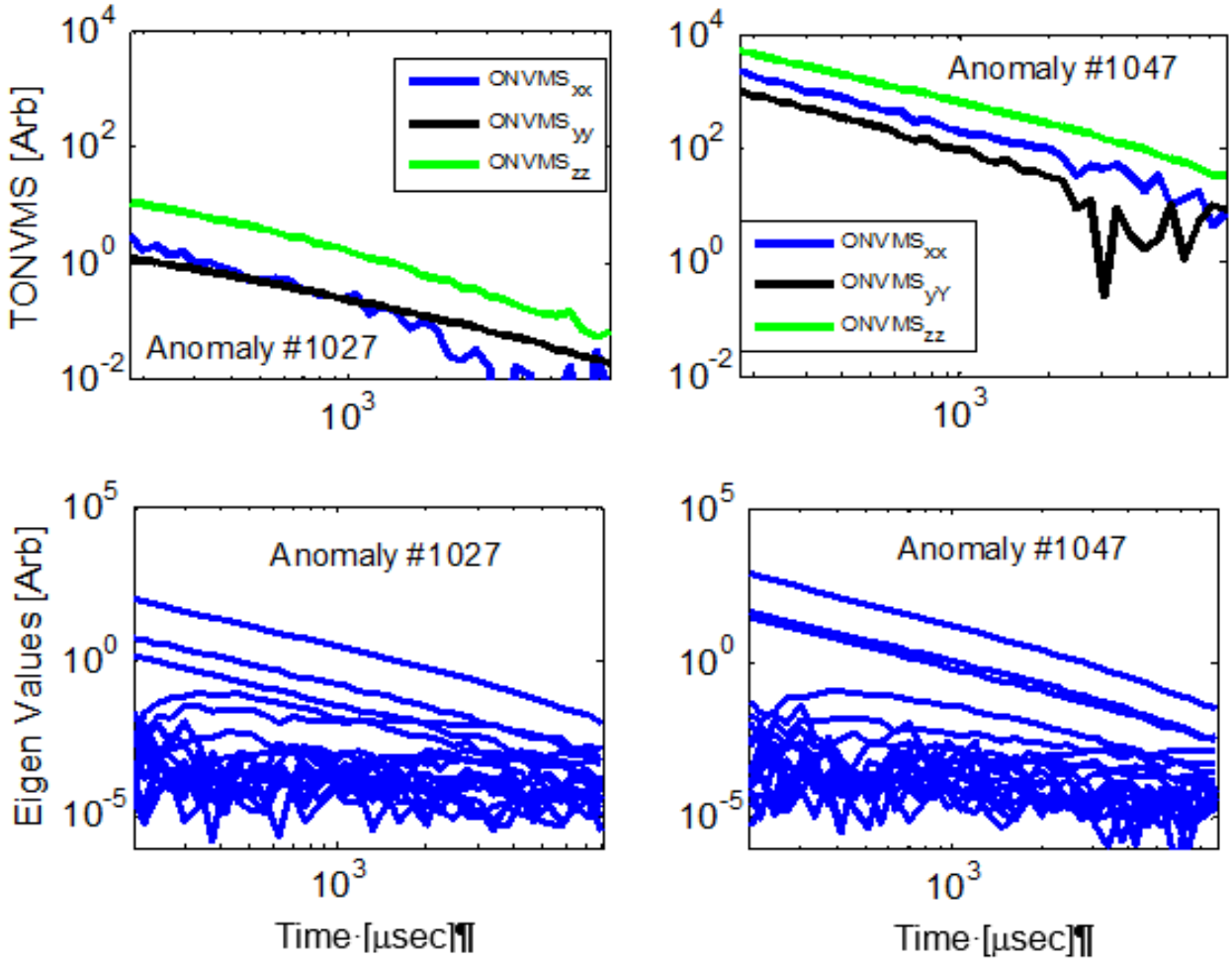

Figure 53. Total ONVMS and Eigenvalues for Missed Small ISO (anomaly #1027) and 60 mm Mortar (anomaly #1047) Targets

For seed WK-1047, the sensor was located 43 cm from the target. This offset is significantly outside the 30 cm objective radius and as a result the extracted polarizabilities values are high but not symmetric. The polarizabilities decay linearly on the log-log scale, and the response looks more like a soil characteristic than the response from a compact 60 mm mortar. While in the case of non-permeable soil conditions, our algorithms were able to obtain accurate classification features at more than 30 cm offsets, we believe the presence of a significant magnetic ground response made it very difficult to extract robust classification features with the sensor at this 43 cm location for anomaly #1047.

Discrepancies Between Classification and Intrusive Results

All intrusive operations at the WMA UXO Live Site were conducted by Parsons's personnel. According to the report MR-201104-DR-Waikoloa: Parsons used the Minelab Explorer SE to determine the initial approach to every target, and as a screening process to assess if either metal was present in the subsurface, or the anomaly was caused by the local geology.

If the Minelab Explorer SE indicated that there was no metal present in the area, the anomaly was considered a “No Contact.” A GPS point was taken at the location of the flag and a photograph collected of the area surrounding the flag. If the Minelab Explorer SE indicated that metal was present in the subsurface, then the UXO technicians excavated the item. Location data captured by GPS were used to document the center of mass and the depth of each item. A photograph was also collected of the item. Lastly, an EM61 unit was used to scan the location to confirm the absence of all metal items from that target location, or that the pre-millivolt reading had been reduced by at least 75%.

Using the above described intrusive investigation approach, Parsons considered anomalies #29, 36, 199, 441, and 442 as “No Contacts” (Figure 54). However, MM data and our classification results depicted in Figure 55, Figure 56 and Figure 57 clearly show that there are compact metallic targets (see eigenvalues vs time and total ONVMS). The effective polarizabilities of these anomalies closely match the polarizabilities of 37-mm projectiles and 60-mm mortar in the library, indicating that the intrusive procedure failed to document all detected targets correctly, or the procedure failed to detect and clear all hazardous targets on the site. If the latter occurred, then we believe that the MineLab explorer SE is not a suitable system for metallic target detection in magnetic soil, and for accurate clearance of UXO sites classification results must be used to guide and validate intrusive investigation results.

Figure 54. Photos of Intrusive Investigated Anomalies #29, #36, #199, #441, #442

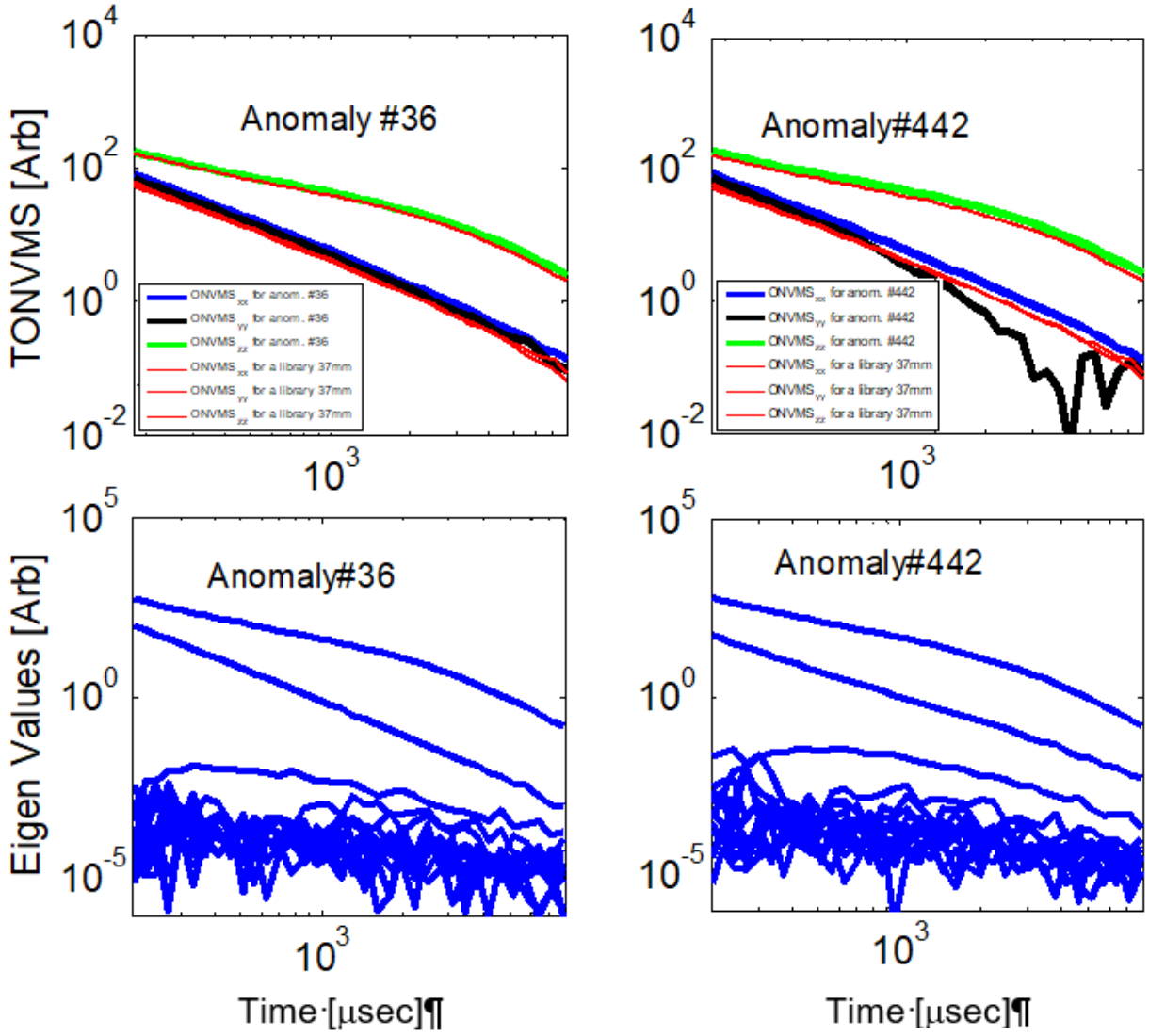

Figure 55. Top Row: Comparisons Between Total ONVMS for a Library 37-mm Projectile (Red Lines), with a Copper Band, and for Anomalies #36 and #442. Bottom Row: Eigenvalues Versus Time for Anomalies #36 and #442

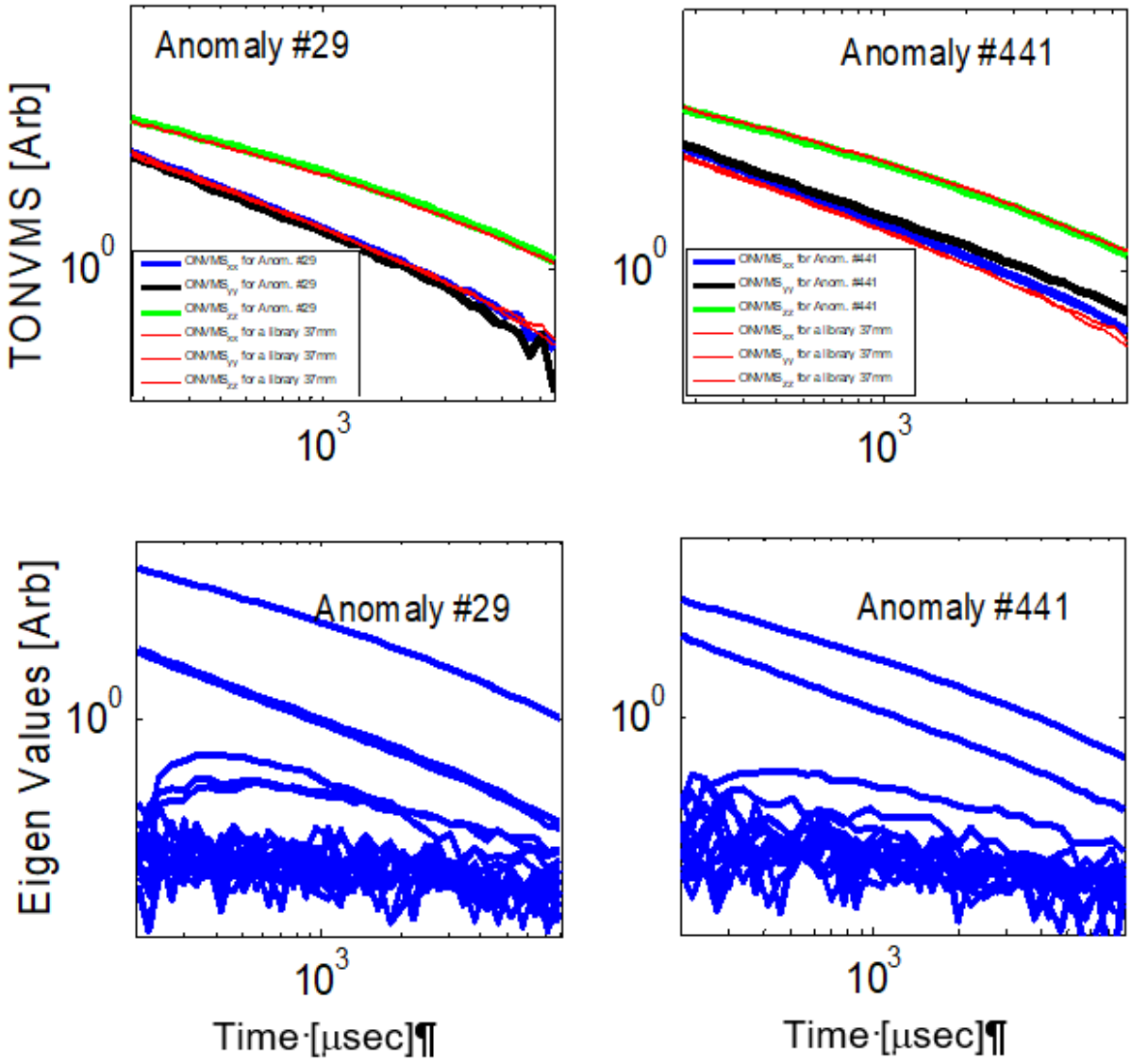

Figure 56. Top Row: Comparison Between Total ONVMS for a Library 37-mm Projectile (Red Lines), Without a Copper Band, and for Anomalies #29 and #441. Bottom Row: Eigenvalues Versus Time for Anomalies #29 and #441

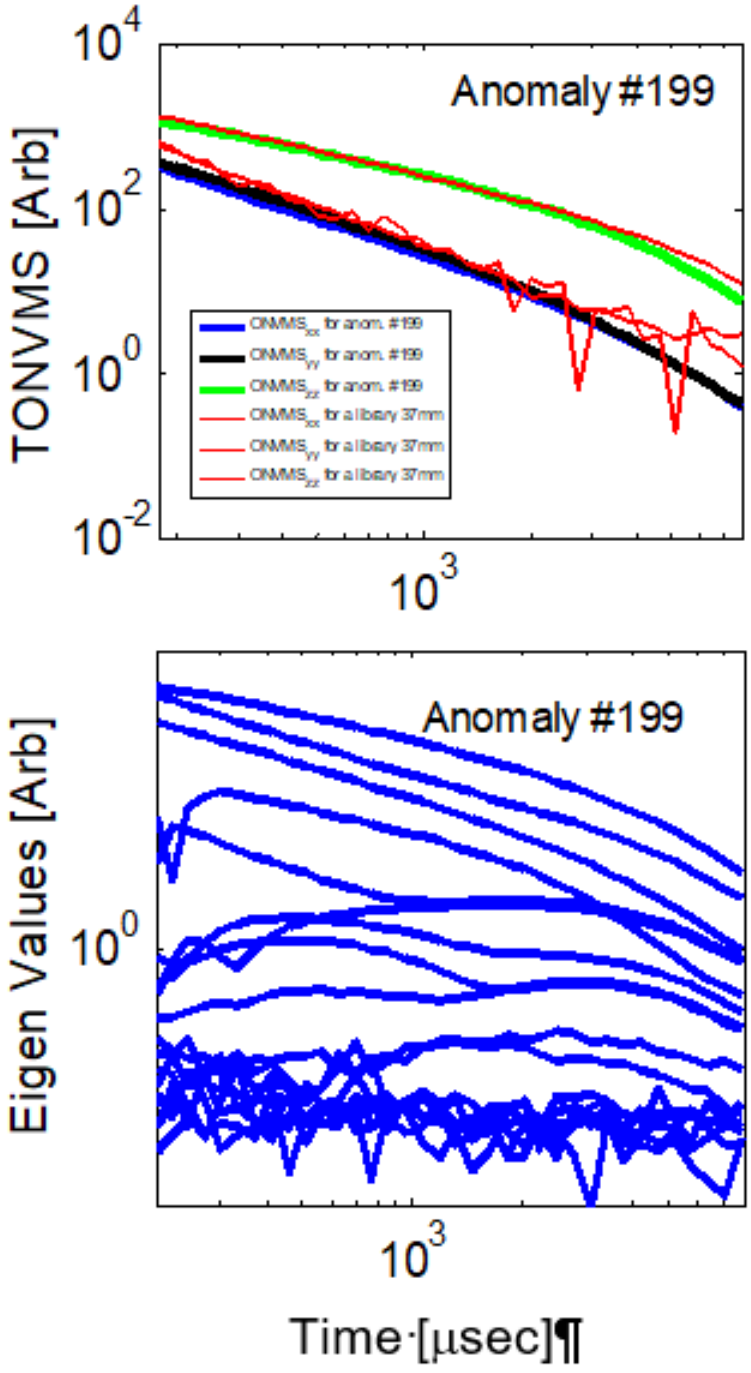

Figure 57. Top: Comparisons Between Total ONVMS for a Library 60-mm Projectile (Red Lines) and for Anomaly #199. Bottom: Eigenvalues Versus Time for Anomaly #199

7.1.8 Andersen AF Base, Guam

This ESTCP UXO Live Site study was performed in the North Ramp Parking (NRP) area of Andersen AFB, (Figure 26) as a part of undergoing a MEC removal action in advance of military construction (MILCON) activities. Geophysical data were collected using the 2x2 TEMTADS system in cued mode. Our team processed data for all anomalies and submitted the final prioritized dig list to the IDA for independent scoring. The scored result in the form of a ROC curve is shown in Figure 58. The result shows that all TOI targets were ranked as "Dig." The study clearly shows that advanced EMI sensing and classification technologies can be used as a part of removal action at active UXO sites. The technology provides the ability to leave at least 91% of clutter items in the ground.

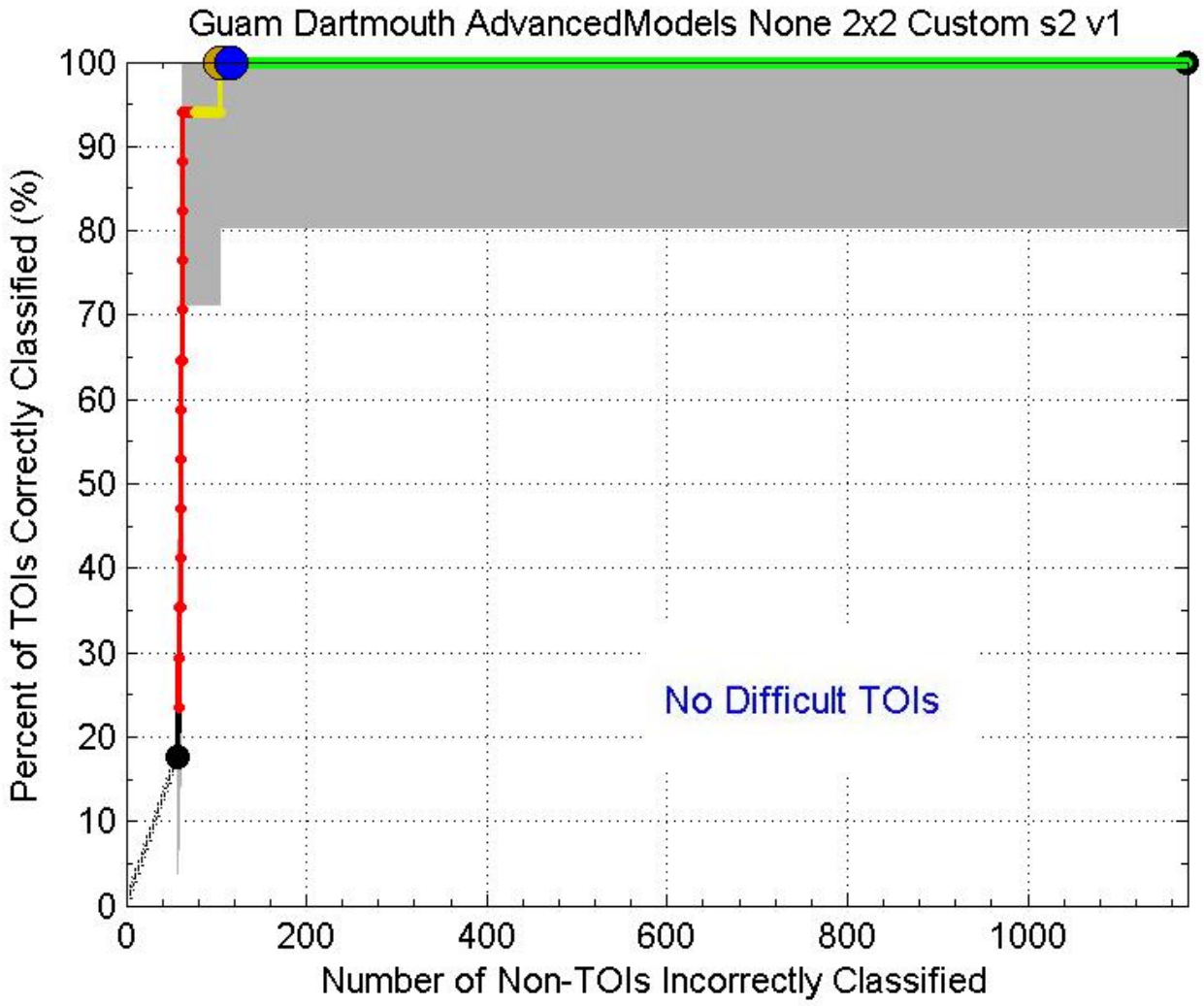

Figure 58. ROC Curve for the Andersen Air Force Base, Guam, 2x2 TEMTADS Data

7.1.9 Castner Range Fort Bliss, TX

The ESTCP demonstration has conducted on a 5 acre subset of the closed Castner Range MRS as shown in Figure 27. The data were collected using the 2x2 TEMTADS system in cued mode. All cued data were processed and intrinsic and extrinsic target parameters were extracted. Using the extracted intrinsic features (i.e., the primary, secondary and tertiary effective dipole polarizabilities) all anomalies were classified as TOI and no-TOI and the final prioritized dig list was created. The dig list was submitted to the IDA for independent scoring. Figure 59 shows the scored result in the form of a ROC curve. The result shows that of the 79 targets that were dug for training, 70 targets were not TOIs (shift along *x*-axis) and 9 were TOIs (shift along *y*-axis); all TOI targets were ranked as "Dig." The result clearly shows that the advanced EMI classification technology provides the ability to leave at least 90% of clutter items in the ground.

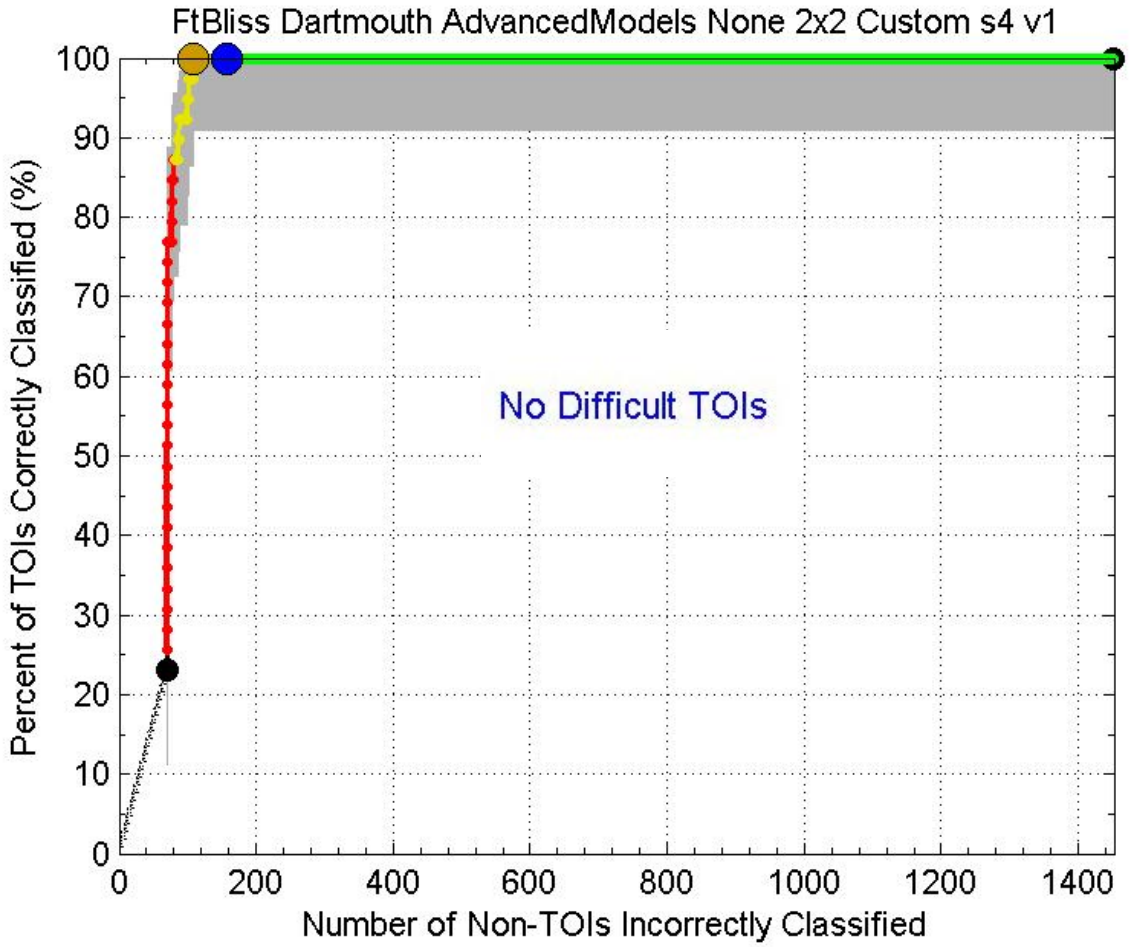

Figure 59. ROC Curve for the Fort Bliss, TX , 2x2 TEMTADS Data

7.1.10 West Mesa, NM

The ESTCP UXO Live Site classification study at the former Kirtland AF Base Precision Pombing Range was conducted on a 10 acre subset of the new demolition bombing site within the high- or medium-anomaly-density target areas (Figure 28). Data were collected in cued-mode using the MM system. All WM targets were classified as TOI and clutter, and a prioritized dig list was created and scored against the ground truth. The Figure 60 shows the scored result of the West Mesa classification study. The study shows that the advanced EMI models are able to detect and classify deep targets without difficulties. Namely, the algorithm was able to classify all hundred thirty-three seeded and nine native TOIs correctly. The nine native targets included four M30GP MEC and five intact 100-lb practice bombs. These results were achieved while keeping 87% non-TOIs in the ground. Thus, the advanced classification is a cost-effective approach for cleanup at West Mesa UXO Live Site.

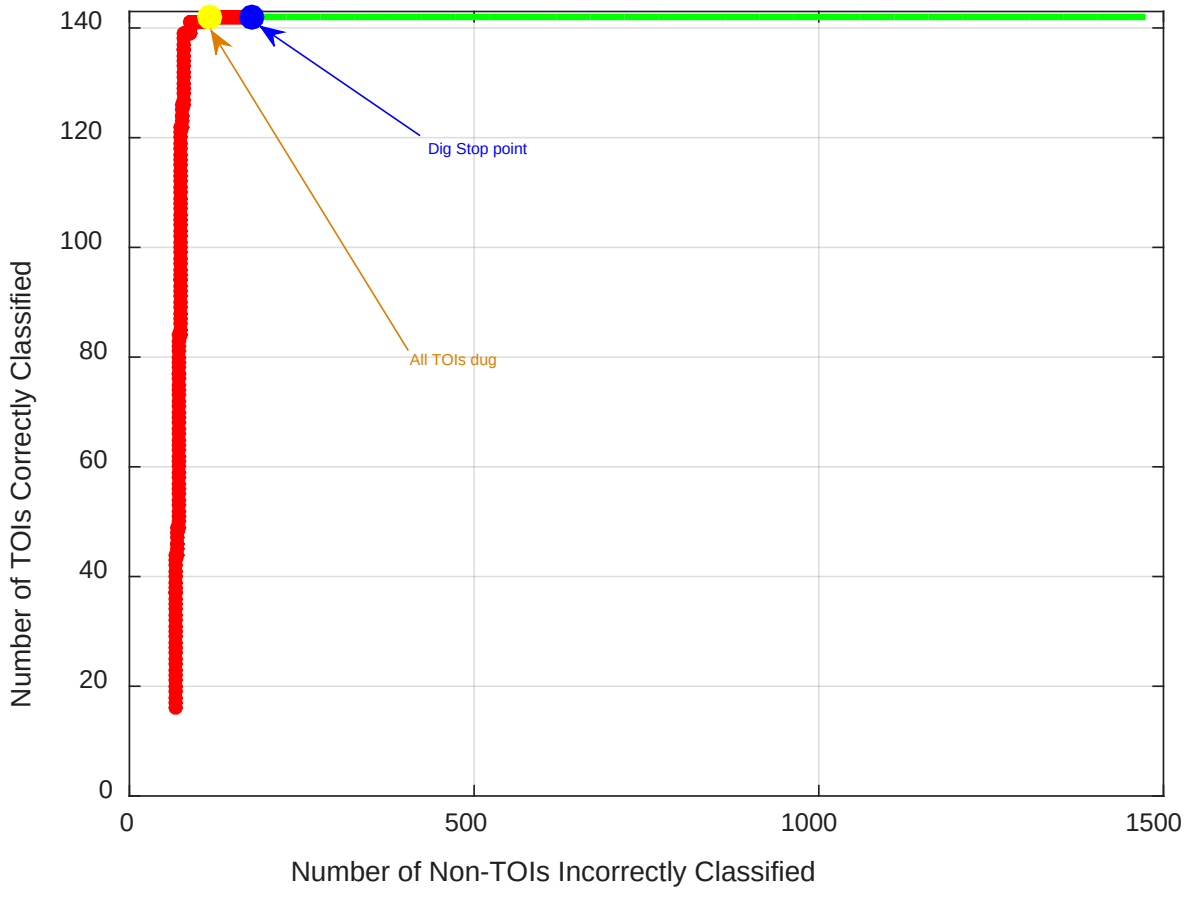

Figure 60. ROC Curve for the West Mesa, NM, MM Data

7.1.11 Fort Ord, CA

The ESTCP UXO Live Site demonstration at Fort Ord was conducted within a 5 acre subset of Units 11 and 12, which are located within the 476 acre Impact Area Munitions Response Area (MRA); see Figure 29. Cued data set was collected using the MM system. There were two main classification objectives: (1) detect and classify all large munitions such as 155-mm projectiles to a depth of 2 feet, with high confidence in medium-to-high metallic density area that exist in the Impact Area at Fort Ord; and (2) assess applicability of advanced classification technology for classifying smaller munitions, such as 40-mm projectiles, within the range of background conditions at Fort Ord (i.e., correctly classify 99% TOIs in all areas of low, medium and high density). Our team processed all cued data and classified anomalies as TOI and non-TOI items. The classification results in form of the ROC curves are depicted in Figure 61 and Figure 62.

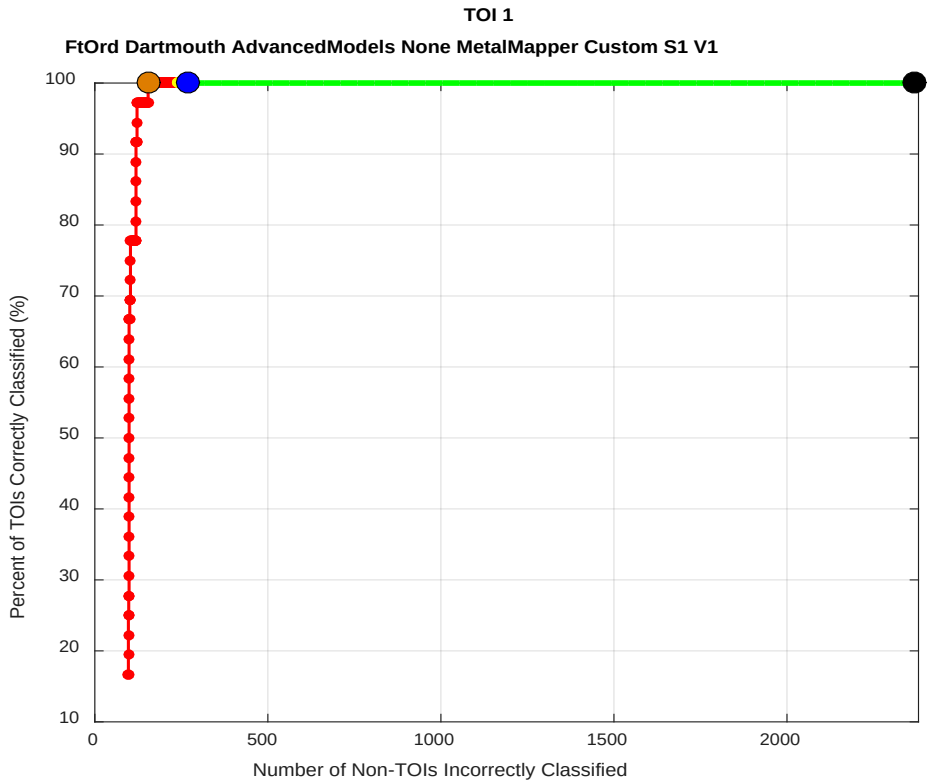

Figure 61. ROC for Fort Ord Primary Objective (Finding all Large TOIs to a Depth of 2 Feet)

The primary objective of classifying all large TOIs at depth of 60 cm was achieved easily, as shown in Figure 61. Namely, result shows that the classification analyst was able to achieve 100% efficiency and 90% false positive rejection rate at the dig stop.

Similarly, the secondary objective of classifying 99% TOIs with high confidence on the site was achieved (see Figure 62). At the final "Stop-Dig" point, our team was able to achieve 99.25% efficiency (we classified 395 out of 398 anomalies) and achieved 76% clutter rejection. Considering all TOI that were classified, we achieved a false positive rejection rate of 47%, see Figure 62.

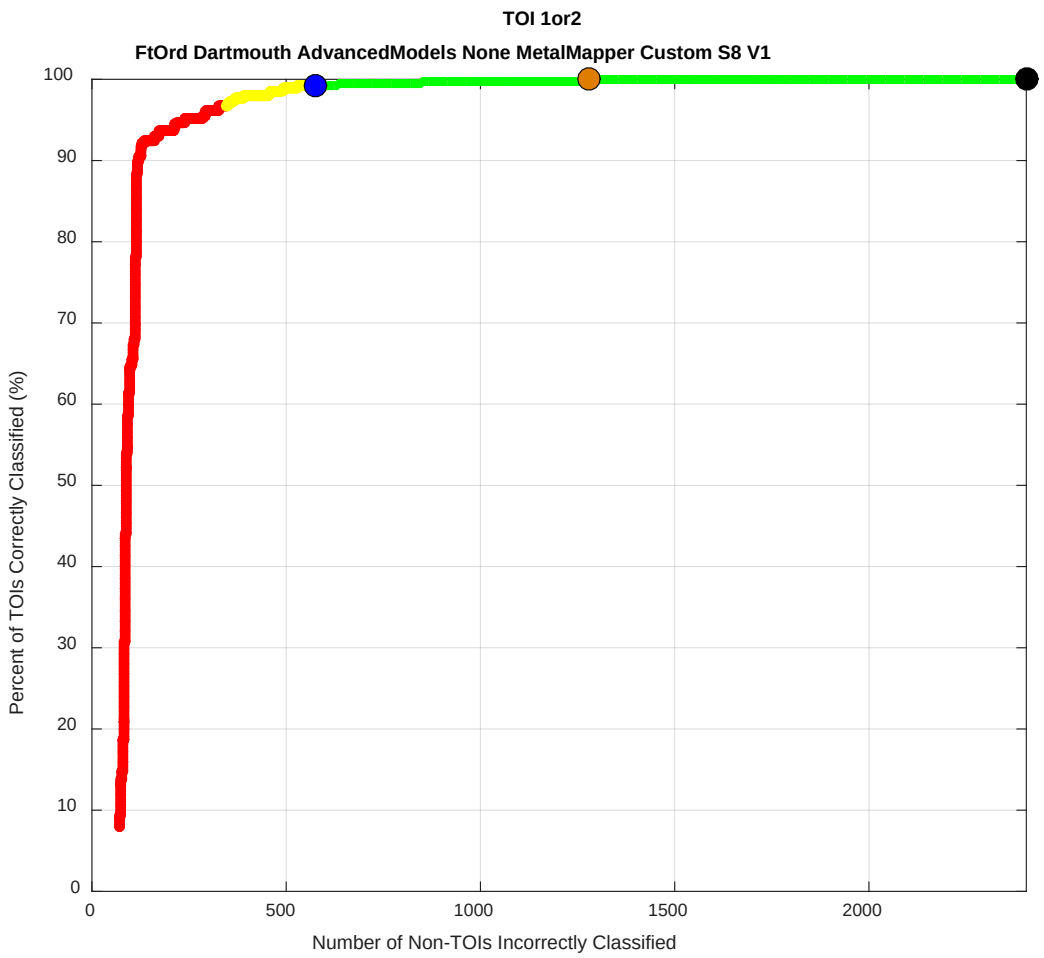

Figure 62. Final Scoring Result for Fort Ord Secondary Objective (Classify all TOI)

7.2 OBJECTIVE: MAXIMIZE CORRECT CLASSIFICATION OF NON-MUNITIONS

The main aim of UXO classification technology is to safely minimize the number of unnecessary digs. To assess the utility of the technology, we compared the number of non-TOI targets that can be left in ground with high confidence using the advanced EMI discrimination technology to the total number of false targets that would be present if the technology were absent. The objective was considered to have been met if the method eliminated at least 75% of targets that did not correspond to a TOI in the discrimination step.

7.3 RESULTS

Our classification results for all eleven demonstrations are summarized in Table 6.

Table 6. Classification Performance Results for all Eleven UXO Live Sites

ESTCP Demo #	Site	Data Set	Efficiency at "Stop-Dig" Point	False Positive Rejection Rate		Number of TOIs Incorrectly Classified
				At "Stop-Dig" Point	With All TOI Classified	
1	Spencer Range, TN, Open Area	MM	100%	90%	93%	0
		5x5 TEMTADS	100%	92%	95%	0
	Spencer Range, TN, Dynamic Area	MM	100%	86%	90%	0
		2x2 TEMTADS	100%	90%	94%	0
		MPV	100%	75%	78%	0
	Spencer Range, TN, Wooded Area	2x2 TEMTADS	98.6%	91%	26.25%	1
		MPV	98.6%	86%	41%	1
2	MMR, MA	MM	99%	76%	67%	1
		2x2 TEMTADS	100%	75%	78%	0
3	Camp Ellis, IL	MM	98%	88%	82.5%	1
		2x2 TEMTADS	97%	84%	63%	1
4	Fort Rucker, AL	MM	100%	45%	57%	0
5	New Boston AF Station, NH	2x2 TEMTADS	100%	20%	44%	0
6	SWPG, AR	MM	100%	94%	96%	0
		2x2 TEMTADS	100%	92.5%	98%	0
7	WMA, HI	MM	98%	78%	51%	2
8	Andersen AF Base, Guam	2x2 TEMTADS	100%	91%	92%	0
9	Castner, Ft. Bliss, TX	2x2 TEMTADS	100%	90%	94%	0
10	West Mesa, NM	MM	100%	87%	92%	0
11	Fort Ord, CA TOI-1	MM	100%	90%	94%	0
	Fort Ord, CA, TOI or 2	MM	99.25%	76%	47%	3

Color codes:

	The objective was met: All TOIs were classified as "Dig" before at the "Stop-Dig" point while reducing of false alarms by more than 75% of TOIs
	The objective was not met: All TOIs were classified as "Dig" before at the "Stop-Dig" point, however due to high ratio between number TOIs to number of clutters on the site the classification was declared as non-sufficient.
	The objective was not met: 98.6% of TOIs classified as "dig" at the dig stop point. The missed classifications due to number of targets and sensor to target separation distances.
	The objective was not met due to insufficient data for the library item.
	The objective was not met partially due to insufficient data quality, magnetic soil and inaccurately documenting the intrusive results.

7.4 OBJECTIVE: SPECIFY A NO-DIG THRESHOLD

One of the main criteria for acceptance of the classification technologies by the end user community is the "Stop-Dig" specification. Over the past 10 years our group has developed a robust EMI data inversion, training, and "Stop-Dig" section approach (see Section 2). This approach was thoroughly tested during this demonstration project. Namely, we compared an analyst's "Stop-Dig" threshold point to the point where 100% of munitions were correctly identified. Our success criterion was considered to be met if a sensor-specific dig list placed all the TOIs before the "Stop-Dig" point and if additional digs (false positives) were requested after all TOI were identified correctly.

7.5 RESULTS

Cued data processing and classification: Our advanced EMI classification technology was applied to all cued data sets collected at eleven UXO Live Sites. During data analysis and classification studies, for each anomaly, advanced EMI sensors data were inverted and the targets intrinsic (total volume magnetic source (NVMS) i.e., the size, shape and material properties) and extrinsic (location, depth, orientation) parameters were estimated.

This objective was successfully met for the majority of ESTCP UXO Live Sites. The classification efficiency at the "Stop-Dig" point and false alarm rejection rate for all eleven sites are summarized in Table 6.

The intrinsic parameters were used for classification and ranked dig-lists were generated for each data set independently. The ranked dig-lists were submitted to the ESTCP office for scoring. All classification results were scored against intrusive results by The Institute for Defense Analyses (IDA), as a third party. The scored results were used to assess the five performance criteria and to determine pons and cons of the advanced classification technology for subsurface targets detection and classification at UXO live sites. We compared the number of non-TOI targets that can be left in ground with high confidence using the advanced EMI discrimination technology to the total number of false targets that would be present if the technology were absent. The objective was considered to have been met if the method eliminated at least 75% of targets that did not correspond to a TOI in the discrimination step. The independently scored results for all eleven sites are summarized in Table 6. The results showed that the main object: to rank all TOIS as "Dig" before at the "Stop-Dig" point while reducing of false alarms by more than 75%, were met for the majority sites. The objective was not met for few sites see Table 6. These were due to density of anomalies and sensor to target separation distance; insufficient data quality, magnetic soil and inaccurately documenting the intrusive results. However, in all cases the classification approach was able to rank more than 98% of TOI correctly as "Dig".

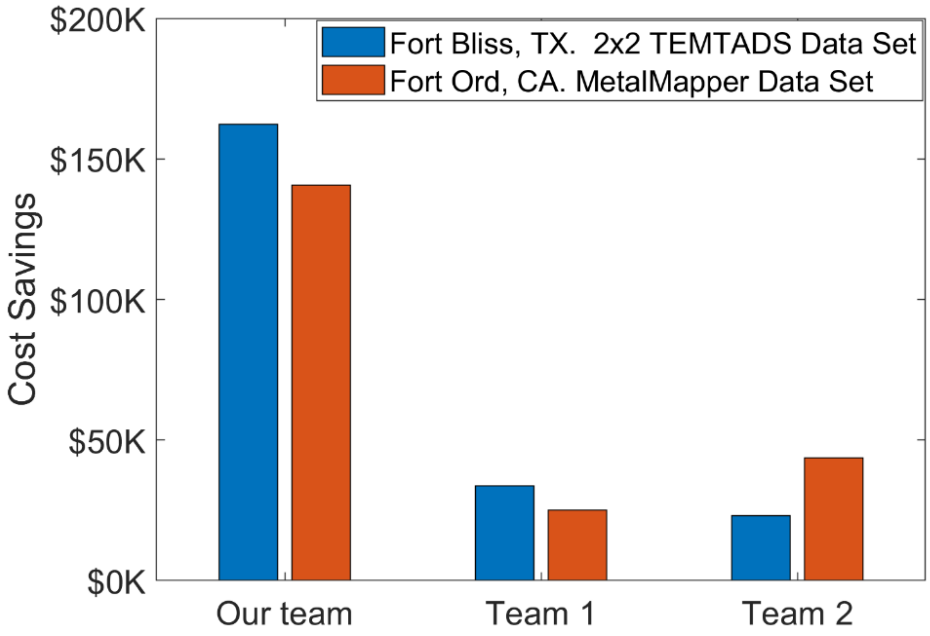

Figure 63. Cost Savings for Achieved by Our and Two Other Teams at Fort Bliss, TX, and Fort Ord, CA, UXO Live Sites

In addition, the independently scored classification results for all sites showed that our classification approach was able to deliver much better classification results than any other approach. Specifically, for very challenging sites, such as for MMR, MA, Fort Bliss, TX, WMA, HI and Ford Ord, CA, our approach was able to classify all seeded items as well as site-specific 20 mm, 25 mm, 35 mm and 40 mm MEC projectiles. For example, during the Fort Bliss, TX, demonstration, we were able to identify 92% of all clutter items as "NO DIG," whereas Team 1 and Team 2, who processed the same datasets, identified only 13% and 19% of clutter as "NO DIG", respectively. The comparisons between cost savings achieved by our team, using the advanced classification approach, Team 1 and Team 2 are showing in Figure 63. The cost savings was calculated as $125 times number of clutters after last TOI dug. The similar results were achieved for MMR, MA and WMA, HI UXO live sites. The studies have showed that our advanced classification technology provides much more savings than any other classification approach.

Extracting subsurface targets intrinsic and extrinsic parameters accurately is one of main products that our data pre-processing and inversion algorithm provide for mapping and classification subsurface anomalies. Overall the success of classification directly depends on how accurately these parameters are estimated. For all studies reported in this project, the following criteria were set: the target intrinsic parameters were allowed be vary within $\pm$10%, the extracted *x*-*y* location within $\pm$10 cm, and the depth within $\pm$5 cm. This objective was successfully met for all datasets collected at all eleven different demonstration sites.

Dynamic data processing and classification: Our approach for processing dynamic datasets is based on orthogonal methods such as the JD and ONVMS techniques, which were originally developed for cued data processing and target classification. These methods have also been successfully applied to dynamic datasets collected during the Camp Hale, CO Live-Site classification demonstration.

Comparisons of the data collected in dynamic survey mode and stationary cued mode revealed that dynamic data is not significantly inferior to cued data in terms of the information that can be extracted and exploited for target classification. Our analysis has shown that when advanced models are applied to dynamic datasets, we are able to completely characterize and classify anomalies and eliminate or reduce significantly the number of cued measurements required for complete target classification across a site.

Comparisons between predicted target locations, estimated by using our target picking/classification algorithm, and actual target locations, measured intrusively, have shown that our advanced models map the subsurface targets accurately and provide significantly improved anomaly selection compared to a simple thresholding or dipole inversions/matched filter approaches. These results are particularly apparent in areas with medium or high dense concentrations of metallic clutter. In addition, the applied advanced EMI models classified each TOI very accurately from multiple dynamic data points, demonstrating the robustness of our dynamic modeling and analysis methods.

7.6 OBJECTIVE: MINIMIZE THE NUMBER OF ANOMALIES THAT CANNOT BE ANALYZED

Fast and cost effective UXO cleanup using the classification approach requires minimizing the number of anomalies that cannot be analyzed. During the execution of the complete classification process (data collection, inversion, decision/classification) some anomalies may not be classified either because the data are not sufficiently informative—the sensor physically cannot provide the data needed to support classification for a given target at a given depth—or because the extracted feature parameters of the target are inadequate for classification. During the UXO Live Site classification studies, reported here, success criteria was met if at least 95% of the selected anomalies could be analyzed and classified.

7.7 RESULTS

This objective was successfully met for all eleven demonstration sites, except for Spencer Range MPV data set. All data sets, collected at eleven classification demonstrations sites, were analyzed, intrinsic and extrinsic target parameters were extracted and classified. Not a single anomaly, with the data, was ranked as “Cannot Analyze.”

7.8 OBJECTIVE: CORRECT ESTIMATION OF TARGET PARAMETERS

One of main products of our data pre-processing and inversion algorithm, ONVMS-DE, is a set of intrinsic and extrinsic parameters used for subsurface target mapping and classification. The success of classification directly depends on how accurately these parameters are estimated. For all studies reported in this project, the following criteria were set: the target intrinsic parameters were allowed be vary within $\pm$10%, the extracted *x-y* location within $\pm$10 cm, and the depth within $\pm$5 cm.

7.9 RESULTS

The clustering seen in the targets’ inverted intrinsic parameters indicates that this objective was successfully met for all datasets collected at all eleven different demonstration sites, see [42]-[52].

Page Intentionally Left Blank

8.0 COST ASSESSMENT

8.1 COST FOR CUED DATA SET PROCESSING AND CLASSIFICATIONS

Time and resources were tracked for each task to assess the cost of deploying the technology at future UXO Live Sites. Here we report the average time that an analyst spent processing and classifying cued data sets from three sites; Camp Beale, CA, Fort Sill, OK and Camp George West, CO. Costs associated with computer resources and run times are excluded. Note that some of the costs might be further decreased as the technology will be used in production setting and survey procedures become formalized. An average time and cost model of the resources spent during three Live Site anomalies classification using the advanced models is summarized in Table 7. These estimations are done for a geophysicist with salary of $90/hr.

Table 7: Average Time and Cost Model for Processing Cued Data Set Using Advanced EMI Models

Cost Category	Description	Time (Minutes Per Anomaly)	Cost Per Anomaly
Preprocessing	Perform eigenvalue extraction, check data quality, and estimate the number of potential anomalies	0.5	$0.75
Parameter extraction	Run code and extract target feature parameters	0.25	$0.375
Classifier training	Optimize classifier design and train	0.25	$0.375
Classification and construction of a ranked anomaly list	Classify anomalies in the test set and construct the ranked anomaly list	1	$1.5
Reporting	Generate and document classification results and write reports.	1	$1.5
	Total	3	$4.5

8.2 COST FOR DYNAMIC DATA SET PRE-PROCESSING, DATA INVERSION AND CLASSIFICATIONS

The dynamic data processing consists: background selection, background subtraction, data inversion, targets selection, classifier training, targets classification and construction of a prioritized dig list. Table 8 summarizes an average time spent Camp Hale, CO dynamic data processing and targets classification.

Table 8: Average Time Spent by an Analyst on Camp Hale, CO, Dynamic Data Processing and Classification

Cost Category	Description	Time (Hours Per Acre)	Cost (Per Acre)
Dynamic Data Processing and Targets Selection			
Background data selection	Process and analyze dynamic background data sets	4	$360
Background subtraction	Import, normalize by maximum on Tx current and remove background data sets	8	$720
Anomalies selection	Combine inverted locations from each dynamic data point with GPS, and to cluster the extracted coordinates	8	$720
Reporting	Write dynamic data pre-processing and anomaly section reports	6	$540
	Total	26	$2340
Targets Classification Form Dynamic Data Sets			
Preprocessing	Perform eigenvalue analysis, check data quality, and estimate the number of potential anomalies	0.5 min/anomaly	$0.75
Parameter extraction	Extract and analyze target feature parameters	0.5 min/anomaly	$0.75
Classifier training	Optimize classifier design and train	1 min/anomaly	$1.5
Classification and construction of a ranked anomaly list	Classify anomalies in the test set and construct the ranked anomaly list	2 min/anomaly	$3.0
Reporting	Generating and documenting classification results and writing reports	1 min/anomaly	$1.5
	Total	5 min/anomaly	$7.5

9.0 IMPLEMENTATION ISSUES

Advance EMI models and classification approaches described here consist: background corrections, data inversion and target feature parameter estimation, ranking, training, and finally target classification using statistical and library matching techniques. During this project we have developed the software package called "*EMClass*", see Figure 1. *EMClass* software is easy to use. There exist four primary steps:

1. The user should specify an output folder;
2. Background data files are selected for the background level subtraction from the original EMI anomaly dataset;
3. The path to .csv data files is provided and each EMI dataset is normalized by a corresponding transmit (Tx) current and backgrounds are subtracted;
4. After background EMI levels have been applied and corrupted channels removed, the combined ONVMS-DE algorithm is applied to the anomaly datasets using a multiple source inversion approach.

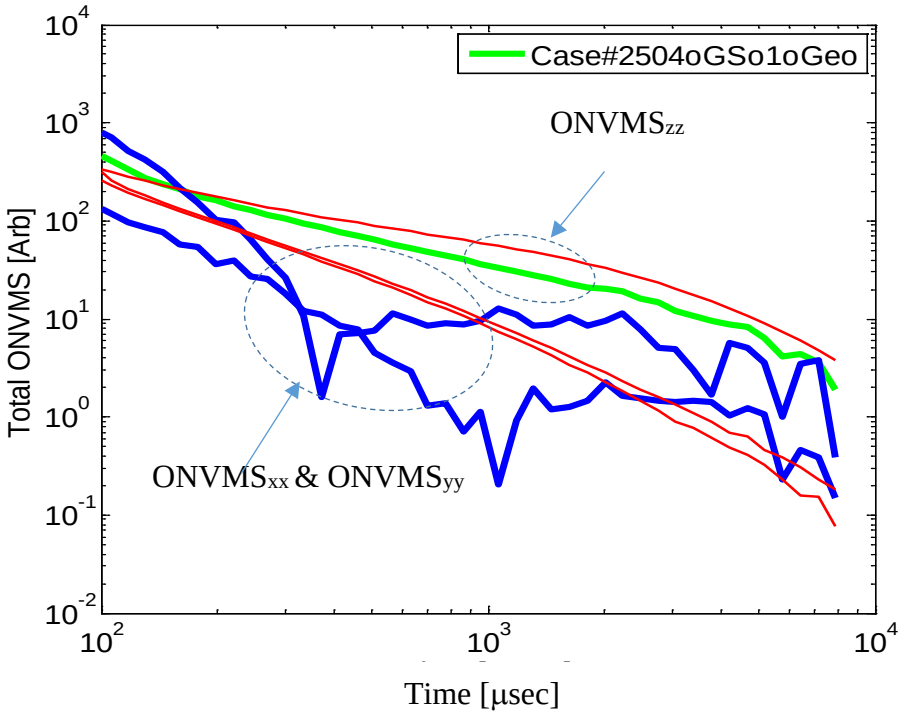

Figure 64. Extracted Total ONVMS Time-decay Profiles for MM Anomaly #2504

The thin red lines show a library signatures, while the thick blue and green lines show the inversion results.

Once intrinsic and extrinsic parameters of the targets are extracted, they are clustered and each anomaly is ranked. During this “Analyze Data” step, target classification features, such as the total ONVMS or the effective polarizabilities, (via one, two and three sources) are evaluated using clustering results, library matching results and visual inspection tools. During this process site-specific training target lists are generated. These training data and built-in DoD library data are used to assess background noise levels, validate inversion results, confirm preliminary target ranking results, and (more importantly) determine an optimal “Stop-Dig” point to optimize classification performance.

To achieve the optimal “Stop-Dig” point the training data are derived from “uncertain anomalies,” which are located in the preliminary ranked list between targets which are definitely targets of interest (TOI), and targets which are definitely clutter. Finally, once the ground truth is obtained from the training targets, all anomalies are classified as TOI or clutter and the optimal “Stop-Dig” point is defined using statistical, library matching, and visual inspection tools. The statistical clustering and library matching techniques are fully automated and only visual inspection step of the inverted effective polarizabilities requires a user with focused attention and the ability to visually identify corrupted effective polarizabilities. For example, in some cases, due to poor signal-to-noise ratio, the feature vectors from UXO targets can be corrupted (See Figure 64) or could be similar with clutter anomalies. In such cases, the user must recognize similarities between the library and test-anomaly polarizabilities for one of three parameters (the primary, secondary and tertiary polarizabilities) and override statistical and/or library matching results using an expert's judgment.

10.0 REFERENCES

[1] Report of the Defense Science Board Task Force on Unexploded Ordnance. Office of the Under Secretary of Defense for Acquisition, Technology, and Logistics. 2003.

[2] S. V. Chilaka, D. L. Faircloth, L. S. Riggs, and H. H. Nelson, "Enhanced discrimination among UXO-like targets using extremely low-frequency magnetic fields," *IEEE Trans. Geosci. Remote Sens.*, vol. 44, pp. 10–21, 2006.

[3] D. McNeill and M. Bosnar, "Application of TDEM techniques to metal detection and discrimination: A case history with the new Geonics EM-63 fully time-domain metal detector," Geonics Technical Note TN-32, 2000 [Online]. Available: http://www.geonics.com/pdfs/technicalnotes/tn32.pdf.

[4] E. Gasperikova, J. T. Smith, H. F. Morrison, A. Becker, and K. Kappler, "UXO detection and identification based on intrinsic target polarizabilities—A case history," *Geophysics*, vol. 74, no. 1, pp. B1–B8, 2009.

[5] D. A. Steinhurst, G. R. Harbaugh, J. B. Kingdon, T. Furuya, D. A. Keiswetter, and D. C. George, "EMI array for cued UXO discrimination," ESTCP project MM-0601 final rep., 2010 [Online]. Available: http://www.serdp.org/Program-Areas/Munitions-Response/Land/Sensors/MR-200601/MR-200601.

[6] I. J. Won, D. A. Keiswetter, D. Hansen, E. Novikova, and T. M. Hall, "GEM-3: A monostatic broadband electromagnetic induction sensor," *J. Environ. Eng. Geophys.*, vol. 2, pp. 53–64, 1997.

[7] K. O'Neill, I. J. Won, A. Oren, C.-C. Chen, H.-S. Youn, X. Chen, and K. Sun, "Data diversity for UXO discrimination in realistic settings with a handheld EMI sensor," *Proc. SPIE*, vol. 5415, pp. 253–262, 2004.

[8] J. P. Fernández, B. E. Barrowes, K. O'Neill, I. Shamatava, and F. Shubitidze, "A vector handheld frequency-domain sensor for UXO identification," *Proc. SPIE*, vol. 7303, p. 7303-31, 2009.

[9] H. H. Nelson and J. R. McDonald, "Multi-sensor towed array detection system for UXO detection," *IEEE Trans. Geosci. Remote Sens.*, vol. 39, pp. 1139–1145, 2001.

[10] D. D. Snyder and D. C. George, "The Advanced Ordnance Locator (AOL): A dual-mode TEM and magnetics system for detection and classification of UXO," in *2005 Proc. SAGEEP*, pp. 1244–1253.

[11] M. Prouty, D. C. George, and D. D. Snyder, "MetalMapper: A multi-sensor TEM system for UXO detection and classification," ESTCP Project MR-200603 final rep., 2011 [Online]. Available: http://www.serdp.org/content/download/9593/122667/file/MR-200603-FR.pdf.

[12] J. P. Fernández, B. E. Barrowes, N. Lhomme, A. Bijamov, T. M. Grzegorczyk, K. A. O'Neill, I. Shamatava, and F. Shubitidze, "MPV-II: An enhanced vector man-portable EMI sensor for UXO identification," *Proc. SPIE*, vol. 8017, p. 8017-06, 2011.

[13] F. Shubitidze, J. P. Fernández, B.E. Barrowes, I. Shamatava, A. Bijamov, K. O'Neill, D. Karkashadze, " The orthonormalized volume magnetic source model for discrimination of unexploded ordnance", *IEEE Transactions on Geo-Science and Remote Sensing, Digital Object Identifier 10.1109/TGRS.2013.2283346.*

[14] F. Shubitidze, J. P. Fernández, I. Shamatava, B. E. Barrowes, and K. A. O'Neill, "Joint diagonalization applied to the detection and discrimination of unexploded ordnance," *Geophysics*, Jul 2012, Vol. 77, No. 4, pp. WB149-WB160.

[15] X. Chen, K. O'Neill, B. E. Barrowes, T. M. Grzegorczyk, and J. A. Kong, "Application of a spheroidal-mode approach and a differential evolution algorithm for inversion of magneto-quasistatic data in UXO discrimination," *Inv. Prob.*, vol. 20, pp. S27–S40, 2004.

[16] F. Shubitidze, K. O'Neill, B. E. Barrowes, I. Shamatava, K. Sun, J. P. Fernández, and K. D. Paulsen, "Application of the normalized surface magnetic charge model to UXO discrimination in cases with overlapping signals," *J. Appl. Geophys.*, vol. 61, pp. 292–303, 2007.

[17] "ESTCP Munitions Response, Live Site Demonstrations, former Camp Beale, CA, April 2011, Draft 4," dated June 2, 2011.

[18] ESTCP, "2009 ESTCP UXO Classification Study, San Luis Obispo, CA," Environmental Security Technology Certification Program, Arlington, VA, Demonstration Plan, April 2009.

[19] F. Shubitidze et al., "A complex approach to UXO discrimination: Combining advanced EMI forward models and statistical signal processing," SERDP MR-1572 Final Report, January 2012.

[20] F. Shubitidze, B. E. Barrowes, I. Shamatava, J. P. Fernández, T. M. Grzegorczyk, K. O'Neill, and A. Bijamov, "Advanced UXO discrimination: resolving multiple targets and overlapping EMI signals," in R. S. Harmon, J. H. Holloway, and J. T. Broach, eds., *Detection and Sensing of Mines, Explosive Objects, and Obscured Targets XVI, Proceedings of SPIE* vol. 8017, 8017-09, 2011.

[21] F. Shubitidze, "Advanced EMI models for live-site UXO discriminations". Final Report, ESTCP-MR-201101.

[22] P. Comon, "Independent component analysis, a new concept?" *Signal Processing* 36(3): 287–314, 1994.

[23] A. Belouchrani, K. Abed Meraim, J.-F. Cardoso, and E. Moulines, "A blind source separation technique based on second order statistics," *IEEE Trans. Signal Processing*, 45(2): 434–444, 1997.

[24] S. Harmeling, A. Ziehe, M. Kawanabe, and K.-R. Müller, “Kernel-based nonlinear blind source separation,” *Neural Computation*, 15: 1089–1124, 2003.

[25] J.-F. Cardoso and A. Souloumiac. “Jacobi angles for simultaneous diagonalization,” *SIAM J. Mat. Anal. Appl.*, 17(1): 161–164, 1996.

[26] B. Flury and W. Gautschi. “An algorithm for simultaneous orthogonal transformation of several positive definite symmetric matrices to nearly diagonal form,” *SIAM J. Sci. Stat. Comput.*, 7(1): 169–184, 1986.

[27] A.-J. van der Veen, M. C. Vanderveen, and A. Paulraj, “Joint angle and delay estimation using shift-invariance techniques,” *IEEE Trans. Signal Processing*, 46(2): 405–418, 1998.

[28] S. Harmeling, A. Ziehe, M. Kawanabe, and K.-R. Müller, “Kernel-based nonlinear blind source separation,” *Neural Computation*, 15: 1089–1124, 2003.

[29] J.-F. Cardoso and A. Souloumiac. “Jacobi angles for simultaneous diagonalization,” *SIAM J. Mat. Anal. Appl.*, vol. 17, pp. 161–164, 1996.

[30] F. Shubitidze, J. P. Fernández, I. Shamatava, A. Luperon, B. E. Barrowes, and K. A. O’Neill, “Inversion-free discrimination of unexploded ordnance in real time,” *Proceedings of SPIE* 8357, 8357-04 (2012).

[31] R. Storn, and K. Price, “Differential evolution: a simple and efficient adaptive scheme for global optimization over continuous spaces,” *Journal of Global Optimization*, vol. 11, pp. 341–359, 1997.

[32] R. Storn, “System design by constant adaptation and differential evolution,” *IEEE Trans. Evol. Comput.*, vol. 3, pp. 22–34, 1999.

[33] S. Cazares, M. Tuley, and E. Ayers, “The UXO Classification Demonstration at Former Camp Butner, NC,” 2011 [Online]. Available: http://serdp-estcp.org/content/download/12777/151554/version/1/file/IDA_Camp+Butner_Report_1-13.pdf.

[34] F. Shubitidze, B. E. Barrowes, I. Shamatava, J. P. Fernández, and K. O’Neill, “The orthonormalized volume magnetic source technique applied to live-site UXO data: Inversion and classification studies,” *SEG Expanded Abstracts*, vol. 30, pp. 3766–3770, 2011.

[35] A. Bijamov, J. P. Fernández, B. E. Barrowes, I. Shamatava, K. O’Neill, and F. Shubitidze "Camp Butner Live-Site UXO Classification using Hierarchical Clustering and Gaussian Mixture Modeling", IEEE Transactions on Geo-Science and Remote Sensing, Digital Object Identifier 10.1109/TGRS.2013.2287510

[36] J. P. Fernández, F. Shubitidze, I. Shamatava , B. Barrowes, and K. O’Neill, “Realistic subsurface anomaly discrimination using electromagnetic induction and an SVM classifier”, Journal in Advanced Signal Processing, 2010.

[37] A. P. Dempster, N. M. Laird, and D. B. Rubin, "Maximum likelihood from incomplete data via the EM algorithm," Journal Royal Statistics Society, vol. 39, no. 1, pp. 1-21, 1977.

[38] F. Shubitidze *et al.*, "Advanced EMI models, Camp Beale", ESTCP MR-201101, Demon. Report, http://www.serdp.org/Program-Areas/Munitions-Response/Land/Live-Site-Demonstrations/MR-201101.

[39] F. Shubitidze *et al.*, "Advanced EMI models, Fort Sill,OK", ESTCP MR-201101, Demon. Report, http://www.serdp.org/Program-Areas/Munitions-Response/Land/Live-Site-Demonstrations/MR-201101.

[40] F. Shubitidze *et al.*, "Advanced EMI models applied to Camp George West, CO", ESTCP MR-201101, Demon. Report, http://www.serdp.org/Program-Areas/Munitions-Response/Land/Live-Site-Demonstrations/MR-201101.

[41] CH2MHill. 2009. Final Limited Site Investigation Report, Former Camp Ellis Military Range,Table Grove, Illinois.

[42] F. Shubitidze *et al.*, "Advanced EMI models applied to Spencer Range, TN", ESTCP MR-201227, Demon. Report,http://www.serdp.org/Program-Areas/Munitions-Response/Land/Live-Site-Demonstrations/MR-201227.

[43] F. Shubitidze *et al.*, "Advanced EMI models applied to Camp Edwards Massachusetts Military Reservation (MMR), MA", ESTCP MR-201227, Demon. Report,http://www.serdp.org/Program-Areas/Munitions-Response/Land/Live-Site-Demonstrations/MR-201227.

[44] F. Shubitidze *et al.*, "Advanced EMI models applied to Camp Elis, IL", ESTCP MR-201227, Demon. Report,http://www.serdp.org/Program-Areas/Munitions-Response/Land/Live-Site-Demonstrations/MR-201227.

[45] F. Shubitidze *et al.*, "Advanced EMI models applied to Fort Rucker, AL", ESTCP MR-201227, Demon. Report,http://www.serdp.org/Program-Areas/Munitions-Response/Land/Live-Site-Demonstrations/MR-201227.

[46] F. Shubitidze *et al.*, "Advanced EMI models applied to New Boston Airforce Station, NH", ESTCP MR-201227, Demon. Report,http://www.serdp.org/Program-Areas/Munitions-Response/Land/Live-Site-Demonstrations/MR-201227.

[47] F. Shubitidze *et al.*, "Advanced EMI models applied to Southwestern Proving Ground, AR", ESTCP MR-201227, Demon. Report,http://www.serdp.org/Program-Areas/Munitions-Response/Land/Live-Site-Demonstrations/MR-201227.

[48] F. Shubitidze *et al.*, "Advanced EMI models applied to Waikoloa Maneuver Area (WMA) , HI", ESTCP MR-201227, Demon. Report,http://www.serdp.org/Program-Areas/Munitions-Response/Land/Live-Site-Demonstrations/MR-201227.

[49] F. Shubitidze *et al.*, "Advanced EMI models applied to Andersen AF base, Guam", ESTCP MR-201227, Demon. Report,http://www.serdp.org/Program-Areas/Munitions-Response/Land/Live-Site-Demonstrations/MR-201227.

[50] F. Shubitidze *et al.*, "Advanced EMI models applied to Fort Bliss, TX", ESTCP MR-201227, Demon. Report,http://www.serdp.org/Program-Areas/Munitions-Response/Land/Live-Site-Demonstrations/MR-201227.

[51] F. Shubitidze *et al.*, "Advanced EMI models applied to West Mesa, NM", ESTCP MR-201227, Demon. Report,http://www.serdp.org/Program-Areas/Munitions-Response/Land/Live-Site-Demonstrations/MR-201227.

[52] F. Shubitidze *et al.*, "Contunued Discrimination Demonstration Using Advanced EMI models at Live UXO sites: Data Quality Assessment and Residual Risk Mitigation in Real Time", ESTCP MR-201227, Final Report,http://www.serdp.org/Program-Areas/Munitions-Response/Land/Live-Site-Demonstrations/MR-201227.

[53] ESTCP office,"Advamced EMI Sensor Demomnstration at the Central Impact Area, Camp Edwards, MA", final report, https://serdp-estcp.org/Featured-Initiatives/Munitions-Response-Initiatives/Classification-Applied-to-Munitions-Response/Massachusetts-Military-Reservation/Advanced-EMI-Sensor-Demonstration-at-the-Central-Impact-Area-Camp-Edwards-MA-with-Addendum.

Page Intentionally Left Blank

APPENDIX A HEALTH AND SAFETY PLAN (HASP)

As this effort did not involve the collection of field data, no HASP was required.

Page Intentionally Left Blank

APPENDIX B POINTS OF CONTACT

Points of contact (POCs) involved in the demonstration and their contact information are presented in Table 9.

Table 9. Points of Contact for the Advanced EMI Models Demonstration

Point of Contact Name	Organization Name Address	Phone Fax E-mail	Role in Project
Dr. Fridon Shubitidze	White River Technologies, 115 Etna Road, Lebanon, NH 03766 USA	Tel: 603 727 9549 shubitidze@whiterivertech.com	PI
Erik Russell	White River Technologies, 115 Etna Road, Lebanon, NH 03766 USA	Tel: (603) 678-8386 russell@whiterivertech.com	Project Coordination
Dr. Herb Nelson	ESTCP Program Office, ESTCP Office, 901 North Stuart Street, Suite 303 Arlington, VA 22203-1821	Tel: 571 372-6400 herb.nelson@nrl.navy.mil	ESTCP Munitions Management Program Manager